ABSTRACT

Development of Prediction Technique for the Abrasive Waterjet Generated Kerf

by
Yichung Chung

This study is concerned with the development of a practical and accurate technique for off-line determination of the variables characterizing the macro-geometry of the kerf generated in the course of abrasive waterjet (AWJ) machining of ductile materials. The study involved generation and processing of a database relating operational conditions with kerf dimensions. The total number of generated samples exceeded 1500.

A physical model relating the process results with operational conditions was constructed and used for the selection of a statistical technique for analysis of the acquired experimental information. The semiempirical model developed here is based on a simple theoretical model which assumes that the particle distribution within the AWJ is statistically uniform. The good correlation found between the experimental results and the semiempirical model demonstrate the validity of this assumption. Regression equations, determining the depth of jet penetration, kerf width and taper, were constructed. The correlation coefficients between predicted and measured values of the kerf characteristics exceed 0.94. Only in one case out of 20 was the correlation coefficient 0.9. The observed result demonstrates the geometry of the kerf is controlled by the diameter of the jet and kinetic energy of particles.

A practical, reliable procedure for construction of a prediction technique for AWJ machining of a material in question was suggested and tested. The proposed technique will be used for control of AWJ machining as well as for the development of an expert system.

DEVELOPMENT OF PREDICTION TECHNIQUE FOR THE GEOMETRY OF THE ABRASIVE WATERJET GENERATED KERF

by
Yichung Chung

A Dissertation
Submitted to the Faculty of the
New Jersey Institute of Technology
in Partial Fulfillment of the Requirements for the Degree of
Doctor of Philosophy
Department of Mechanical and Industrial Engineering

May 1992

Blank Page

APPROVAL PAGE
Development of Prediction Technique for the Geometry of the Abrasive Waterjet Generated Kerf

by
Yichung Chung

Dr. Ernest S. Geskin, Dissertation Adviser
Professor of Department of Mechanical and Industrial Engineering, NJIT

Dr. Rajesh N. Dave
Assistant Professor of Department of Mechanical and Industrial Engineering, NJIT

Dr. Avraham Harnoy
Associate Professor of Department of Mechanical and Industrial Engineering, NJIT

Dr. Zhiming Ji
Assistant Professor of Department of Mechanical and Industrial Engineering, NJIT

Dr. Raj Sodhi
Associate Professor of Department of Mechanical and Industrial Engineering, NJIT

BIOGRAPHICAL SKETCH

Author: Yichung Chung

Degree: Doctor of Philosophy

Date: May, 1992

Undergraduate and Graduate Education:

- Doctor of Philosophy in Mechanical Engineering, New Jersey Institute of Technology, Newark, NJ, 1992
- Master of Science in Mechanical Engineering, New Jersey Institute of Technology, Newark, NJ, 1988
- Bachelor of Science in Mechanical Engineering, Tatung Institute of Technology, Taiwan, 1983

Major: Mechanical Engineering

Position Held:

Research Assistant, Department of Mechanical Engineering, New Jersey Institute of Technology, January 1988 - December 1988

Graduate Assistant, Department of Mechanical and Industrial Engineering, New Jersey Institute of Technology, January 1989 - May 1992

Research Engineer,
Waterjet Cutting System, Ingersoll-Rand Company, May 1990 - September 1990

This dissertation is dedicated to
My parents

ACKNOWLEDGMENT

The author wishes to express his sincere gratitude to his advisor, Professor E. S. Geskin, who provided constant supervision, many valuable suggestions, continuous support and encouragement throughout the course of study.

Special thanks to Drs. R. Dave, A. Harnoy, Z. Ji, and R. Sodhi for serving as members of committee, having kindly read through the original manuscript, and providing valuable suggestions. Additionally, sincere thanks to Mr. Jo-Fei Chao for his timely help and suggestions in this study.

The author also wishes to express his sincere gratitute to Dr. P. Singh who offered a great oppertunity working in the Ingersoll-Rand Co. and turned this study much more solid and pratical.

And finally, a greatful thank you to the author's family, especially, his wife, Li-Chuan, for the firm support and encourgement.

TABLE OF CONTENTS

LIST OF TABLES

LIST OF FIGURES

Figure **Page**

CHAPTER 1
INTRODUCTION

Waterjet (WJ) has been used as a cutting, mining and cleaning tool in industrial applications for over twenty-five years. In the formation of the waterjet, water is pressurized up to 345 MPa and expelled through a nozzle to form a coherent and high-velocity jet. Depending on the inside diameter of the nozzle, the diameter of waterjet at the exit of nozzle is generally in the range of 0.1 to 0.5 millimeters for cutting application. Currently, WJ is appropriate for cutting non-metallic and soft materials. Brittle materials may crack under the impact of the WJ.

To improve the machining performance of the WJ, an abrasive waterjet (AWJ) cutting technology as an extension of waterjet cutting technology was developed as a new nontraditional machining tool in 1983. As depicted in Fig. 1, the waterjet is expelled into the chamber of a nozzle body where a vacuum is created and the abrasive particles are drawn into the chamber. The waterjet and abrasive particles are then introduced into a focusing tube which is generally made of tungsten carbide. The turbulent processes in the tube cause the water and abrasive particles to mix together to form an abrasive waterjet. Here, part of the momentum of the waterjet is transferred to the abrasives, whose velocities are abruptly increased. As a result of the momentum transfer between the water and abrasives, a high-velocity stream of abrasives is generated to perform the machining work.

The AWJ is a single-point tool, which may be pointed in almost any direction, is capable of cutting almost every kind of material [1-6], and causes very little, if any, subsurface damage to the material being cut. A number of investigations on the application of AWJ have been reported. Among the investigations, turning, milling, drilling, trimming and deburring have been tested and successful results claimed [7-8].

Along with the aid of a CAD/CAM system, the AWJ is now capable of shaping complicated three-dimensional workpieces [9-11, Appendix I].

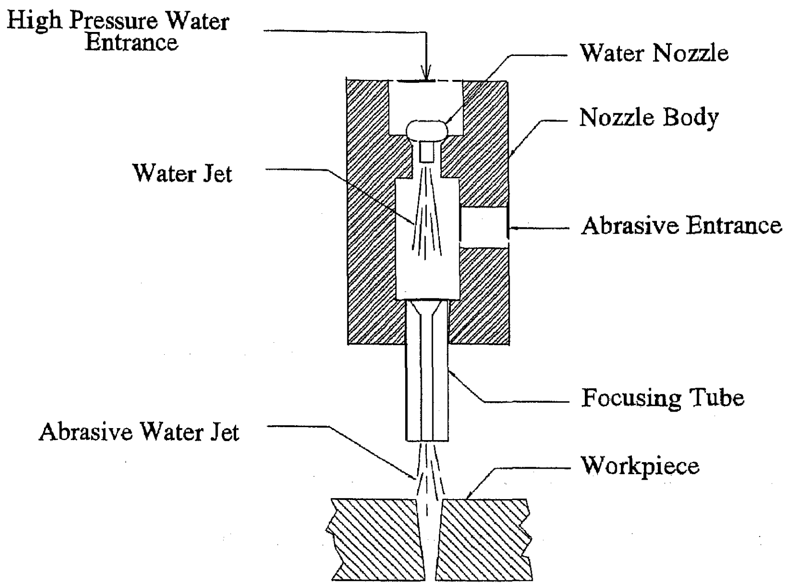

Figure 1 Schematic of Cutting Head.

Despite the tremendous amount of experimental work which has been carried out, the full potential of the AWJ application today has not been completely explored.

The operating parameters affecting the AWJ cutting performance can be categorized, in general, as follows:

- Operating water pressure (Po),
- Water nozzle diameter (Do),
- Focusing tube diameter (Dt),
- Abrasive material, (Garnet sand was used in this study)
- Size of the abrasive particle (Sa),
- Mass flow rate of abrasive (Ma),
- Standoff distance (Sd),
- Traverse speed of AWJ (U).

The AWJ cutting results being investigated include, in general, as follows:

- Depth of cut (H),
- Top kerf width (Wt),
- Bottom kerf width (Wb),
- Taper of kerf (Tp),
- Generated surface roughness.

Some studies relating the operating parameters to the cutting results have been done but only within a small range of consideration [12-20]. These works will be discussed in Chapter 6 together with the results of this study. Due to the lack of a complete scope of knowledge on this technology, as of today, the AWJ machining tasks being carried out in the industries as well as in research labs are still using the trial and error technique for determining the operating parameters in machining a material in question. Such a trial and error process requires large safety factors on the operating parameters to ensure good machining results, and hence, results in a lot of waste in the course of machining.

The first objective of this study is to develop a reliable representative database relating the machining results to the operating parameters for the use of AWJ. The expected features of this database include

- To investigate the effect of all practically important operating parameters on the AWJ machining results within the range of industrial application.
- To identify the information necessary for the construction of prediction models.
- To construct a practical and valid quantitative model relating operational conditions with kerf geometry.
- To evaluate the physical notion used for constructing prediction equations for the AWJ machining results.

The second objective of this study is to create a prediction technique for the AWJ machining results. Such a technique offers a convenient tool for AWJ users to decide the optimal operating parameters for AWJ machining work.

The third objective is to meet the industrial requirement of construction of an expert system (Fig. 2) for the AWJ machining technology. This study is mainly to meet the module of "OPERATING PARAMETERS SELECTION" in the whole structure of the expert system.

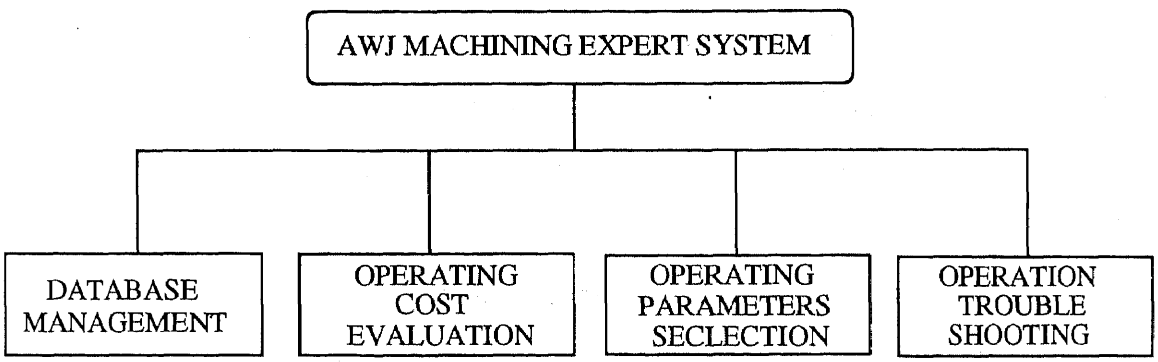

Figure 2 The Structure of An Expert System for AWJ Machining.

The previous fundamental studies on the AWJ working mechanism are discussed in Chapter 2. To avoid the defects of employing unavailable parameters in the past modeling works, a modified simple model for prediction of the depth of cut by AWJ is constructed and presented in Chapter 3. A series of experiments are conducted then (Chapter 4) to improve the accuracy of the model and the results are compared with other results of past studies. The prediction technique by the use of this model accompanied by the experimental results is suggested in Chapter 5. Conclusions and recommendations are made in Chapter 6. A case study on the capability of AWJ three-dimensional machining is given in Appendix I. All the experimental databases of over 1000 cutting and grooving tests are listed in the Appendix II.

CHAPTER 2
LITERATURE SURVEY

2.1 Study of the Erosion Mechanism in the Course of the AWJ Machining

An AWJ consists of liquid water, bubbles, and abrasive particles. When impinging at a solid material, each of them is capable of making some damage on the solid surface. However, in the study of the AWJ machining process, when compared with the effect of abrasive particles on the amount of material removal, the effect of liquid water and bubbles is too small to be considered. Erosion by solid particles, which was defined as the material removal mechanism in the course of particles impacting on a solid surface, was hence accepted as the main mechanism of the AWJ machining. In the long history of the study of erosion by solid particles, there were two main models created by Finnie [21] and Bitter [22], respectively.

Finnie derives equations to describe the trajectory of an individual particle of mass **m** striking a solid surface at an angle **α**, and with a velocity **V** as shown in Fig. 3.

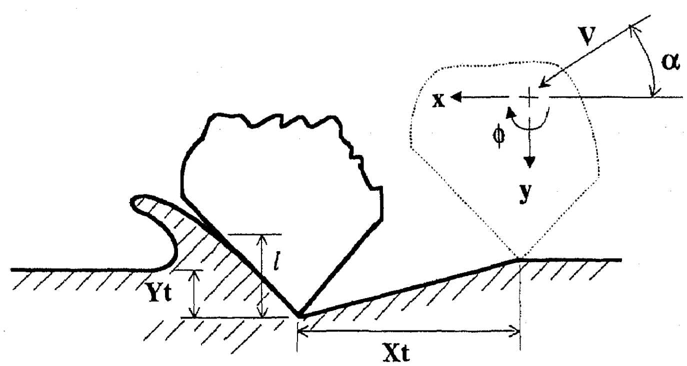

Figure 3 An Idealized Two-dimensional Model of a Rigid Abrasive Grain Impinging into a Ductile Metal.

In this analysis it is assumed that the center of the particle translates in **x** and **y** directions while rotating at an angle ϕ. The particle is considered as the cutting edge of a tool for the erosion of a ductile material. The volume removal **W** can be found by integrating the equations of motion for the penetrating tip of the particle over the period of penetration. The final result yields:

$$W = \frac{mV^2}{p\psi K}\left(\sin(2\alpha) - \frac{6}{K}\sin^2\alpha)\right) \qquad \text{if} \quad \tan\alpha \le \frac{K}{6} \tag{1}$$

$$W = \frac{mV^2}{p\psi K}\left(\frac{K\cos^2\alpha}{6}\right) \qquad \text{if} \quad \tan\alpha \ge \frac{K}{6} \tag{2}$$

where p : horizontal component of the stress on the particle face

ψ : the ratio l / Y_t

K : ratio of vertical to horizontal force component on particle

The results of the above analysis had been compared with test results from a specially designed "sandblast" type tester in which the velocity, direction, and amount of abrasive may be carefully controlled. It was concluded that for ductile materials it is possible to predict the manner in which material removal varies with the direction and velocity of the eroding particles.

Bitter [22] also makes a theoretical analysis of the erosion by solid particles in which the type of wear analyzed in Finnie's work was classified as the cutting wear. In addition, however, Bitter accounts for deformation wear which corresponds to the erosion at normal angles of attack in ductile materials, and which is not accounted for in Finnie's analysis. Bitter derived the equation for deformation wear using the energy balance of collisions at large angles. The resulting equation for deformation wear and the equation for cutting wear derived by Bitter [22] are given below:

$$W_D = \frac{1}{2}\frac{M(V\sin\alpha - V_C)^2}{\varepsilon}, \qquad 0 \le \alpha \le 90^\circ \tag{3}$$

$$W_C = \frac{2MC(V\sin\alpha - V_C)^2}{\sqrt{V\sin\alpha}}\left(V\cos\alpha - \frac{C(V\sin\alpha - V_C)^2}{\sqrt{V\sin\alpha}}\rho\right) \qquad \text{if } \alpha \le \alpha_0 \tag{4}$$

$$W_C = \frac{\frac{1}{2}M\left(V^2 \cos^2 \alpha - K_1 (V\sin\alpha - V_C)^{3/2}\right)}{\rho} \qquad \text{if } \alpha \geq \alpha_0 \tag{5}$$

where W_D, W_C : units volume loss due to deformation wear and cutting wear, respectively.

M : total mass of impinging particles.

V : particle velocity.

α : impact angle.

V_C : maximum particle velocity at which the collision still is purely elastic.

ε : the energy needed to remove a unit volume of material from the body by deformation wear (deformation wear factor).

ρ : the energy needed to scratch out a unit volume from a surface (cutting wear factor).

constant $C = \frac{0.288}{y} \sqrt[4]{d/y}$,

constant $K_1 = 0.82 y^2 \sqrt[4]{y/d} \left(\frac{1-q_1^2}{E_1} + \frac{1-q_2^2}{E_2}\right)^2$

y : elastic load limit.

d : density.

E : Young's module.

q : Poisson's ratio.

Bitter's work is an exhaustive and extremely intricate study, accounting for both elastic and plastic properties of the particle and specimen materials.

The experimental results and the analyses of Finnie [21] and Bitter [22] indicate that the following factors should be accounted for in the modeling of erosion damage.

(a) The normal component of kinetic energy of the impacted particles is absorbed in the specimen surface and accounts for deformation wear.

(b) For certain hard materials, subjected principally to deformation wear, there is a limiting component of velocity normal to the surface below which no erosion takes place. This limiting value dependents on the particle shape.

(c) The kinetic energy component parallel to the surface is associated with cutting wear.

(d) For cutting wear and large angles of attack the particles come to rest in the surface and the total parallel component of kinetic energy contributes to cutting wear. For the small angle of attack, however, the particles may sweep into the surface and finally leave again with a residual amount of parallel kinetic energy.

Based on the above results, Neilson and Gilchrist [23] constructed a simplified model for erosion by a stream of solid particles as:

$$W = \underbrace{\frac{\frac{1}{2}MV^2\cos^2\alpha\sin n\alpha}{\rho}}_{(A)} + \underbrace{\frac{\frac{1}{2}M(V\sin\alpha - K)^2}{\varepsilon}}_{(B)} \qquad \text{if } \alpha < \frac{\pi}{2n} \tag{6}$$

$$W = \underbrace{\frac{\frac{1}{2}MV^2\cos^2\alpha}{\rho}}_{(C)} + \underbrace{\frac{\frac{1}{2}M(V\sin\alpha - K)^2}{\varepsilon}}_{(B)} \qquad \text{if } \alpha > \frac{\pi}{2n} \tag{7}$$

where W is the erosion produced by M pounds of particles at the angle of attack α and particle velocity V. K is the velocity component normal to the surface below which no erosion takes place. Part B accounts for deformation wear and part A and C account for cutting wear at the small angle of attack and large angle of attack, respectively.

Through experimental studies, Neilson and Gilchrist [23] claimed that the erosion by a stream of particles has the same characteristics as by an individual particle. Therefore, the actual material removal amount by a stream of particles can be approximated through the superposition of the material removal by individual particles.

More recently, Hashish [24] has developed an improved model of the erosion by solid particles in a liquid jet. The Hashish's model uses a single material property to characterize the erosion resistance of a material over the entire range of impact angles. The model also incorporates particle's shape expressed by sphericity and roundness numbers. This improved model is best suited for shallow angles of impact and is expressed as

$$E_V = \frac{7}{\pi}\left(\frac{V}{C_K}\right)^{2.5} \sin 2\alpha\sqrt{\sin\alpha}, \qquad \alpha \le \alpha_0 \tag{8}$$

where E_V is the ratio of the material volume removed to the volume of the abrasive particle; V is the particle velocity and α is the impact angle.

In the above equation C_K is defined as a modified characteristic velocity that combines the particle and material characteristics

$$C_K = \sqrt{\frac{3\sigma \cdot R_f^{\,3/5}}{\rho_P}} \tag{9}$$

where σ : material flow stress

R_f : particle roundness

ρ_P : density of particle

As can be seen in the above created erosion models, the information of the condition of particles size as well as velocity are necessary for these models to be used in the study of AWJ machining mechanism. In the following sections, some of the previous study in this aspect will be discussed.

2.2 Modeling of the AWJ Machining

Based on the past study of erosion by solid particles, there have been a number of works on the mathematical modeling of the AWJ machining. Among those studies, Hashish's work had been considered the most comprehensive [25]. In a series of visualization experiments of AWJ cutting [26], it has been suggested that the total depth of cut should be divided into two distinct zones due to different modes of interaction between impinging abrasive particles and the target material as indicated in Fig. 3. In the upper zone, the material is removed by particles impacting at shallow angles, which has been defined by Finnie as cutting wear mode. In the lower zone, sequential steps are formed which lead to large angle impact which is defined by Bitter as the deformation wear mode.

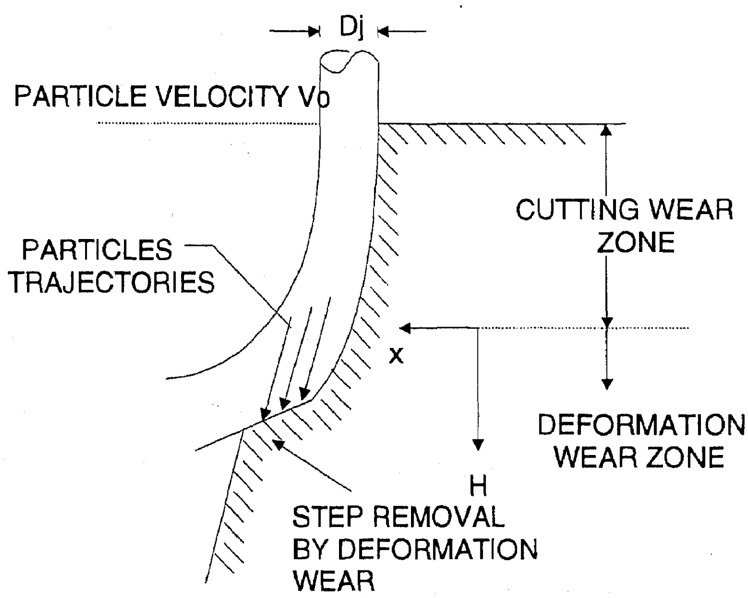

Figure 4 Wear Modes Defined by Hashish.

With these backgrounds, a global cutting equation was derived as listed below.

$$h_C = \frac{(V_0 / C_K) D_j}{\left(\frac{\pi \cdot \rho_P \cdot U \cdot D_j}{14Ma}\right)^{2/5} + \left(\frac{V_e}{C_K}\right)} \tag{10}$$

$$h_d = \frac{1}{\frac{\pi \cdot D_j \cdot \sigma \cdot U}{2C_1 \cdot Ma \cdot (V_0 - V_e)^2} + \frac{C_f}{D_j} \frac{V_0}{(V_0 - V_e)}} \tag{11}$$

where $C_k = \sqrt{\frac{3 \cdot \sigma \cdot R_f^{3/5}}{\rho_P}}$: characteristic velocity

hc, hd : depth of cut due to cutting wear mode and deformation wear mode, respectively

V_o : initial particle velocity

V_e : threshold particle velocity

D_j : jet diameter

ρ_P : density of particle

σ : material flow stress

R_f : particle roundness factor

C_f : coefficient of friction on kerf wall

Ma : abrasive flow rate

C_l : ratio of Ma in which particles cause material removal

U : jet traverse rate

The above derived model considers almost all factors involved in AWJ machining. However, part of the parameters such as R_f, C_l and C_f are decided on free will and thus cause quite different prediction results when employed by different people. More than this, the values of V_o and V_e are either unavailable or also decided on free will.

Except for Hashish's model, there have been other empirical modeling works. Blickwedel et. al. [13] suggested an semiempirical method which is also used in this dissertation and constructed the following prediction equation:

$$H = Cs\frac{P - P_o}{U^{(0.86+2.09/U)}} \tag{12}$$

where P is the water pressure; P_o is the pressure limit for material removal; U is the traverse rate and Cs is a constant to be decided by experiments.

Such a constructed equation considers only two operating parameters, which are pressure and the traverse rate and only predicts one machining result -- depth of cut. However, part of the results of the equation have quite a similar tendency as given in this study.

Most of the previous studies focused on the control of the operating parameters, but very few study the effect of material properties. Matsui et. al. [16] made some efforts in such study and constructed the following equations from experiments:

$$A = 10^{4.74}(H \cdot \varepsilon)^{-0.67} \qquad \text{(for ductile materials)} \tag{13}$$

$$A = 10^{4.98}\left((\sigma_u + \sigma_y)\cdot\frac{\varepsilon}{2}\right)^{-0.64} \qquad \text{(for ductile materials)} \tag{14}$$

$$A = 10^{0.91}\left(\frac{\sigma_u^2}{2E}\right)^{-1.97} \qquad \text{(for brittle materials, except stones)} \tag{15}$$

where $A = U \cdot h$: kerf area generation rate (mm^2 / min)

U : traverse rate (mm/min)

h : depth of cut (mm)

H : Vickers hardness (Hv)

ε : elongation (%)

σ_u, σ_y : tensile and yield stress, respectively (MPa)

E : Young's modulus (MPa)

Experiments that have been conducted in the above works show some good correlation between predicted and experimental results, but no exact correlation coefficient was reported. Much more effort is still needed in this aspect.

2.3 Study of the Abrasive Particles Distribution and Destruction in an AWJ

In the course of the formation of a AWJ, the abrasive particles (Fig. 5) are drawn into the nozzle body, being mixed and accelerated by the waterjet. The abrasive particles are hence broken into smaller particles during this process (Fig. 6).

Due to the high turbulence and complicated multi-phase condition in an AWJ, there has been very limited research in the study of the abrasive particles distribution and destruction. The works of Hashish [27] demonstrated that the amount and size of abrasive significantly affect the wear in the focusing tubes. Labus et. al [28] investigated the correlation between the mixing chamber geometry and the change in particles size distribution. This work showed that the typical operating pressure has a specific effect on altering particles size distribution. Works of Mazurkiewicz et. al [29] established that 70% to 80% of the abrasive particles are disintegrated during the ejection process. This determines the need for a high concentration of abrasive particles over a narrow base to ensure an effective cutting jet. The later work of Simpson [30] showed that as the pressure is increased, the abrasive particles size distribution shifts towards a greater percentage of smaller particles due to disintegration. Larger particles are more easily susceptible to the destruction. Depending on pressure, up to 50% of the initial abrasive particles are disintegrated. More recently, Yang [31] examined the effect of the nozzles' diameter, original abrasive size, water pressure, and abrasive flow rate on the condition of particles destruction by collecting abrasive particles in the AWJ ejected into a barrel with half full of plain water. It was concluded that the particles' size distribution after mixing depends on available force of the waterjet, available space of mixing, and number of particles involved.

Figure 5 Abrasive Particles Before Destruction

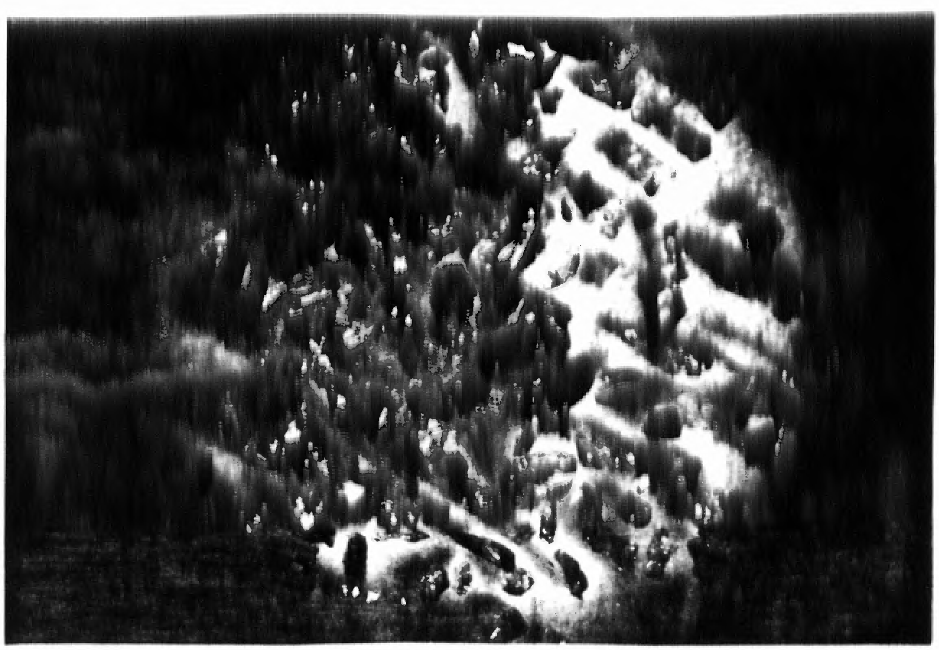

Figure 6. Abrasive Particles After Destruction

The results drawn from the works discussed prior give the tendency of effect of different operating parameters on the particles distribution and destruction. However, they are still far from the exact quantitative description which is necessary for turning the mathematical modeling in Section 2.2 into practical usage.

2.4 Study of the Velocity of Abrasive Particles in the AWJ

The motion of particles entrained in a stream of fluid has been investigated in connection with a variety of industrial applications. Several equations have been proposed for particles entrained in a laminar flow. The forms of these equations depends on the forces considered in a particular study. Finnie [32] employed an equation governing the motion of a particle subjected to the drag force. This equation has the form:

$$\frac{4}{3}\pi \cdot r^3 \cdot \rho_P \cdot \frac{dv}{dt} = \frac{Cd}{2} \cdot \rho_A \cdot \pi \cdot r^2 \cdot (U - V)^2 \tag{12}$$

where r : particle radius

V : particle velocity

ρ_P : particle density

U : air velocity

ρ_a : air density

Cd : drag coefficient

The motion of particles in a turbulent flow is discussed in [33] and in some other studies. Hjelmfelt and Mockros [34] derived an equation of the motion of particles and discussed the particle response to the oscillatory motion of the carrying fluid. As a result of their work, the following equation was proposed:

$$\begin{aligned}\frac{\pi d^3}{6} \cdot \rho_p \cdot \frac{dU_p}{dt} = 3\pi \cdot \mu \cdot \rho_p \cdot d \cdot (U_f - U_p) + \frac{\pi d^3}{6} \cdot \rho_f \cdot \frac{dU_f}{dt} + \frac{1}{2} \cdot \frac{\pi d^3}{6} \cdot \rho_f \cdot \left(\frac{dU_f}{dt} - \frac{dU_p}{dt}\right) \\ + \frac{3}{2} \cdot d^2 \cdot \sqrt{\pi \cdot \rho_f \cdot \mu} \cdot \int_{t_0}^{t} dt' \cdot \frac{(dU_f / dt') - (dU_p / dt')}{t - t'} + Fe\end{aligned} \tag{13}$$

Here

t is the starting time

the index f refers to the fluid

the index p refers to the particle

U is the velocity

d is the particle diameter

ρ is the density

Fe is an external force

A numerical solution of this equation at various initial and boundary conditions is given in [35-40].

Despite the intensive study of the motion of particles entrained in a fluid stream for different engineering applications, the information about the motion of particles in the AWJ are limited. Particularly, there is no direct determination of particle velocity. Due to the high turbulence and the multi-phase condition in AWJ, the conventional probe instruments cannot be applied to measure the velocity of the flow. The non-intrusive instruments hence have been considered and utilized for the AWJ velocity measurement.

An experimental technique for estimation of the particle velocities has been developed by Swanson[41]. In his experiment conventional garnet sand mixed with steel particles of comparable size are entrained by the waterjet and the resulting mixture is directed through a pair of current-carrying coils spaced 1.2" apart. The particle velocity is determined by the measurement of the time between the signals induced by the steel particles entrained in the AWJ. This technique, however, allows us to measure only the mean velocity of a particle traveling through a considerably long distance, compared to the jet diameter which is only 0.05". Also, in this method, since the coil encloses the jet completely, the obtained velocity may represent the velocity of a particle on the periphery of the jet. Moreover, the obtained velocity is the velocity of the added steel particles, rather than the actual abrasive particles used for cutting.

An optical instrument, laser velocimeter has also been applied for this non-intrusive measurement purpose. In general, there two different types of laser velocimeter, Laser Transit Anemometer (LTA) and Laser Doppler Anemometer (LDA), based on the difference of their operational principles. The LTA had been employed in AWJ technology to measure the velocity of abrasive particles. In LTA, there is a unique lens system that splits a single incoming laser beam into two equal intensity beams and focuses the beams into a small region called measurement volume as shown in Fig. 7.

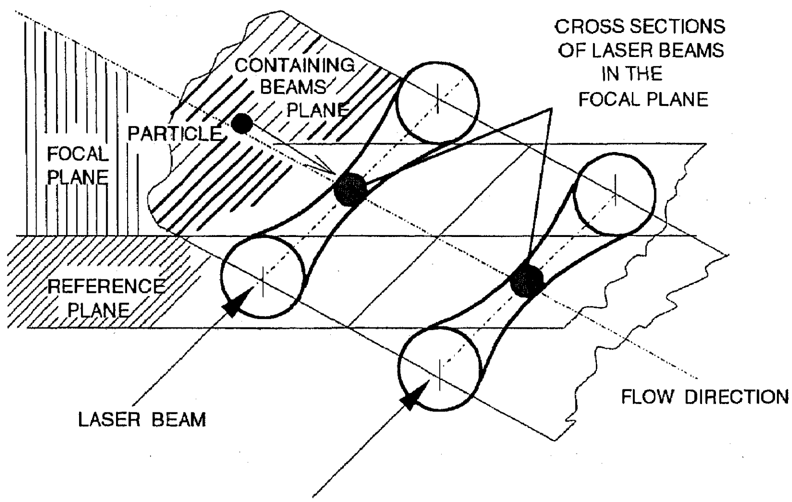

Figure 7 Working Concept of the LTA.

Thus, a particle passing through the focal point of either of these split beams generates a scattering light of high intensity. A sensor is designed to collect these scattering lights and turn them into analog signals to be processed later in the processing unit. With a knowledge of the distance between the two foci and the time taken for a particle to travel through these two focal points, it is possible to calculate the velocity of the particle. Chen [42] used LTA to measure the velocity of the waterjet and the velocity of abrasive particles in AWJ up to 345 MPa of water pressure. A regression equation which correlated the results of velocity measurement with the operating parameters has been constructed. This regression equation has a form :

$$\frac{V_{c.w.} - V_a}{V_{s.w.}} = 0.627 \cdot \left(\frac{Q_a}{Q_w} \right)^{2.557 \cdot (D_o / D_t)^2} \tag{14}$$

where Va : velocity of abrasive particles

Vc.w. : velocity of pure water jet at the exit of focusing tube

Vs.w. : velocity of pure water jet at the exit of water nozzle

Qa : volume flow rate of abrasive particles

Qw : volume flow rate of water

Do : diameter of water nozzle

Dt : diameter of focusing tube

A similar work also has been conducted by Himmelreich and Riess [43] by the use of a Laser-2-Focus method which has the same mechanism as LTA. The measurement was focused on water pressure up to 100 MPa. The results suggested the same tendency as of Chen's, but no regression equation has been derived.

It seems that the technology of laser velocimeter offers quite a potential tool for the study of AWJ fluid dynamics; but constrained by the low signal-to-noise ratio in such a high turbulence and complicated multi-phase flow. This instrument can only be used for investigating a velocity range. When trying to calculate the available kinetic energy of abrasive particles to relate the machining results, this information of velocity range is obviously not enough. Moreover, the laser velocimeter is not readily available for the AWJ industries and the accuracy dramatically depends on the condition of setup.

2.5 Comments on the Previous Studies

1. The theoretical study or mathematical modeling on the AWJ machining mechanism is still far from the practical application without complete information of particles distribution, destruction, and velocity.

2. The condition of particles distribution and destruction in an AWJ has only been evaluated in a less quantitative level.

3. The study of particles velocity offers the information of a range of velocity distribution but is not enough for machining process control.

4. The effort of development of prediction technique for AWJ machining results is not adequate for practical use.

5. The semiempirical method is a economic and efficient way for constructing the prediction equations.

CHAPTER 3
A MODEL FOR PREDICTION OF DEPTH OF CUT

From the discussion in Chapter 2, it follows that the existing mathematical models of AWJ machining process at microscopic level are not sufficient. Empirical methods, under this situation, are to be a more direct way for development of prediction technique in AWJ machining process. Absolute empirical methods, on the other hand, is uneconomic. To get a balance, a semiempirical method was employed in this study. It started from generating a simple model on a macroscopic level with some fundamental assumptions and then modifying the model through a series of designed experiments. In this chapter, the simple model construction is discussed.

Consider the cutting process as shown in Fig. 8, the material removal does not happen until the jet impacts on the workpiece.

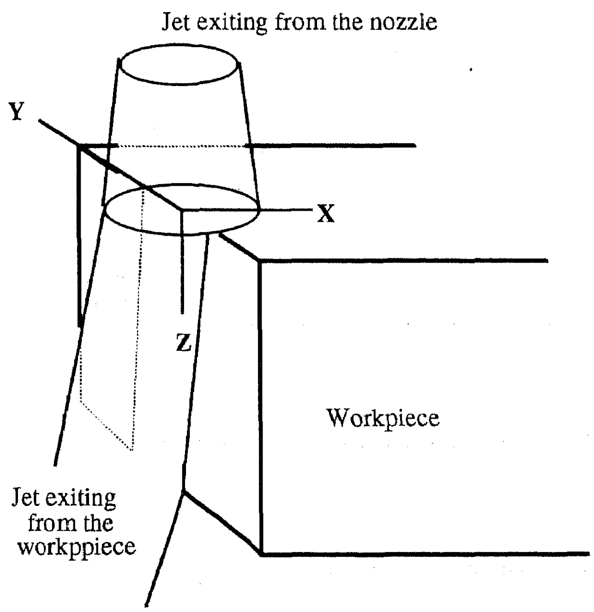

Figure 8 Schematic of AWJ Cutting Process

The geometry of the impingement zone is shown in Fig. 9 in which the jet is moving on the x direction with a traverse speed U. As it follows from this figure,

$$\overline{AB} = \overline{CD} = \overline{OD} - \overline{OC}$$

thus, $\overline{AB} = (\sqrt{r^2 - y^2}) - x$

The length of $\overline{AB}$ represents the portion of the jet swept through point A from time 0 to time t.

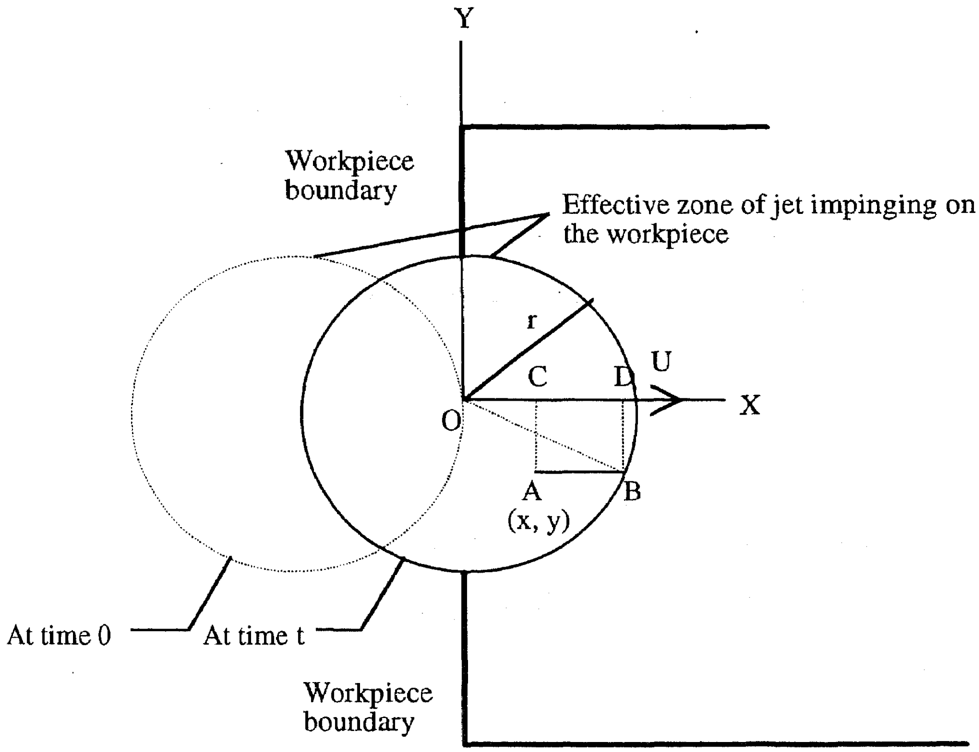

Figure 9 Effective Zone of AWJ for Material Removal.

Let us assume that the abrasive particles in the jet are uniformly distributed so that the amount of particles N impinging at a unit of area in a unit time can be expressed as:

$$N = \frac{Ma}{\pi \cdot r^2 \cdot 60} \tag{15}$$

where Ma is the abrasive flow rate mixed in the jet in g/min and N is in g/(sec·mm²).

The total amount of particles impinging at point A after time t is N·t.

$$N \cdot t = N \cdot \frac{\overline{AB}}{U \cdot 10} = N \cdot \frac{(\sqrt{r^2 - y^2}) - x}{U \cdot 10} \tag{16}$$

where U is the traverse rate of the jet in cm/min, r is the radius of the effective zone of jet in mm and x and y are in mm.

In considering the available energy of an AWJ to remove material, excluding the potential energy which is too small to be considered, there is kinetic energy of water liquid, bubbles, and abrasive particles. According to the previous experiments, the effect of water liquid and bubbles on the depth of cut can be neglected when compared with the abrasive additives. Assume the depth z at point A in the workpiece impinged by abrasive particles after time t is proportional to the total kinetic energy of particles applied, i.e.

$$z = k \cdot \frac{1}{2}(N \cdot t) \cdot Va^2 = k \cdot \frac{1}{2} \cdot \frac{Ma}{\pi \cdot r^2 \cdot 60} \cdot \frac{\sqrt{r^2 - y^2} - x}{U \cdot 10} \cdot Va^2 \tag{17}$$

where k is a proportionality factor.

As discussed in Chapter 2, the value of Va is not readily available. However, for a first evaluation, we can assume Va is proportional to the waterjet velocity and hence is proportional to the square root of operating pressure. The equation (17) can be rewritten as:

$$z = k \cdot \frac{1}{2} \cdot \frac{Ma}{\pi \cdot r^2 \cdot 60} \cdot \frac{\sqrt{r^2 - y^2} - x}{U \cdot 10} \cdot Po \tag{18}$$

The above equation is valid for points of $\sqrt{x^2 + y^2} \leq r$; when $\sqrt{x^2 + y^2} > r$ or $t \geq 2r/U$ on which the jet is no more impinging, the equation becomes

$$z = k \cdot \frac{1}{2} \frac{Ma}{\pi \cdot r^2 \cdot 60} \cdot \frac{2\sqrt{r^2 - y^2}}{U \cdot 10} \cdot Po \tag{19}$$

The resultant geometry of equations (18) and (19), when the operating parameters are fixed, is shown in Fig. 10.

From the above equations and schema, the phenomena of the dragging backward jet front and the convergent kerf shape from top to bottom during cutting are explained.

The maximal depth of cut (H) will locate at y=0 which is

$$H = k \cdot \frac{Ma \cdot Po}{600\pi \cdot r \cdot U} \tag{20}$$

The above equation is to be used as a first evaluation in the semi-experimental modeling of this study.

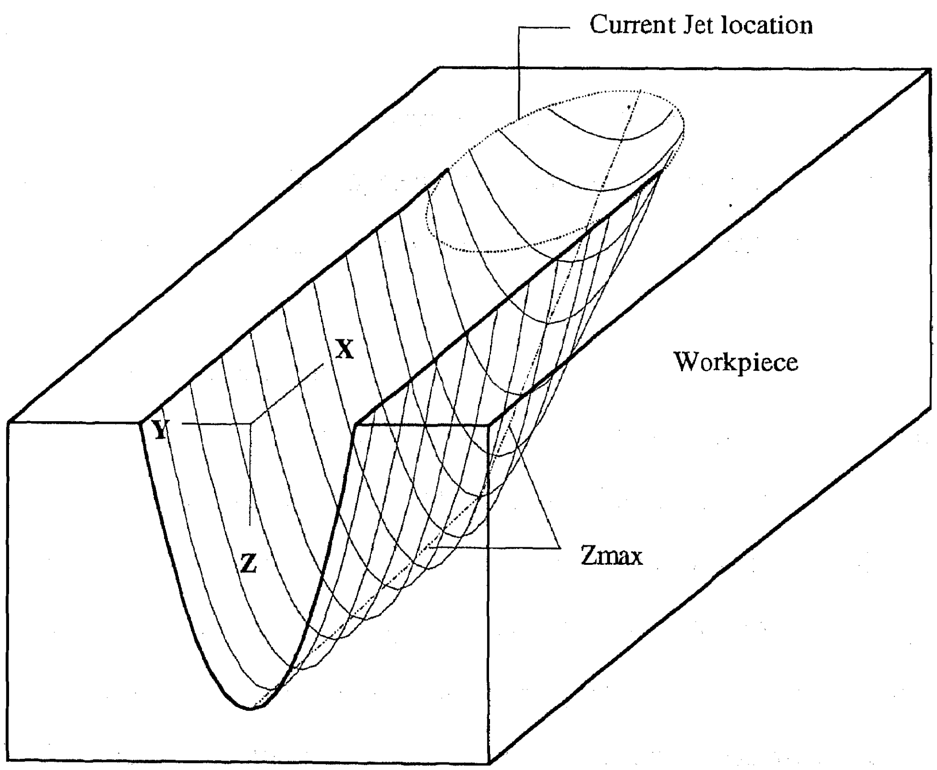

Figure 10 Resultant Kerf Geometry of Equation (18) and (19).

CHAPTER 4.
EXPERIMENTAL PROCEDURE AND APPARATUS

The objectives of performed experiments were the study of the effect of processing parameters of AWJ on the material machining results to construct prediction model. An industrial scale abrasive waterjet cutting system was employed for machining test and a Videometrix was used for machining results measurement. The experimental facilities, samples preparation, the test matrices, the measurement instruments and procedure are described in the following sections.

4.1 Experimental Facilities

The abrasive waterjet cutting system used in this study was manufactured by the Ingersoll-Rand. The system consists of the units (Fig. 11) described below.

4.1.1 Water Preparation Unit

The major components of this unit are the booster pump, filters, water softener, prime mover, intensifier, accumulator, control and safety instrumentation. The major functions of the unit is to continuously feed pure water pressurized to the required pressure. To ensure continuous flow into the high pressure cylinder, the booster pump supplies the water into the low pressure water circuit (180 psi). The iron and calcium compounds contained in the water tend to come out of solution at high pressure and damage the small orifice. In order to remove these compounds, low pressure filters (1-10 microns) and softener are used. This pump also adds polymer additives to the water and blends the water and polymer mixer.

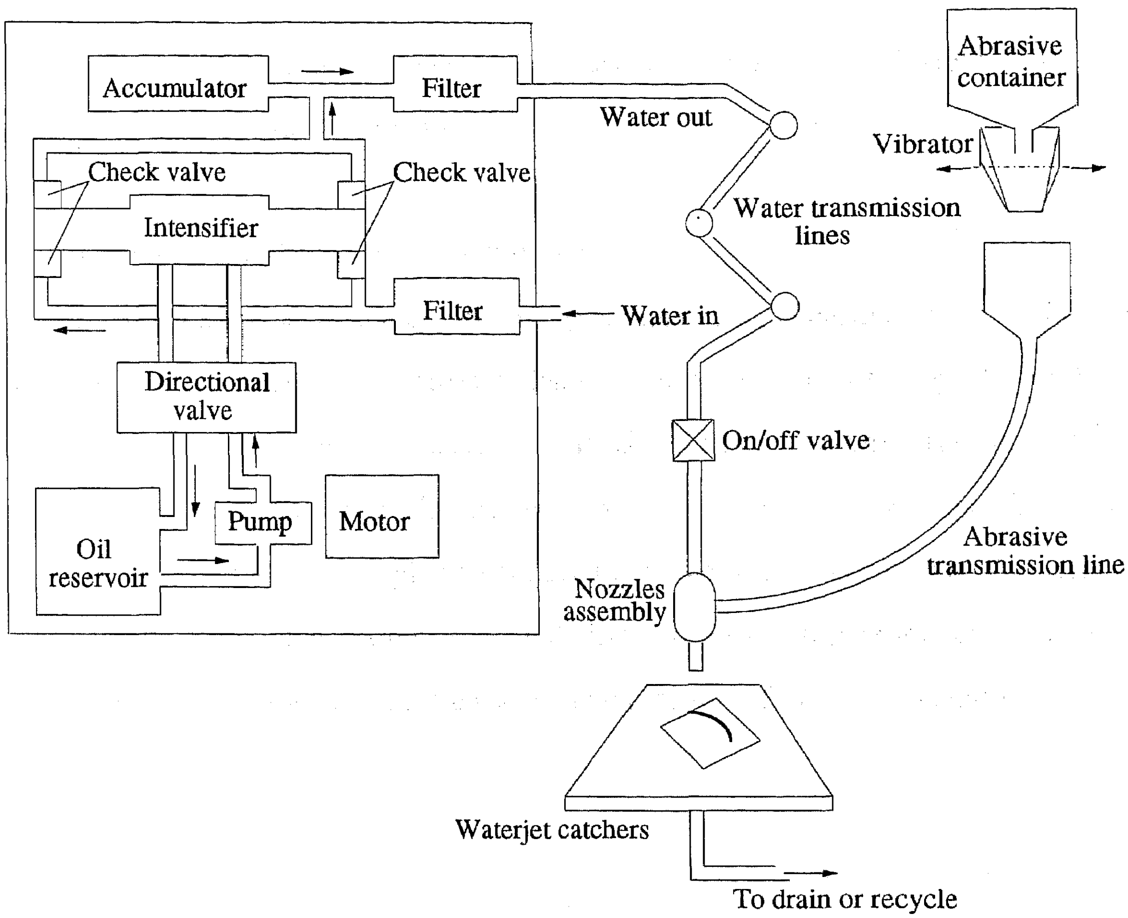

Figure 11 AWJ Machining System

A hydraulic driven (10-40 hp) oil intensifier is the most important part of the system. It develops pressure up to 60,000 psi in the water feed from the booster pump. There are two separate circuits for oil and water. An oil circuit is a closed circuit and water circuit is an open one. The oil pressure of about 3000 psi developed by a rotary pump is used to drive an intensifier. The intensifier is double acting reciprocating (6-inch diameter) type pump. It is operated every few seconds by an adjustable controller.

The high pressure emergency damp valve is a rapid acting two way position valve used to turn the jet ON or OFF in response to control commands. The high pressure water from both sides of the intensifier is discharged to an accumulator where the pressure is stabilized. Since the compressibility of the water at 55,000 psi is 12 percent [44], water is not discharged uniformly from intensifier at all piston position. Thus, it needs the accumulator to provide uniform discharge pressure and flow. The water preparation unit is shown in Fig. 12.

4.1.2 High Pressure Water Distribution System

The output from the accumulator, the high pressure water, is carried away to the work station through a series of hard pipes, swivels, flexible joints, and fittings. Up to 20 ksi, hose can be used to eliminate the need for swivels, which greatly simplifies the pumping. beyond 20 ksi, hard pipes, swivels, flexible joints and fittings must be used. The number of joints, elbows, and the total pipe length determine the line pressure drop. The principal advantage of distribution system is to centralize the water preparation unit for one or more work station, located at different suitable places for different application.

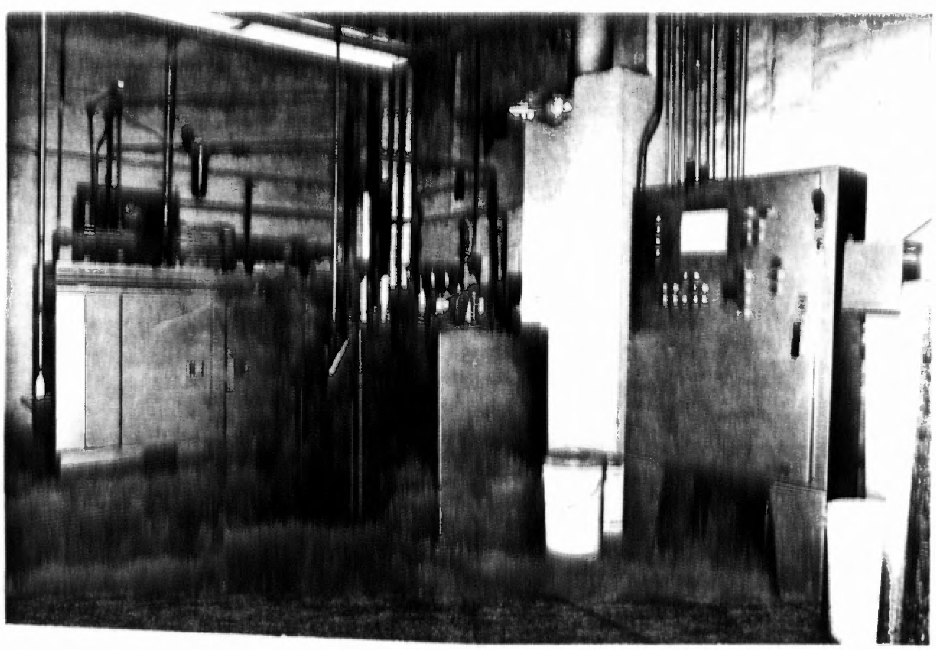

Figure 12 The Water Preparation Unit.

4.1.3 Work Station

It is the place where actual cutting operation is performed. It can be of variety of types and located at different places depending on application. The work station used in this study consists of following major parts.

4.1.3.1 Robotic Work Cell

Shown in Fig. 13 is the gantry CNC 5-axis robotic work cell controlled by the Allen-Bradley 8200R controller (Fig. 14).

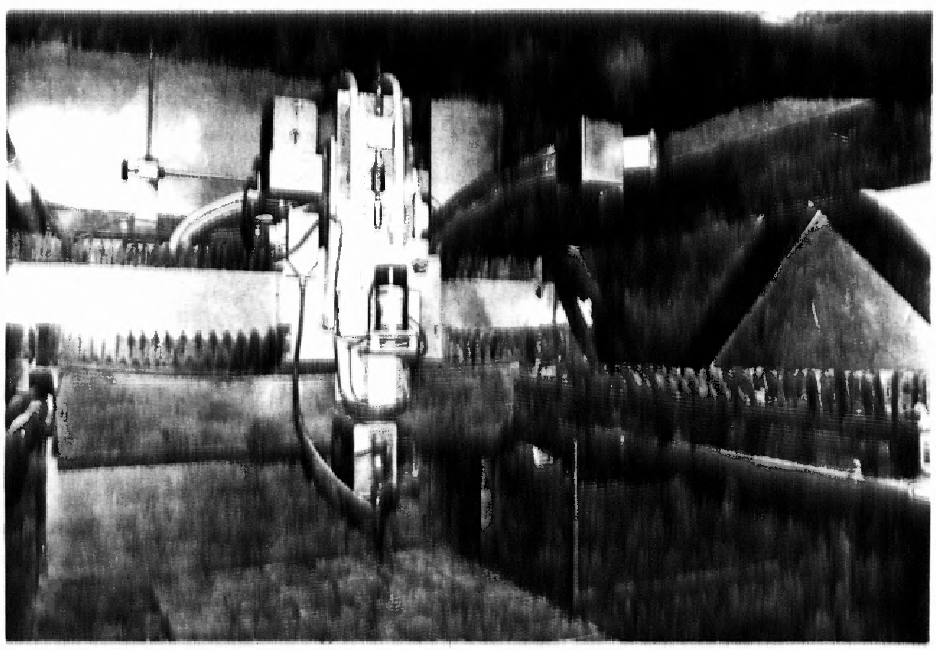

Figure 13 The Gantry CNC 5-axis Robotic Work Cell.

Following is the technical data of the robot.

Table 1 Robot Technical Data

Positioning accuracy	+/- 0.005 inches
Repeatability	+/- 0.005 inches
Working range of linear axes	
Working range of rotary axes	A: 200 degrees, B: 360 degrees
Maximum acceleration	Linear: 75 inches/sec^2 Rotary: 320 deg/sec^2
Maximum velocity	2400 inches/min
Controller resolution	0.0007 inches
Control feedback	Encoders for position Tachometers for velocity
Programmable dwell time	Minimum 0.02 seconds Maximum 320 seconds
X-axis motion driver	Precision ground rack & pinion, driven by 2 inches diameter drive shaft to both sides
Y-axis motion driver	1-1/2 inches diameter precision ground ball screw of 1.875 inches pitch
Z-axis motion driver	1 inch diameter precision ground ball screw of 1 inch pitch
Motor shieve ratios	X-axis 3:1 Y-axis 2:1 Z-axis 1.375:1 A-axis 3:1 B-axis 1:1
Null offset multipliers	X-axis 0.001047198 inches/count Y-axis 0.00062500 inches/count Z-axis 0.00048889 inches/count A-axis 0.01 degrees/count B-axis 0.01 degrees/count

The robot controller consisting of the following standard features.

- Simultaneous continuous path control of all axes
- Linear interpolation
- Circular interpolation
- Digital readout for all axes
- Incremental feed for all axes

- Jog control for all axes
- Inch/metric switchable input
- Absolute/incremental input
- Manual data input
- Sequence number search/display
- Feedrate override
- Edit lookout
- Multiple part storage and edit
- Memory retention during power outage
- Dry run function
- Tool life timer

Figure 14 The Allen-Bradley 8200R Controller.

The controller is capable of receiving input from keyboard entry, punched tape, and/or magnetic tape in accordance with EIA standards RS-232, 244, 358 and 274. Standard G, F and M codes are utilized.

4.1.3.2 Abrasive Feeder

In the abrasive feeding system (Fig. 15), the bulk abrasive is stored in a larger hopper whose exit is located on an electronically controlled vibrating tray. Through the control of the amplitude of vibration, the tray meters the flow of abrasive to a catch hopper. It is then aspirated through a short section of a flexible tube into the mixing chamber of the nozzle body.

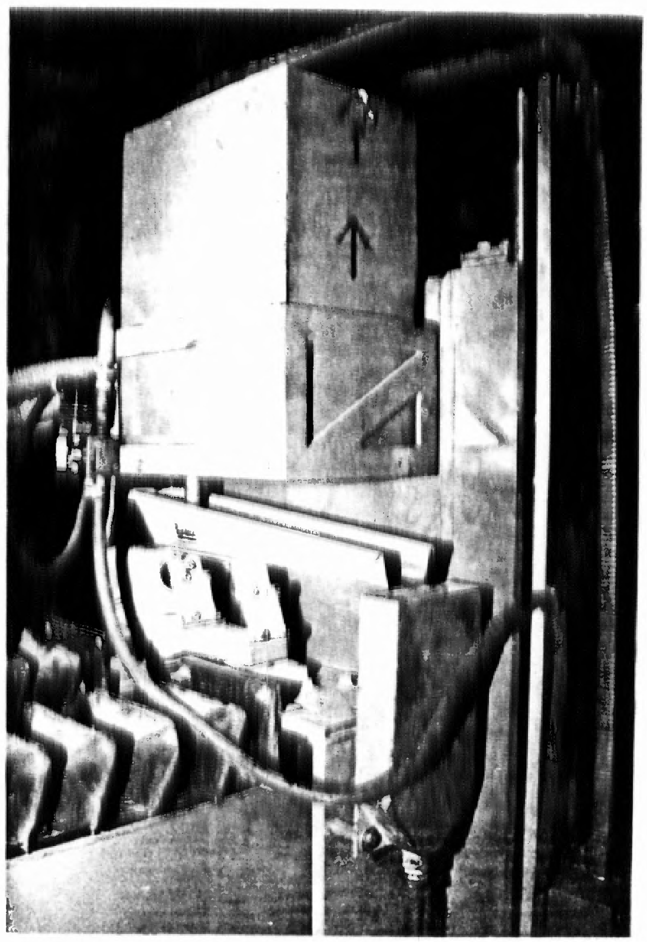

Figure 15 Abrasive Feeder.

4.1.3.3 Catcher System

The catcher tank (Fig. 16) installed below the suspended cutting head collects the spent abrasive, the water and the cutting debris, which settle to the bottom of the tank. The size of the tank enables us to contain the noise of the high pressure jet. A drain near the base of the catcher tank is provided. Through the drain, the water and the abrasive flow into a settlement tank where the water drains out and the abrasive grit settles down. The grit is disposed of periodically from the tank.

Figure 16 Catcher System.

4.2 Measurement Instrument

A Matrix Videometrix Econoscope (hereafter called Econoscope) is used for the measurement of experimental results such as depth of cut and width of kerf. This instrument is a fully automatic, 3-D video inspection system. It uses noncontact technique to provide rapid dimensional verification of complete parts or specified features of a part.

The Econoscope comprises a General Purpose Computer, a 3-axis Positioning Control System, a Digital Image Processor and Part Monitor Section as shown in Fig. 17. Specifically designed to be easy for use, the Econoscope operates at a high speed, producing very accurate (with resolution up to 0.1 micron) and repeatable results. The software is menu/prompt driven so the operator need not learn cumbersome computer language.

Figure 17 The Matrix Videometrix Econoscope

4.3 Experimental Procedures

The experimental cutting and grooving were carried out in the Ingersoll-Rand 5-axis robotic workcell equipped with the intensifier "Streamline". The whole processes of machining experiments were conducted under the following prudential considerations:

1) The workcell was always in normal conditions during experiments.
2) All experiments were carried out by one person who was well trained to operate the workcell.
3) Experimental setups were in the similar conditions in the whole experiments.
4) Measurement instruments were always fine tuned in normal conditions.
5) Measurements were conducted by the same person who carried out the experiments so that the experimental results were collected in the consistent situation.

The following will be the step-by-step experimental procedures.

4.3.1 Samples Preparation

In the course of experiments the samples of steel AISI 1018, aluminum Al 6061-T6 and titanium Gr-2 have been used. The chemical compositions and mechanical properties of these materials are listed in Table 2 and 3, respectively.

Table 2 Chemical Compositions of Experimental Materials

Material	Compositions					
Al 6061-T6	% Mg 1.0	% Si 0.6	% Cr 0.2	% Cu 0.27	% Al 97.93	
AISI 1018	% C 0.15-0.2	% Mn 0.6-0.9	% P 0.4	% S 0.05max	% Fe remainder	
Ti Gr2	% N 0.03	% C 0.1max	% H_2 0.015max	% Fe 0.3max	% O_2 0.25max	% Ti remainder

Table 3 Mechanical Properties of Experimental Materials.

Material	Tensile Strength (MPa)	Yield Strength (MPa)	Elongation (% in 2 in.)	Vickers Hardness (HV)
Al 6061-T6	310	275	12	111
AISI 1018	450	380	16	131
Ti Gr2	345	275	20	

In order to find the maximal depth of cut at different operating parameters, the steel and aluminum samples have been prepared as wedge blocks (Fig. 18, 19).

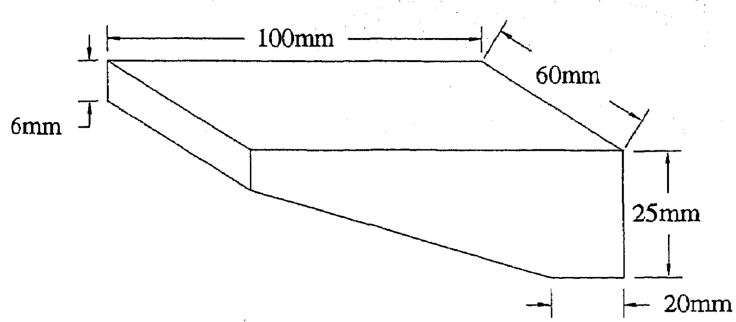

Figure 18 Schematic of the Sample for Cutting Experiment.

4.3.2 Machining Experiments Setup

The prepared samples are firmly held by a vise for cutting experiments as shown in Fig. 20-21. Grooving experiments are conducted also in order to develop prediction technique for non-through cutting (milling) condition. For titanium and other hard-to-machined materials grooving is the only practical technique for this study.

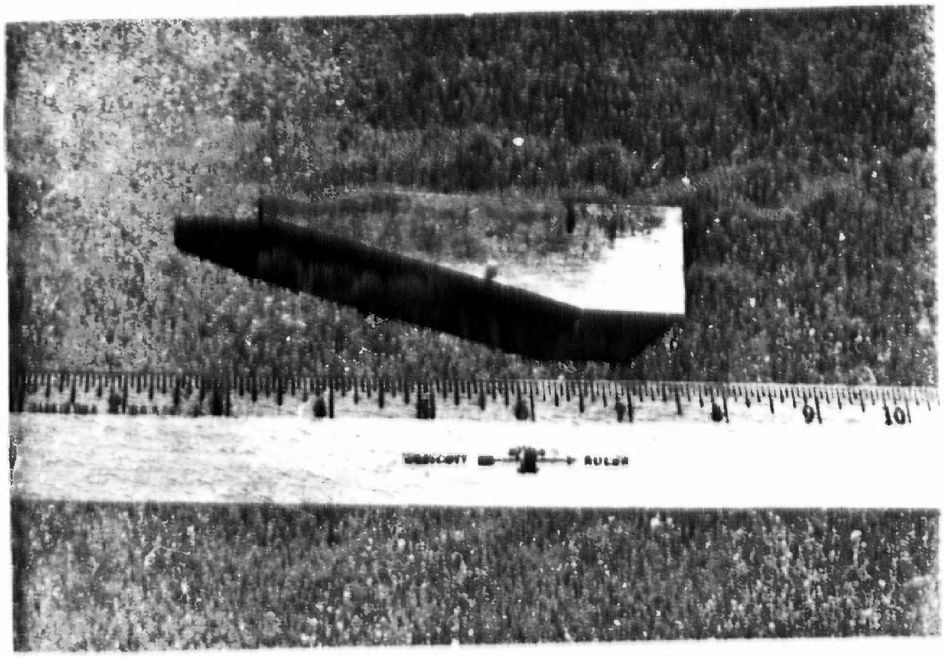

Figure 19 Photograph of the Sample for Cutting Experiment.

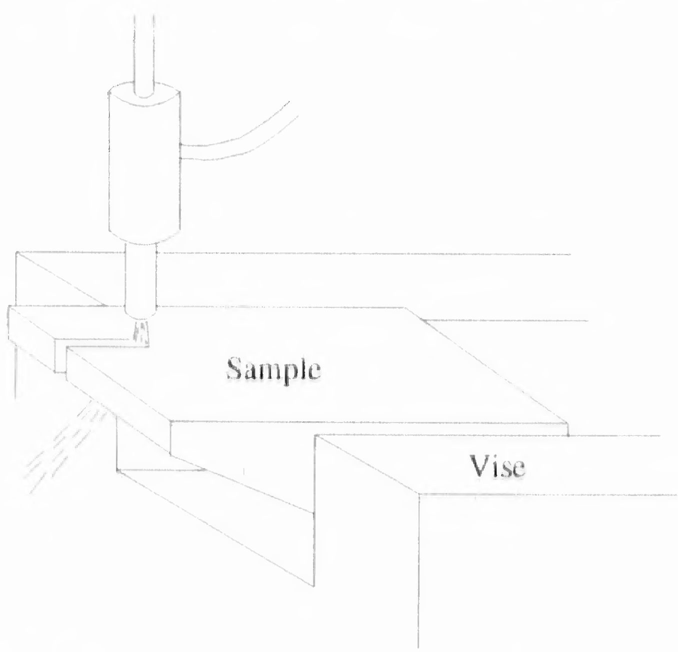

Figure 20 Schematic of Experimental Setup.

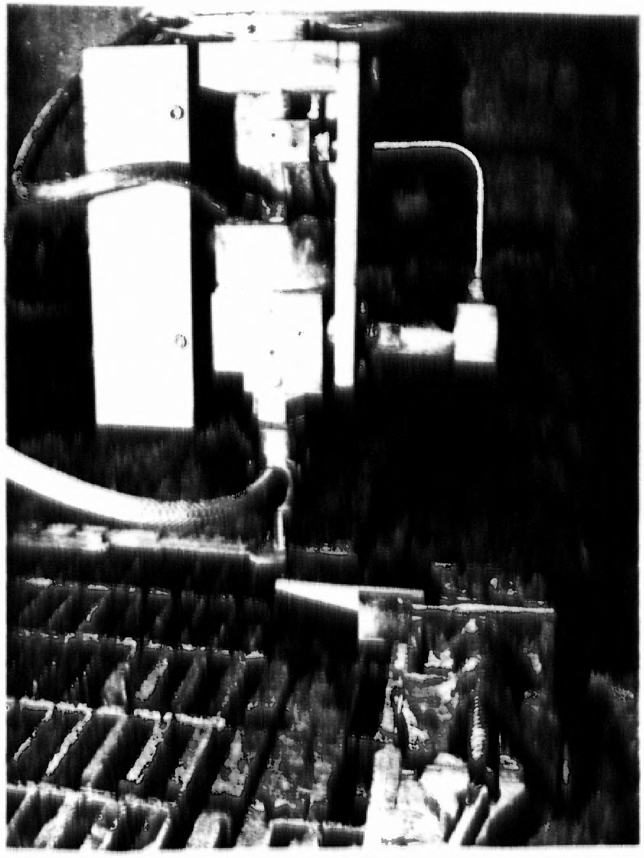

Figure 21 Photograph of Experimental Setup.

4.3.3 Calibration of the Abrasive Flow Rate

The garnet sands manufactured by the Barton Company has been employed as the abrasive particles in this study. The properties and size distribution of the abrasive particles are listed in Table 4.

As mentioned in the section 4.1.3.2, the abrasive flow rate is controlled by the change of amplitude of a vibrator. There is a tray attached to the vibrator to transport the abrasive particles from the bulk tank to the flexible hose as shown in Fig. 15. In order to get an accurate abrasive flow rate for the experiments, the abrasive particles accumulated on the tray are flowed out and replaced with the new particles of the expected flow rate. This process was carried out each time a new value of vibrator switch was set to change the current abrasive flow rate. The calibration of abrasive flow rate was then conducted by collecting and weighing the abrasive particles flowed out in one minute.

Table 4 Properties and Size Distribution of Abrasive Particles

Abrasive Material: Garnet, Density: 3.9-4.0 g/cm³, Hardness: 800-1000 HV					
Abrasive Size Distribution					
Tyler Mesh Size (#)	Sieve Opening (microns)	Percent Retained (%)			
		#50 HP	#80 HP	#120 HP	#220 HP
28	600	0.6			
32	500	0.8			
35	425	4.3			
42	355	21.8	0.6		
48	300	41.2	8.1		
60	250	26.7	19.8		
65	212	4.1	22.1		
80	180		26.8	14.2	
100	150		16.1	20.1	
115	125		4.6	34.2	5.5
150	106			19.7	25.7
170	90			8.0	27.9
200	75			2.4	14.4
250	63			1.4	6.6
270	53				7.3

4.3.4 Starting the Machining Experiments

Cutting or grooving experiments are conducted by straight traversing the jet on the workpiece. The stand off distance between the nozzle and the workpiece is always checked and maintained at 2.5 mm height. There are 4 mm intervals consistently between each cutting or grooving path as shown in Fig. 22.

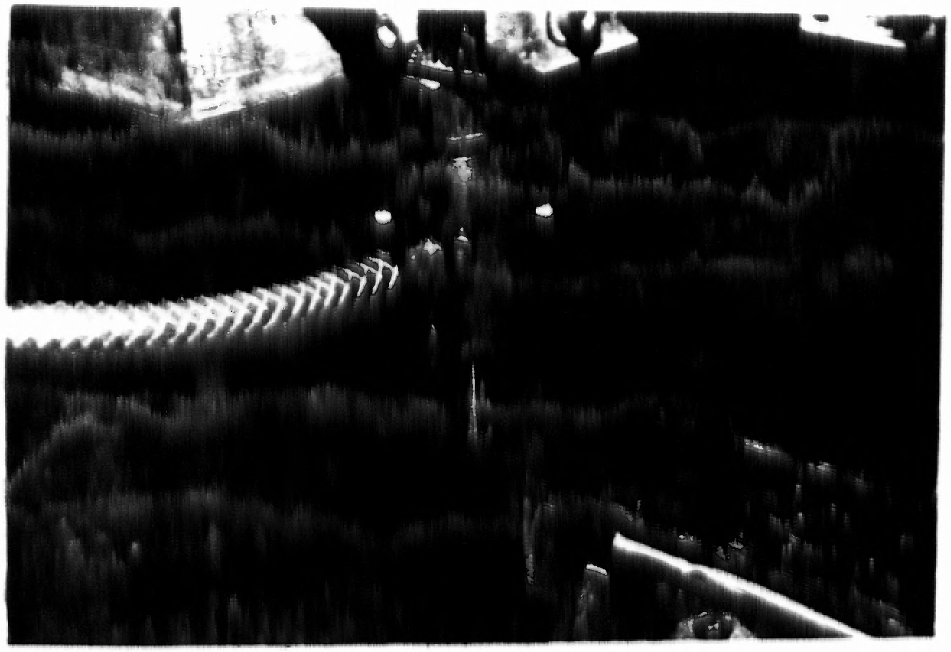

Figure 22 Experimental Setup After Cutting.

4.3.5 Measurement of the Experimental Results

The measured results of cutting experiments include depth of cut, top kerf width and bottom kerf width (Fig. 23) while the grooving experiments exclude the bottom kerf width only. The existing monitoring technique (Econoscope) is used for the measurement of the kerf geometry (Fig. 24). For the consistent bases of experimental results, the top kerf width and bottom kerf width are measured at the depth of 8 mm (Fig. 25).

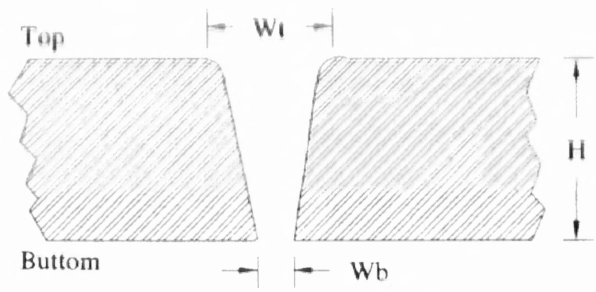

Figure 23 Schematic of Kerf Geometry.

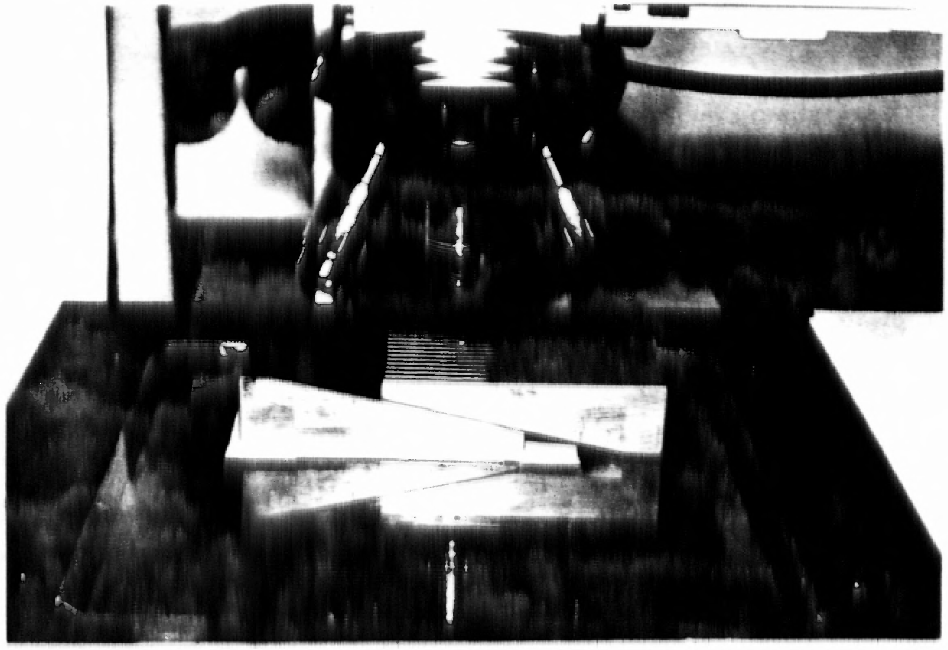

Figure 24 Experimental Results Measurement Setup

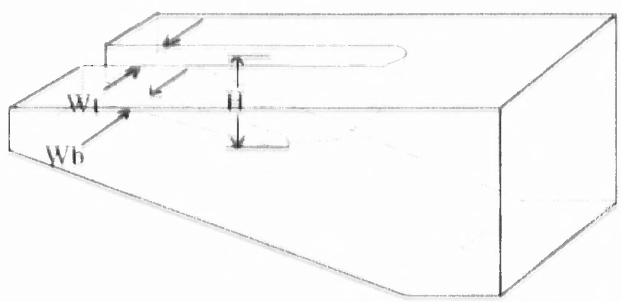

Figure 25 Location of Kerf Width Measurement

The taper of kerf is calculated by following equation.

$$Tp = Tan^{-1}\left(\frac{Wt - Wb}{16}\right) \tag{21}$$

where Tp is the taper of kerf in degrees, Wt and Wb are the top and bottom kerf width, respectively.

In this equation the kerf shape is considered as convergent. The validity of this geometry is demonstrated in [17].

In the cutting experiments, all the kerf geometry includes depth of cut, top kerf width, bottom kerf width as well as kerf taper can be readily measured under the Econoscope. While in the grooving experiments, the kerf geometry is described in depth of cut and top kerf width only. The depth of cut in the grooving experiments is measured by averaging six points on the bottom of kerf as shown in Fig. 26.

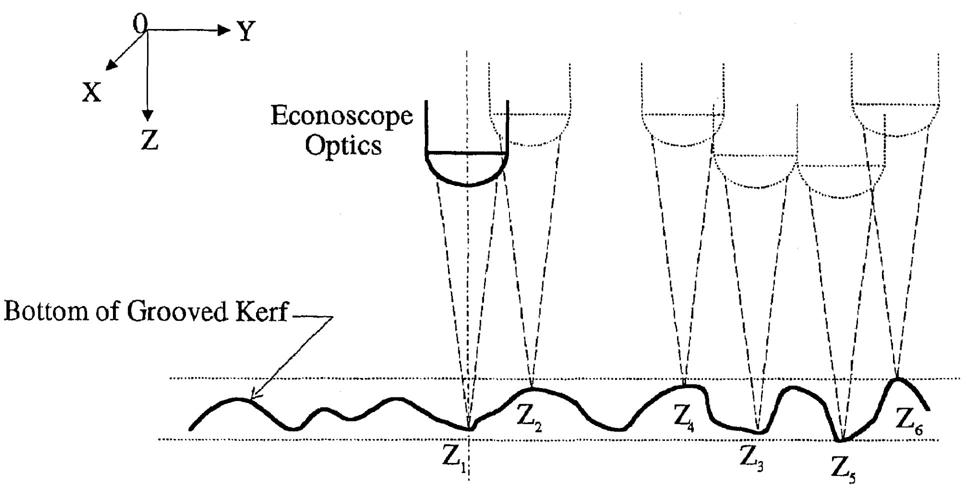

$$H_{min} = (Z_2 + Z_4 + Z_6) / 3$$
$$H_{max} = (Z_1 + Z_3 + Z_5) / 3$$
$$H = (H_{max} + H_{min}) / 2$$

Figure 26 Measurement of the Depth of Cut in the Grooving Experiments

CHAPTER 5
RESULTS AND DISCUSSION

In total 1000 experimental cutting and 100 experimental grooving are carried out in a wide range of process variables (Table 5) on three different ductile materials. The results of these experiments enable us to identify the effect of the following process variables on the kerf geometry.

TABLE 5 Range of Operating Parameters in the Course of Experiments.

Operating Parameters	Notation	Empirical Range
Operating pressure	Po	103 - 338 MPa
Water nozzle diameter	Do	0.1778, 0.2286, 0.254, 0.3048 & 0.3556 mm
Focusing tube diameter	Dt	0.838, 1.092 & 1.6 mm
Abrasive size	Sa	65, 125, 177 & 300 μm
Abrasive flow rate	Ma	40 - 360 g/min
Traverse speed	U	6 - 60 cm/min
Stand-off distance	Sd	1 - 12.5 mm

5.1 Effect of Traverse rate (Fig. 27 - 30)

The depth of cut is inversely proportional to the traverse rate (Fig. 27, 28) which prove the validity of the equation (20). Similar experimental results of the linearity between H and 1/U is presented in [13, 15]. Wt does not depend on U (Fig. 29, 30). According to our phenomenological model this width depends on the diameter of the flow containing fast active particles. The slow particles distributed at the jet periphery do not remove materials. Wb, and consequently, Tp are inversely proportional to U (Fig. 29, 30). This effect is due to energy dissipation in the slurry flow which effects mostly peripheral particles and, thus, reduces the width of flow penetrating into the material.

5.2 Effect of Abrasive flow rate (Fig. 31 - 34)

The relationship between H and Ma is shown in Fig. 31 and 32. This form of correlation is also suggested in [15]. It is assumed that material removal is actually carried out only by "fast" particles. The fraction of particles sufficiently accelerated by the water stream is reduced as the total amount of particles increases. Beyond a specific level, farther increase in the abrasive flow rate does not effect machining results. Regression analysis by the use of second order polynomials has been carried out on the region before "saturation". The results are listed in Table 6. Such results do not agree with the equation (20). The first model, hence, needs to be modified.

Since the abrasive flow rate also effects the active cross section of the slurry flow, it can be seen (Fig. 33, 34) that Wt increases linearly with increase of Ma. No clear correlation between Wb, Tp and Ma was observed.

5.3 Effect of Water pressure (Fig. 35 - 38)

From the Bernoulli equation it follows that the kinetic energy of a particle is proportional to the water pressure. Thus, it is expected that the depth of cut is directly proportional to P (Fig. 35, 36) which agrees with the equation (20). Similar experimental results are reported in [13, 27]. There is, however, the threshold pressure which is determined by the minimum required energy for material destruction. In the experiments of this study, no correlation between the threshold pressure and standard strength characteristics of a metal is determined.

No effect of the water pressure on kerf width is found. Most probably, the accelerated particles are concentrated in the inner part of the jet (Fig. 37, 38).

Table 6 Results of Regression Analysis Between Depth of Cut and Abrasive Flow Rate

Regression Equation: $H = C_1 \cdot Ma + C_2 \cdot Ma^2$						
Material	Operating Parameters	C_1	C_2	Corr. Coeff.	Critical Ma (g/min)	Maximal H (mm)
Steel	Po=317MPa, Do=0.254mm, Dt=0.838mm, Sa=177μm, U=14cm/min	0.110233	-0.00017	0.9945	324	17.87
Steel	Po=331MPa, Do=0.1778mm, Dt=0.838mm, Sa=177μm, U=14cm/min	0.088284	-0.00018	0.9957	245	10.82
Steel	Po=197MPa, Do=0.1778mm, Dt=0.838mm, Sa=177μm, U=10cm/min	0.037318	-0.00006	0.9957	311	5.8
Aluminum	Po=317MPa, Do=0.254mm, Dt=0.838mm, Sa=177μm, U=32cm/min	0.130299	-0.00022	0.9849	296	19,29
Titanium	Po=317MPa, Do=0.254mm, Dt=0.838mm, Sa=177μm, U=14cm/min	0.163863	-0.00036	0.9953	317	18.65

5.4 Effect of Stand-off Distance (Fig. 39, 40)

It has been found that for the experiment conditions the depth of cut can be approximated by a function inversely proportional to the stand off distance (Fig. 39). But when compared with other parameters, the influence of stand-off distance can be neglected for most practical cutting situations in which the stand-off distance is maintained within a range of a little variance in which the energy dissipation of the jet due to the friction between the air and the jet is neglectable small. Due to the jet divergence, the top width of the kerf is directly proportional to the stand-off distance (Fig. 40). No correlation between Sd and Wb has been found.

5.5 Effect of Nozzle diameter (Fig. 41, 42)

Because the slurry jet is formed by two nozzles, the available energy, and thus, the penetrative ability of the jet depends on the ratio of the nozzles diameters (Fig. 41). The similar results are given in [45, 46].

The top kerf width is directly proportional to the diameter of the focusing tube (Fig. 42) because this tube determines the diameter of the slurry flow.

5.6 Effect of Cutting and Grooving (Fig. 43)

Figure shows that the results obtained for non-through cut can be used for the prediction of the maximal depth of cutting.

5.7 Effect of Material Properties (Fig. 44, 45)

Three different ductile materials have been used in this study. Their properties are listed in Table 3. To study the effect of material properties on the machining results, the terms of flow stress $(\sigma_u + \sigma_y)/2$ and fracture energy $(\sigma_u + \sigma_y) \cdot \varepsilon / 2$ in Equation (14) are evaluated as shown in Fig. 44 and 45. It suggests a good correlation between the fracture energy and the depth of cut. The linear regression results are listed in Table 7. Comparing with Equation (14), the results are different. More advanced studies on material properties are required.

Table 7 Results of Regression Analysis Between the Kerf Area Generated Rate and the Material Fracture Energy

Regression Equation: $A = C_1 + C_2 \cdot (\sigma_u + \sigma_y) \cdot \varepsilon / 2$			
Operating Parameters: Po=317MPa, Do=0.254mm, Dt=0.838mm, Sa=177μm,	C_1	C_2	Corr. Coeff.
Ma=100g/min	5819.587	-0.66653	0.9927
Ma=150g/min	7866.365	-0.90778	0.9982
Ma=200g/min	9337.798	-1.08768	0.9999

5.8 Summary of the experimental results

The results of the performed experiments are summarized in Table 8.

TABLE 8 The Effect of Operating Parameters on the Kerf Geometry.

	Po	Do	Dt	Sa	Ma	Sd	U
H	*	*	+	*	*	+	*
Wt	-	-	*	-	+	*	-
Wb, Tp	*	+	+	+	*	*	*

* Strong + Light - No effect

The constructed equations are presented in Table 9.

These equations are integrated into following prediction model:

$$H = A \cdot \frac{Ma^B \cdot (Po - Pth)}{U \cdot Wt} + C \tag{22}$$

$$Wt = a + b \cdot Dt + c \cdot Ma + d \cdot Dt \cdot Ma \tag{23}$$

$$Tp = e + f \cdot U + g \cdot Dt + h \cdot U \cdot Dt \tag{24}$$

where coefficients A, B, C, Pth, a, b, c, d, e, f, g, and h are to be determined from regression analysis.

TABLE 9 Correlation Between the Operating Parameters and the Kerf Geometry.

Element of Kerf Geometry	Operating Parameter	Regression Equations
Depth of cut (H)	Operating pressure (Po)	$H = a \cdot (Po - b)$
	Focusing tube diameter (Dt)	$H = a / Dt$
	Traverse speed (U)	$H = a / U$
	Abrasive flow rate (Ma)	$H = a \cdot Ma^2 + b \cdot Ma$
	Stand-off distance (Sd)	$H = -a \cdot Sd + b$
Top kerf width (Wt)	Focusing tube diameter (Dt)	$Wt = a \cdot Dt + b$
	Abrasive flow rate (Ma)	$Wt = a \cdot Ma + b$
	Stand-off distance (Sd)	$Wt = a \cdot Sd + b$
Taper (Tp)	Traverse speed (U)	$Tp = a \cdot U + b$
	Stand-off distance (Sd)	$Tp = a \cdot Sd + b$
	Focusing tube diameter (Dt)	$Tp = a \cdot Dt + b$

a , b = regression coefficients.

Some results of the application of this model are given in Fig. 46-49. The values of the coefficients A and C are given in Table 10. The accuracy of the prediction by the use of equation (22) is demonstrated in Table 10 by the correlation coefficients between computed and measured values of the cutting depth. The minimal value of these coefficients exceeds 0.9 and the average value exceeds 0.95.

5.9 Dimensional Analysis

The operating parameters involved in equations (22-24) are all dimensional. The value of regression coefficients are to be changed along with the change of different dimensional units employed. This dimensional consideration must be taken into account carefully when apply those prediction equations. Following is some effort to evaluate the possibility of constructing dimensionless group(s) for those variables involved in the equation (22). The approach is suggested by Ipsen [48].

In general consideration, the depth of cut (H) can be affected by the operating pressure (Po), diameter of the water nozzle orifice (Do), diameter of the focusing tube

(Dt), the abrasive flow rate (Ma), and the traverse speed of jet (U). By including all these significant variables in a functional equation, we have

$$H = f\,(Po, Do, Dt, Ma, U).$$

where the basic dimensions $[H] = L$

$$[Po] = F / L^2$$

$$[Do] = L$$

$$[Dt] = L$$

$$[Ma] = F\,T / L$$

$$[U] = L / T$$

There are 6 variables H, Po, Do, Dt, Ma, and U involved and 3 basic dimensions *F, L, T* included in the variables. According to the Buckingham Π theorem [49], the number of independent dimensionless groups of variables needed to correlate the variables in our process is equal to 6-3 which is 3. This prediction will be validated after the following process.

(i) Eliminate *F* as a dimension by combining Po with all variables that have the force dimension in them in such a way that *F* is canceled:

$$H = f_2(Do, Dt, \frac{Ma}{Po}, U)$$

where $[H] = L$

$$[Do] = L$$

$$[Dt] = L$$

$$[\frac{Ma}{Po}] = TL$$

$$[U] = L / T$$

(ii) Eliminate the time dimension *T* by combining U with the remaining groups of variables that include the time dimension:

$$H = f_3(\text{Do}, \text{Dt}, \frac{\text{Ma}}{\text{Po}} \cdot \text{U})$$

where $[\text{H}] = L$

$[\text{Do}] = L$

$[\text{Dt}] = L$

$[\frac{\text{Ma}}{\text{Po}} \cdot \text{U}] = L^2$

(iii) Eliminate the last length dimension by combining Do with the remaining groups of variables:

$$\frac{\text{H}}{\text{Do}} = f_4(\frac{\text{Dt}}{\text{Do}}, \frac{\text{Ma} \cdot \text{U}}{\text{Po} \cdot \text{Do}^2}) \qquad (25)$$

Now there are 3 dimensionless groups of variables left which meet the prediction of the Buckingham Π theorem.

Comparing with the equation (22), it can be seen that the relationship between the three dimensionless groups does not match the tendency of experimental results. When keeping all other parameters fixed, the relationship in equation (25) suggests that the depth of cut (H) has a tendency of ascending with the abrasive flow rate (Ma) and descending with the operating pressure (Po) or vice versa. Such a tendency violates the fact that the depth of cut will be ascending both with abrasive flow rate or operating pressure.

It will need more consideration on the dimensional analysis to construct dimensionless groups of variables in the equation (22). Before acquiring advanced information, the dimensions must be selected consistently in using the equations (22-24) along with the table 10.

TABLE 10 Regression Results of Prediction Equations for the Depth of Cut. (A, B, Pth, C = regression coefficients).

Material	Sa (μm)	Do (mm)	Amount of Data	A	B	Pth (MPa)	C	Corr. Coef.
Steel	300	0.254	48	0.03648	0.6	70	-0.6376	0.909
		0.3048	24	0.03972			-0.0850	0.957
	177	0.1778	30	0.03825			-2.4149	0.982
		0.2286	36	0.04314			-1.5356	0.942
		0.254	300	0.04470			-0.2074	0.965
		0.3048	72	0.05129			-1.6054	0.954
		0.3556	72	0.04901			1.29386	0.948
	125	0.254	12	0.05008			0.04928	0.981
	65	0.254	72	0.02847			1.54696	0.963
		0.3556	72	0.04010			0.46849	0.946
Titanium	177	0.1778	24	0.04156	0.7	60	-.82704	0.985
		0.254	36	0.02170			-0.3343	0.995
Aluminum	300	0.2032	12	0.05425	0.65	63	-0.3738	0.998
		0.254	60	0.07285			-0.6156	0.97
		0.3048	12	0.08547			-0.3373	0.999
	177	0.2032	12	0.06016			-0.7164	0.998
		0.254	60	0.08985			-0.5203	0.967
		0.3048	12	0.10932			-0.1808	0.996
	65	0.254	24	0.08823			-0.9869	0.985
		0.3048	12	0.09336			-0.9869	0.993

5.10 Prediction Technique

Table 10 and Equation (22-24) enables us to develop a practical technique for prediction of the kerf geometry. The suggested procedure of prediction technique consists of the following steps:

5.10.1 Procedure for Prediction of the Depth of Cut

- experimental grooving at variable Ma is carried out to determine B. At least 3 experiments are required and regression between LnH and Ma is sought;

- experimental grooving at variable P to determine Pth is carried out. At least two grooving are required and regression between P and H is sought;

- coefficients A and C are sought as regression coefficients of Equation (22). Results of previous grooving can be used for this analysis.

5.10.2 Procedure for Prediction of the Top Kerf Width

- experimental grooving at variable Dt and Ma. At least four experiments (two variable Dt and two variable Ma) are required.

- coefficients a, b, c and d are sought by doing regression between Wt and Dt and Ma.

5.10.3 Procedure for Prediction of the Taper of Kerf

- experimental cutting at variable U and Dt. At least four experiments (two variable U and two variable Dt) are required.

- coefficients a, b, c and d are sought by doing regression between Tp and U and Dt.

A statistical technique [47] is used at each step to determine the minimal number of experiments.

CHAPTER 6
CONCLUSIONS AND RECOMMENDATIONS

6.1 Concluding Remarks

- The acquired experimental data enable us to evaluate the effect of traverse rate, abrasive size, abrasive flow rate, water pressure, nozzle diameters and stand off distance on the kerf geometry.

- The depth of cut is mainly decided by the available kinetic energy of abrasive particles before impingement.

- The top kerf width is mainly affected by the diameter of jet before impingement.

- The taper as well as bottom kerf width is affected by the energy dissipation during impingement.

- It was found that except for abrasive flow rate, the relation between process conditions and kerf geometry can be approximated by the straight line.

- The simple prediction equations are given. The results are valid for the investigated span of process conditions. These equations, however, provide substantial information for description of the phenomena which take place in the course of AWJ machining in general.

- The prediction technique offers an effective tool for selecting the optimal operating parameters for AWJ machining.

- Dimensional analysis for the prediction equations needs more study.

6.2 Recommendations for Future Studies

To have a complete understanding of the mechanism of AWJ machining, following studies are necessary:

1) The complete knowledge of the effect of material properties on the AWJ machining results.

2) The effect of operating parameters on the destruction and distribution of abrasive particles.

3) The velocity distribution of abrasive particles in the AWJ.

Even lots of special applications of the AWJ had been investigated, the potential of AWJ machining capability is still not clear. One of the reasons is the lack of proper fixture to hold the workpieces without interference with the cutting head. Such a fixture must be rustproof, firm to resist the jet force, tough to avoid wearing and ready for loading and unloading the workpiece. Study on the fixture design is valuable and urgent for the three-dimensional machining.

The working enviroment needs more improvement in noise control and recycling or handling of the waste water and abrasive.

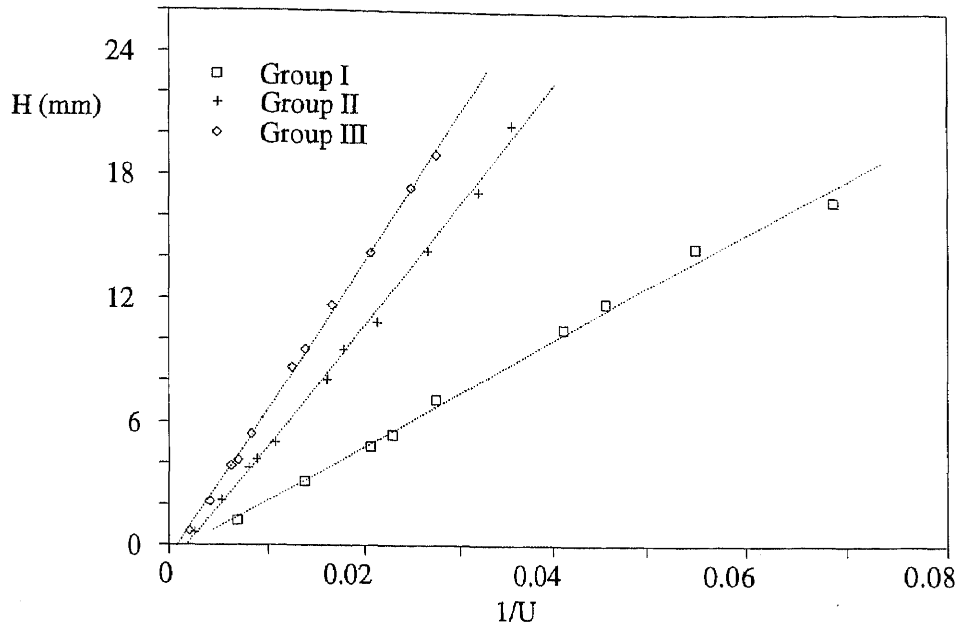

Figure 27 Effec of Traverse Speed on the Depth of Cut.
(Aluminum Al 6061-T6, Po=310MPa, Do=0.254mm, Dt=0.838mm;
Group I: Ma=86g/min; Group II: Ma=221g/min; Group III: Ma=286g/min)

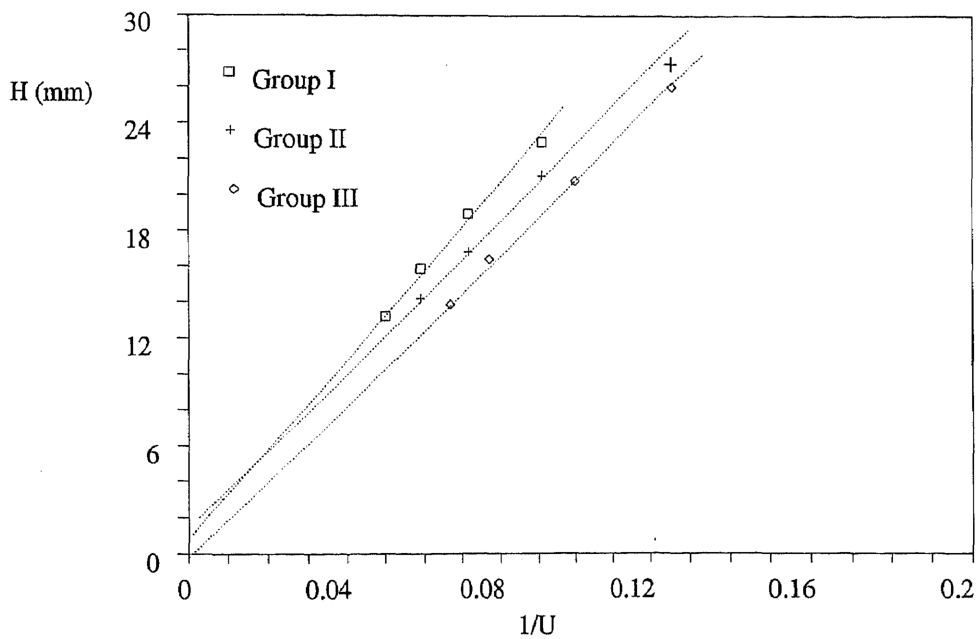

Figure 28 Effec of Traverse Speed on the Depth of Cut.
(Steel AISI1018, Pi=345MPa, Sa=177μm; Group I: Do=0.254mm, Dt=0.838mm, Ma=256g/min;
Group II: Do=0.305mm, Dt=0.838mm, Ma=212g/min; Group III: Do=0.356mm, Dt=1.092mm,
Ma=280g/min)

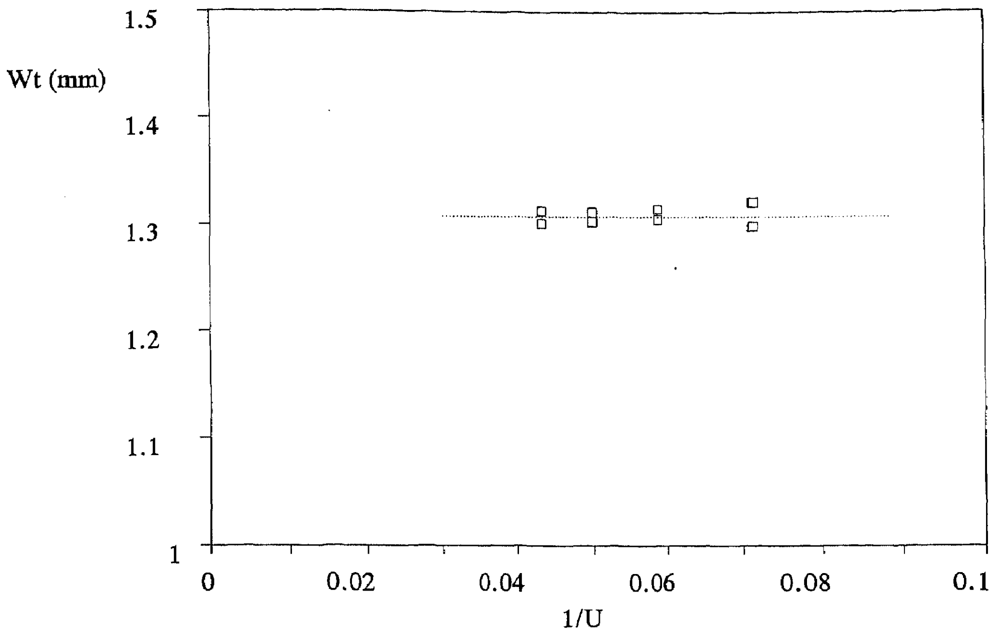

Figure 29 Effect of Traverse Speed on the Top Kerf Width.
(Titanium Ti Gr-2, Po=310MPa, Do=0.254mm, Dt=0.838mm, Ma=162g/min)

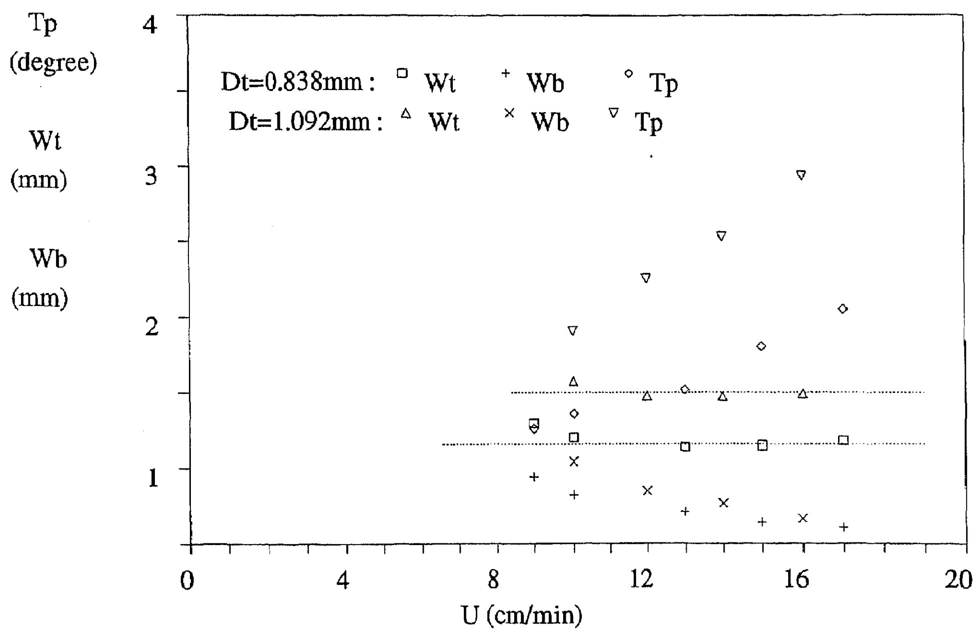

Figure 30 Effect of Traverse Speed on the Kerf Geometry.
(Steel AISI1018, Sa=177μm, Po=317MPa, Do=0.254mm, Ma=210g/min)

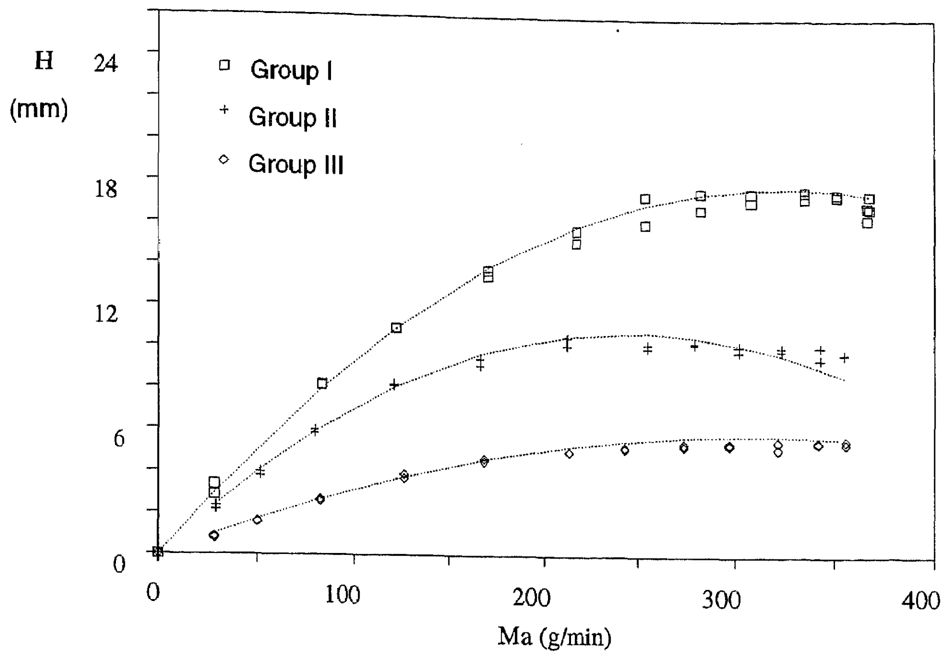

Figure 31 Effect of Abrasive Flow Rate on the Depth of Cut.
(Steel AISI1018, Sa=177μm; Group I: Po=317MPa, Do=0.254mm, Dt=0.838mm, U=14cm/min; Group II: Po=331MPa, Do=0.178mm, Dt=0.838mm, U=14cm/min; Group III: Po=197MPa, Do=0.178mm, Dt=1.092mm, U=10cm/min)

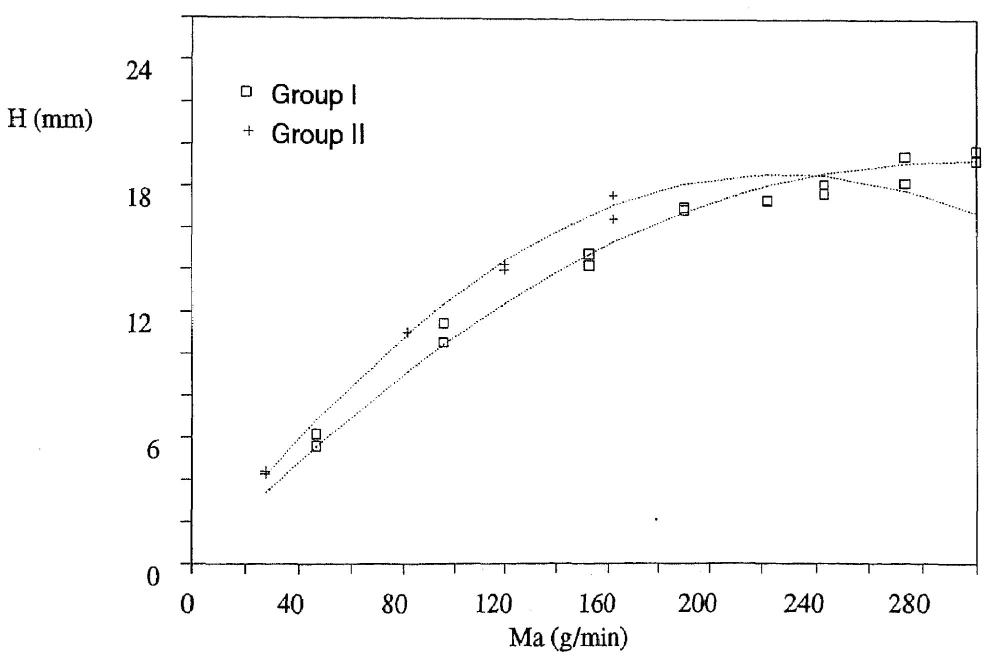

Figure 32 Effect of Abrasive Flow Rate on the Depth of Cut.
(Po=317MPa, Do=0.254mm, Dt=0.838mm, Sa=177μm;
Group I: Aluminum Al 6061-T6, U=32cm/min; Group II: TitaniumTi Gr2, U=14cm/min)

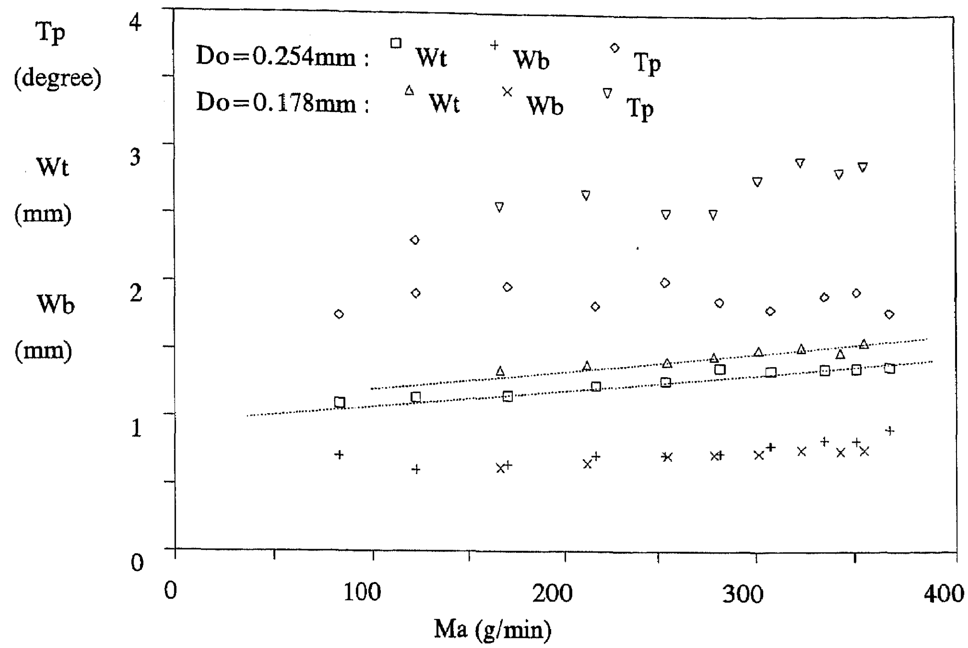

Figure 33 Effect of Abrasive Flow Rate on the Kerf Geometry.
(Steel AISI1018, Sa=177μm; Pi=345Mpa, Dt=0.9mm, U=14cm/min)

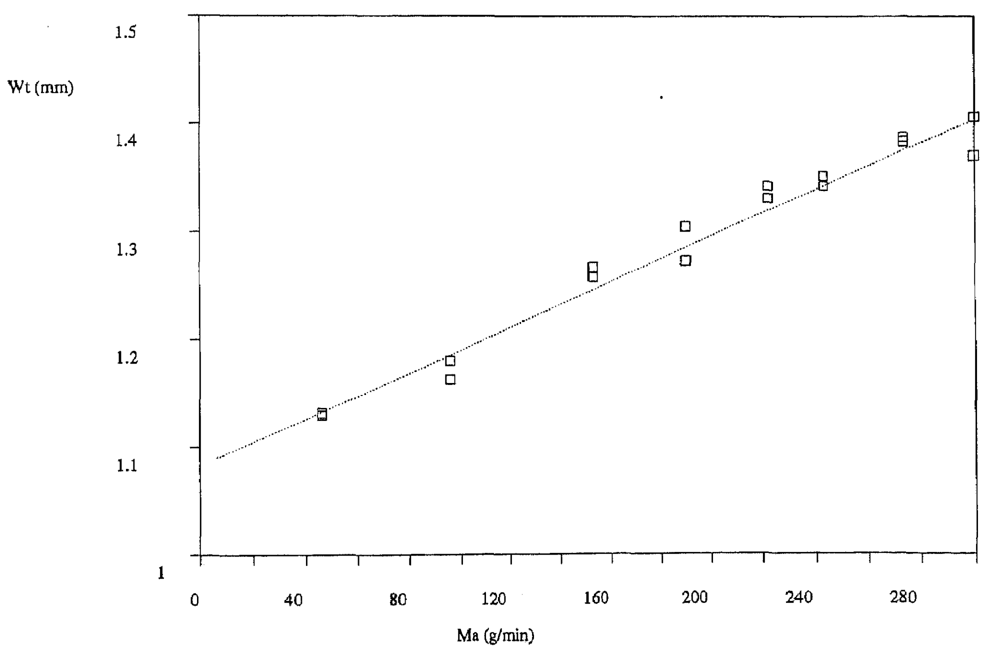

Figure 34 Effect of Abrasive Flow Rate on the Top Kerf Width
(Aluminum Al 6061-T6, Po=310MPa, Do=0.254mm, Dt=0.838mm, Sa=177μm, U=32cm/min)

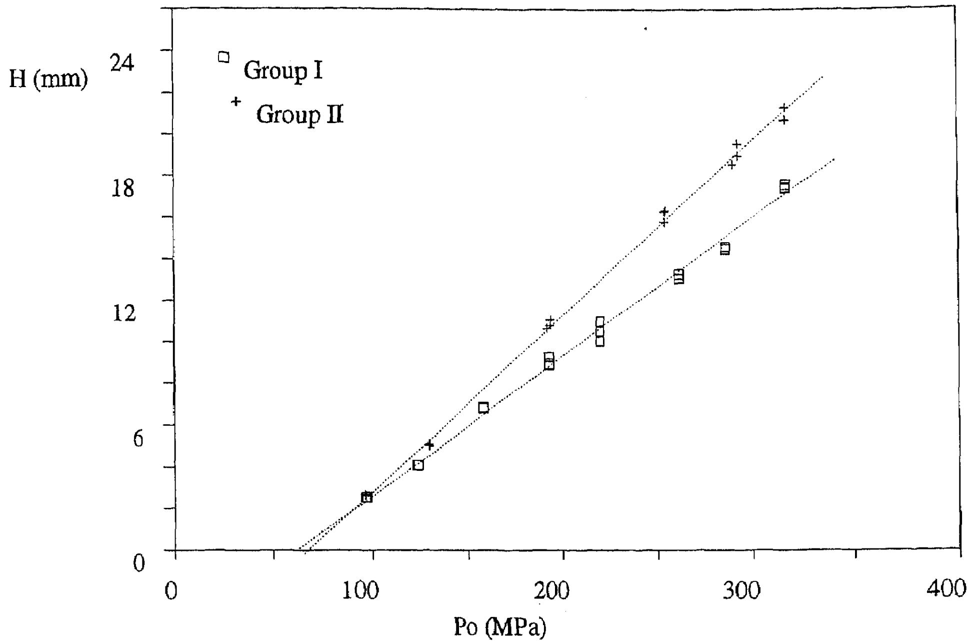

Figure 35 Effect of Operating Pressure on the Depth of Cut.
(Steel AISI1018, Sa=177μm, Po=317MPa, Do=0.254mm, U=12cm/min; Group I: Dt=1.092mm, Ma=242g/min; Group II: Dt=0.838mm, Ma=303g/min)

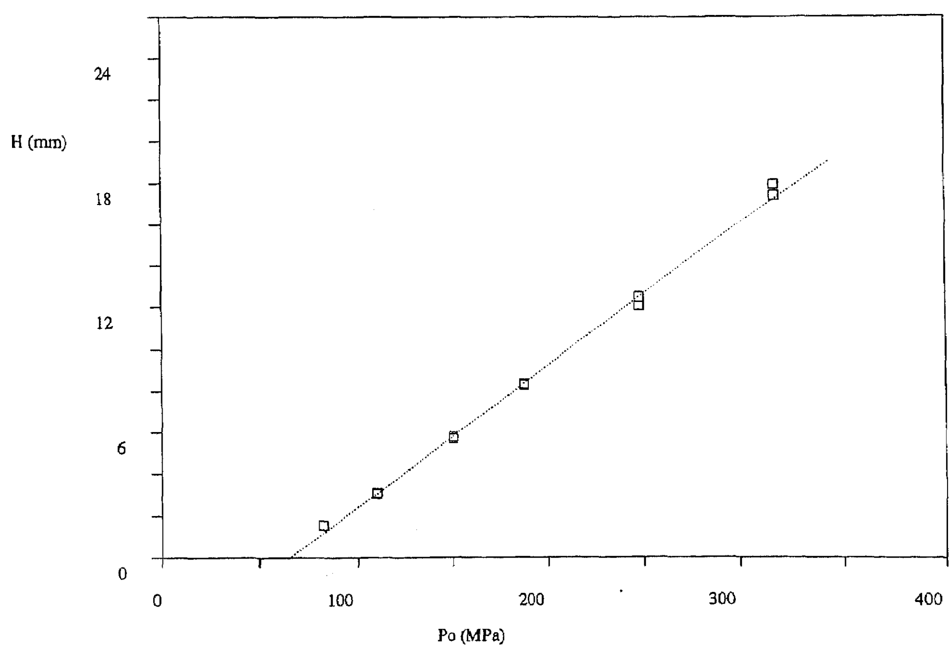

Figure 36 Effect of Operating Pressure on the Depth of Cut.
(Aluminum Al 6061-T6, Do=0.254mm, Dt=0.838mm, Sa=177μm, Ma=220g/min, U=32cm/min)

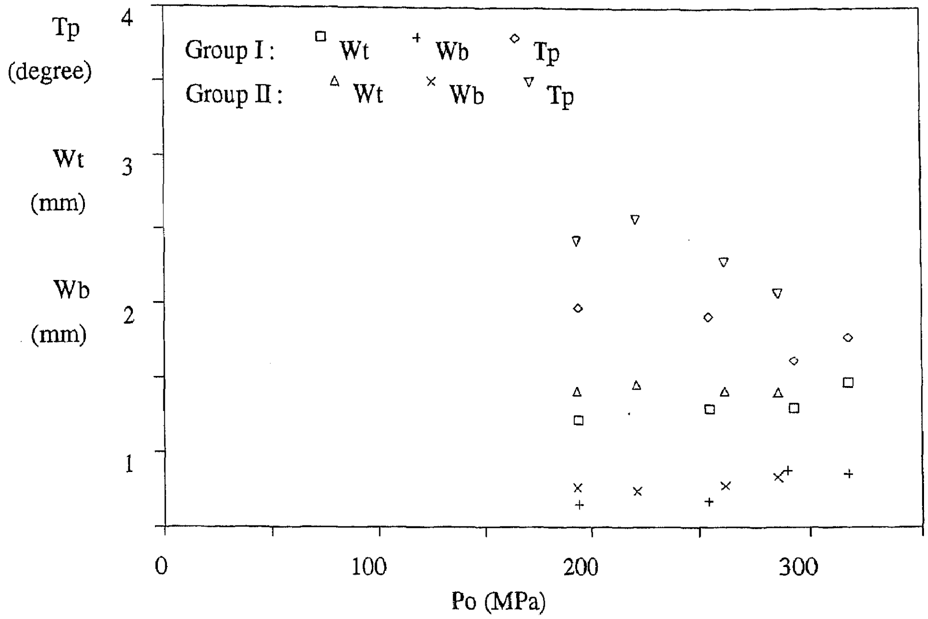

Figure 37 Effect of Operating Pressure on the Kerf Geometry.
(Steel AISI1018, Do=0.254mm, Sa=177μm, U=12cm/min; Group I: Dt=0.838mm, Ma=303g/min; Group II: Dt=1.092mm, U=12cm/min)

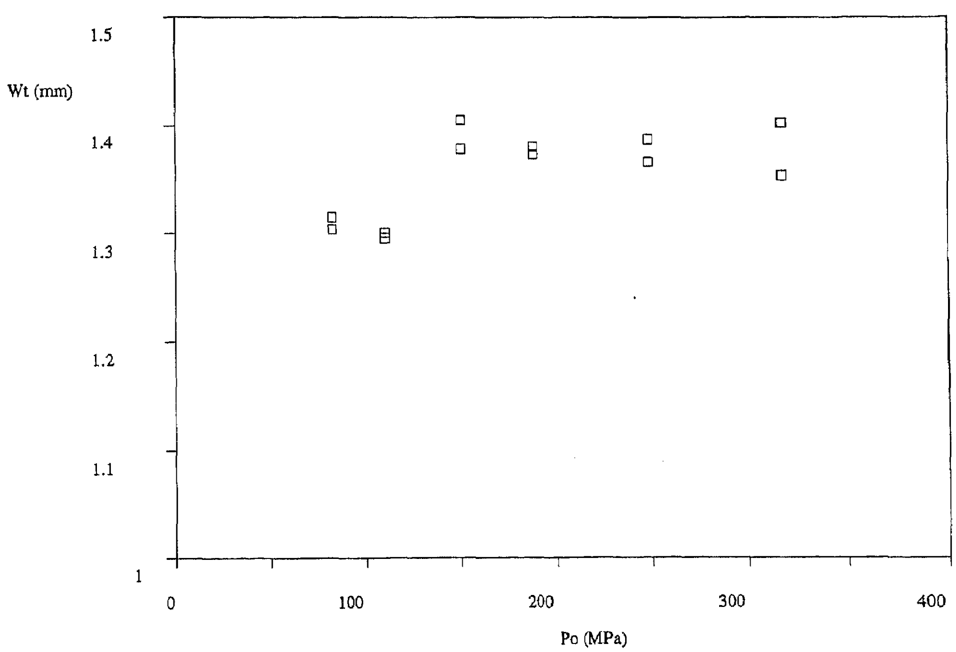

Figure 38 Effect of Operating Pressure on the Top Kerf Width.
(Aluminum Al 6061-T6, Do=0.254mm, Dt=0.838mm, Sa=177μm, Ma=220g/min, U=32cm/min)

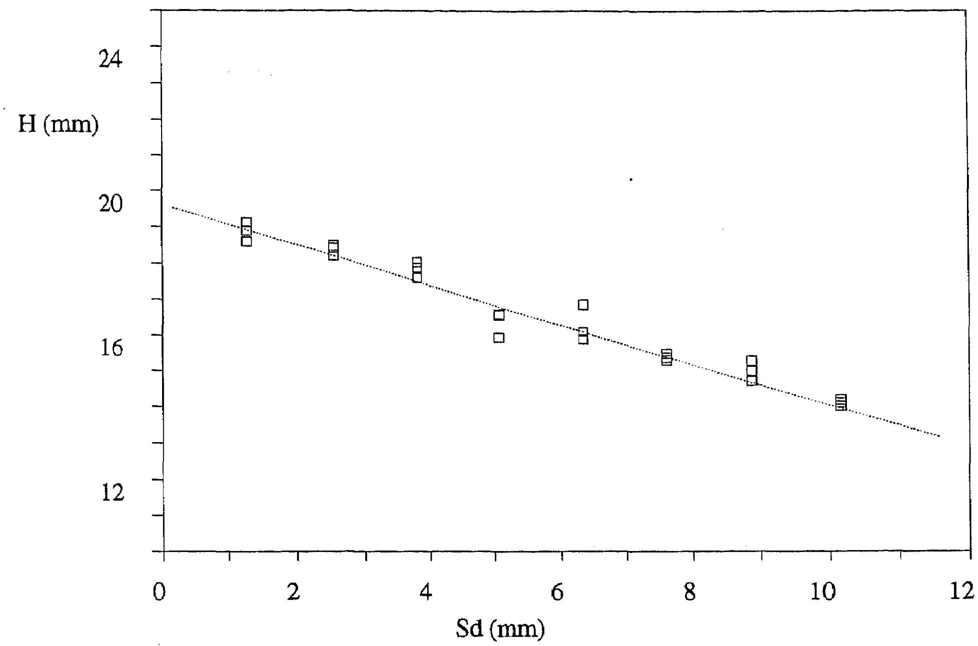

Figure 39 Effect of Stand-off Distance on the Depth of Cut.
(Steel AISI1018, Sa=177μm, Po=317MPa, Do=0.254mm, Dt=0.838mm, Ma=272g/min, U=12cm/min)

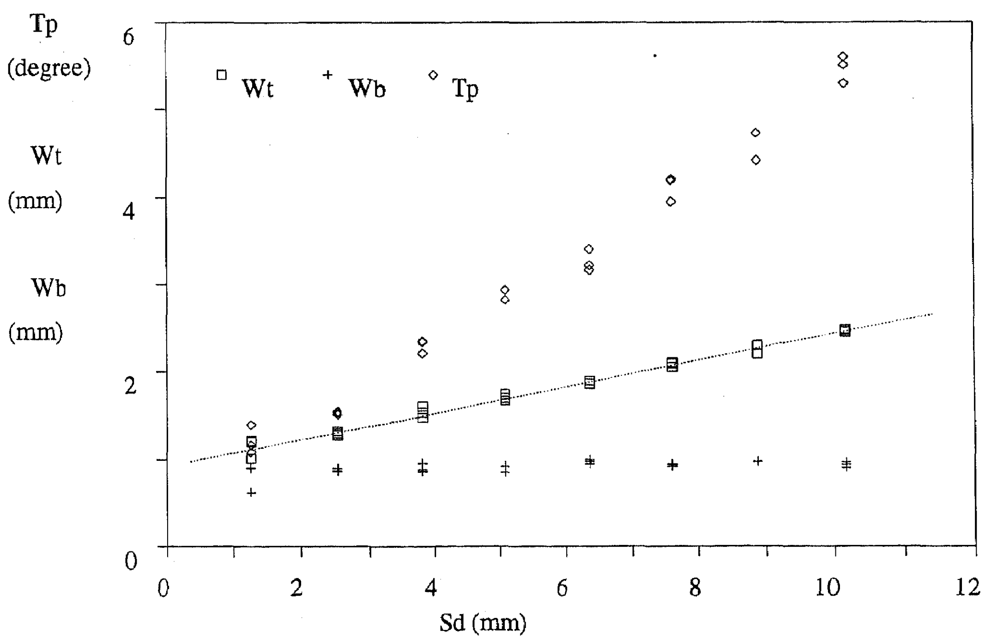

Figure 40 Effect of Stand-off Distance on the Kerf Geometry.
(Steel AISI1018, Sa=177μm, Po=317MPa, Do=0.254mm, Dt=0.838mm, Ma=272g/min)

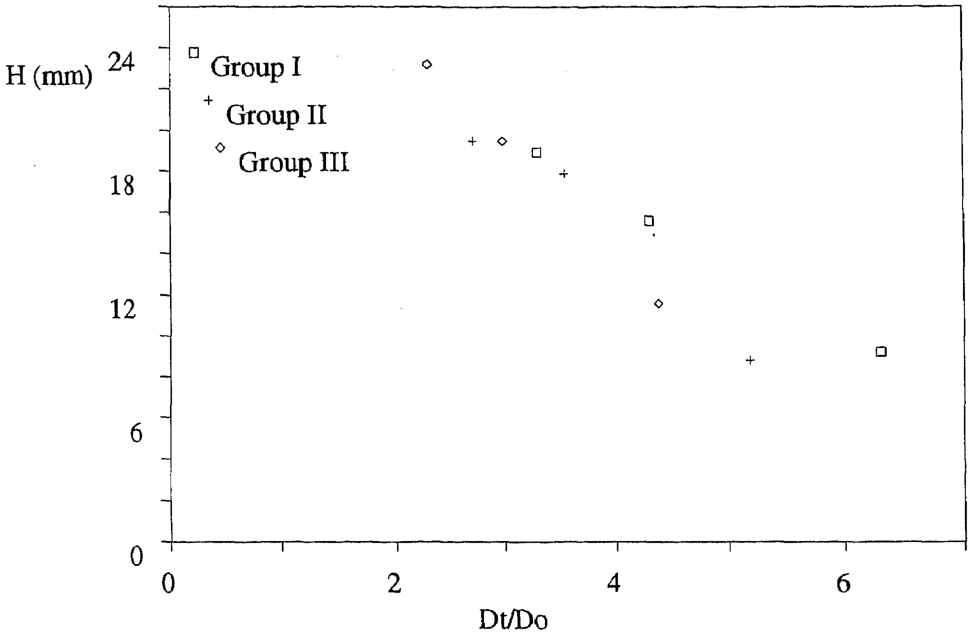

Figure 41 Effect of Nozzle Combination on the Depth of Cut.
(Steel AISI1018, Sa=177μm, Pi=345MPa; Group I: Do=0.254mm, Ma=260g/min, U=14cm/min; Group II: Do=0.305mm, Ma=275g/min,U=14cm/min; Group III: Do=0.356mm, Ma=280g/min, U=13cm/min)

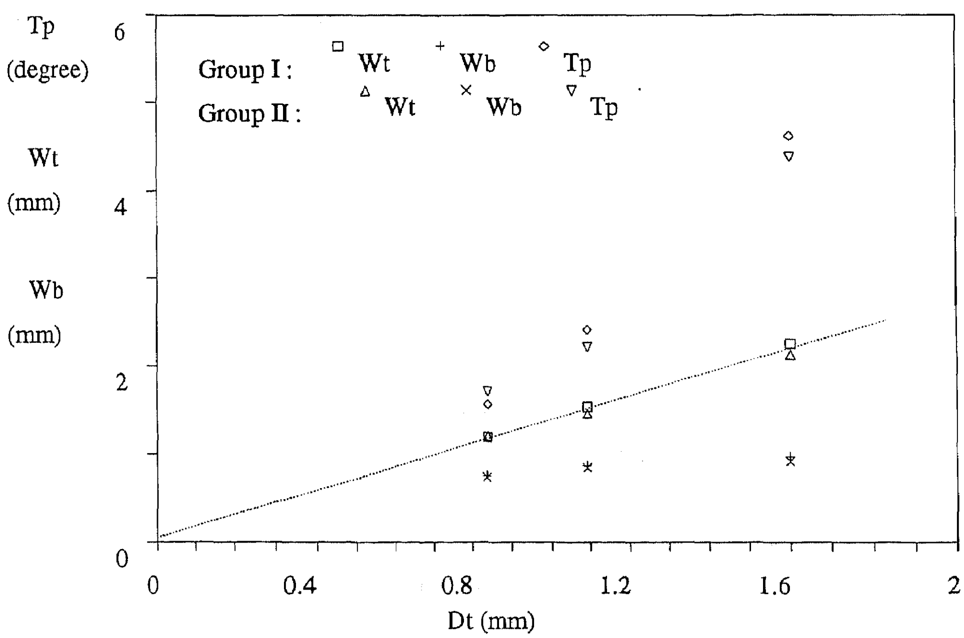

Figure 42 Effect of Focusing Tube Diameter on the Kerf Geometry.
(Steel AISI1018, Sa=177μm; Group I: Po=317MPa, Do=0.254mm, Ma=260g/min, U=14cm/min; Group II: Po=290MPa, Do=0.356mm, Ma=280g/min, U=13cm/min)

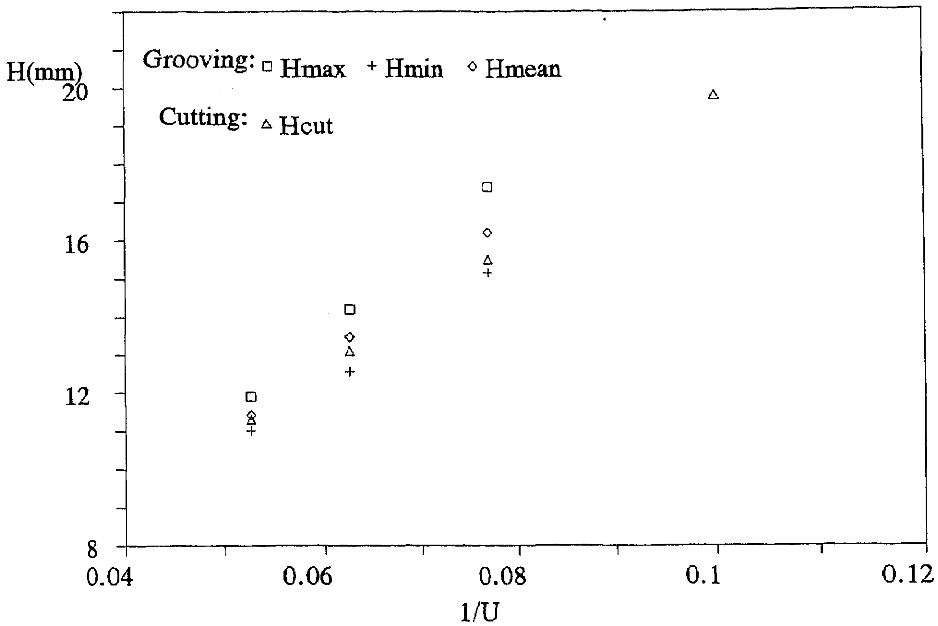

Figure 43 Effect of Machining Process on the Depth of Penetration.
(Machining AISI1018, Sa=177μm, Po=324MPa, Do=0.229mm, Dt=0.838mm, Ma=215g/min)

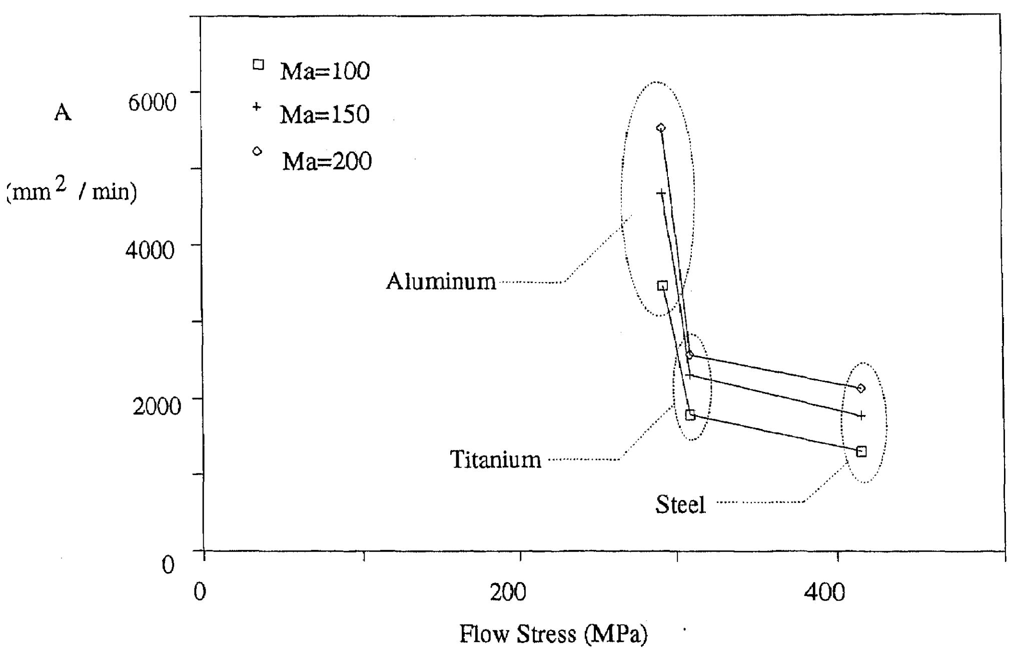

Figure 44 Effect of Material Flow Stress on the Depth of Cut
(Po=317MPa, Do=0.254mm, Dt=0.838mm)

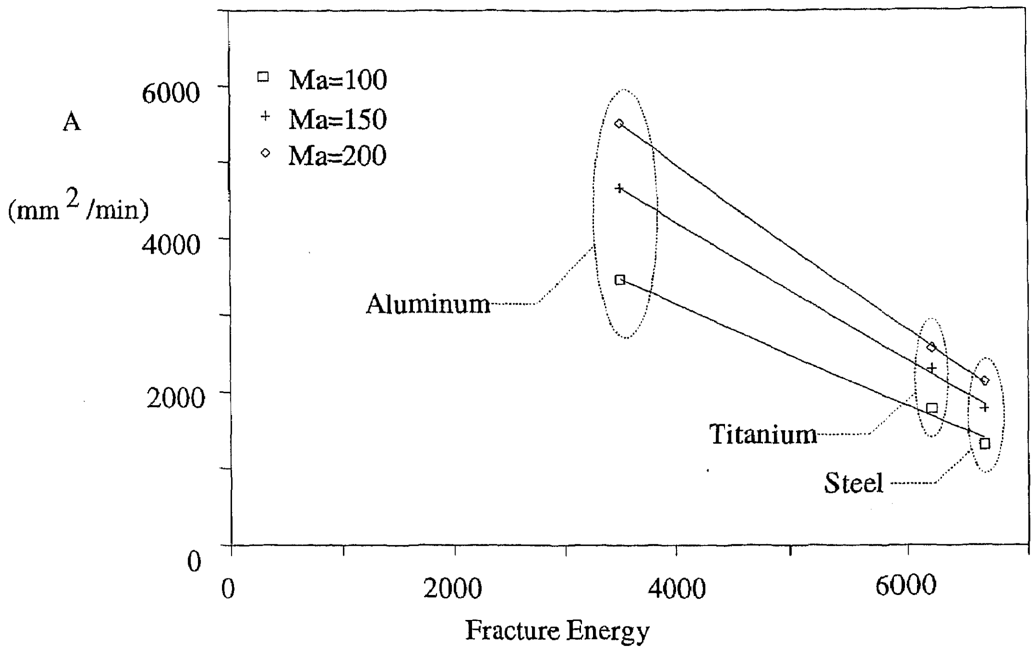

Figure 45 Effect of Material Fracture Energy on the Depth of Cut (Po=317MPa, Do=0.254mm, Dt=0.838mm)

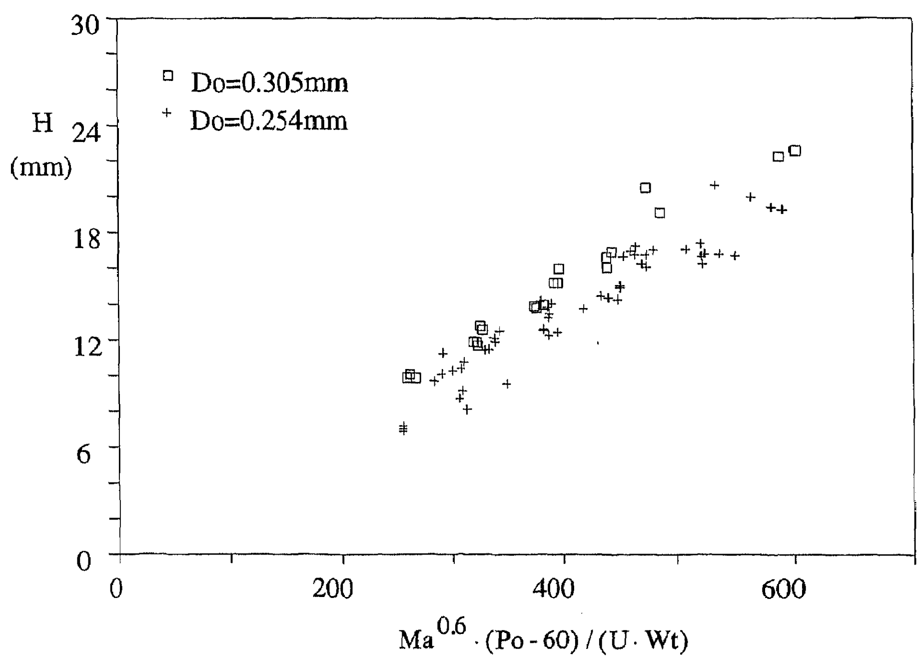

Figure 46 Prediction Results on the Depth of Cut. (Steel AISI 1018, Sa=300μm, Sd=2.54mm)

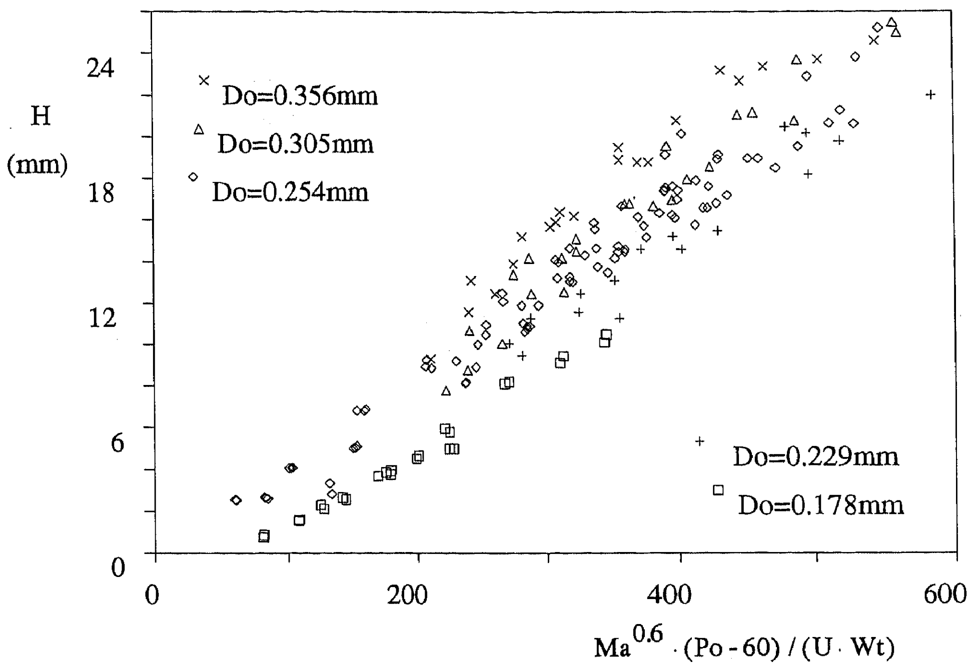

Figure 47 Prediction Results on the Depth of Cut.
(Steel AISI1018, Sa=177μm, Sd=2.54mm)

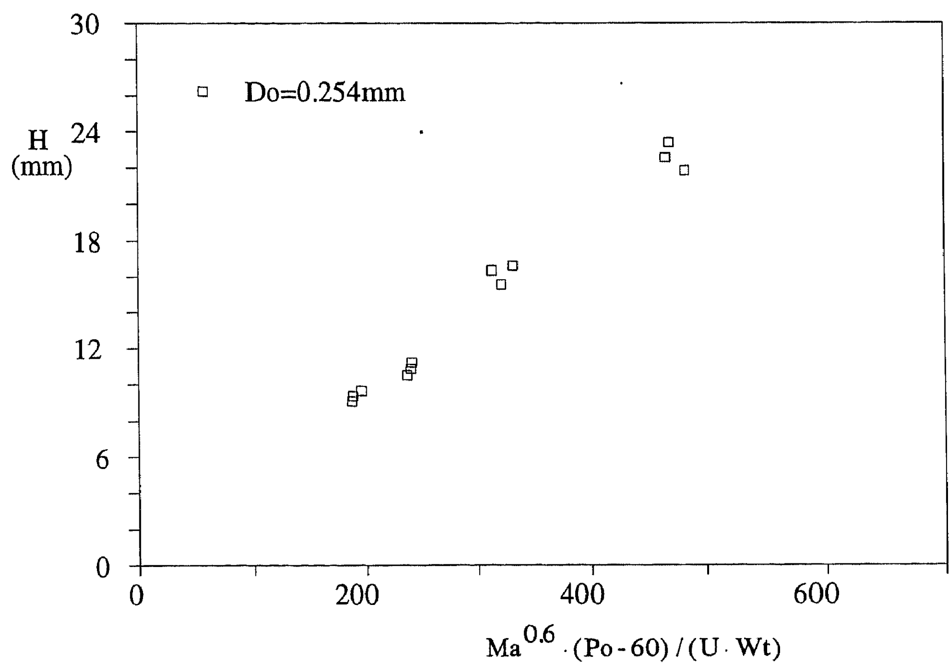

Figure 48 Prediction Results on the Depth of Cut.
(Steel AIS1018, Sa=125μm, Sd=2.54mm)

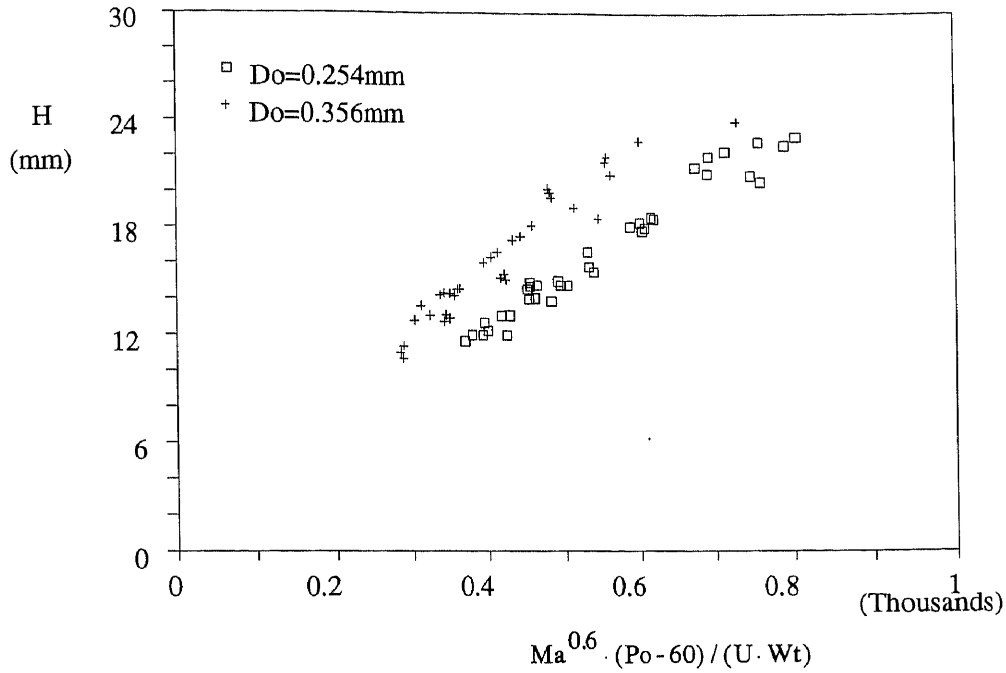

Figure 49 Prediction Results on the Depth of Cut.
(Steel AISI1018, Sa=65μm, Sd=2.54mm)

APPENDIX I.
A CASE STUDY OF AWJ 3-D MACHINING ABILITY

I.1 Project History Review

March 12 : Dr. Geskin made the first discussion with Mr. Edward Simonson of the Corning Glass in the telephone. Received faxed drawing of the dimension of workpiece to be trimmed. (The 5-axis AWJ machine was not working because of broken motor.)

March 19 : Received two original glass workpiece to be trimmed.

March 20 - 22 : Inside discussion and dimension investigation.

March 25 : Discussed with Ed on detail plan. Made the following decision:

1. The robot NC program will be prepared by Corning.
2. Fixture will be made by Corning.
3. All 65 pieces of glass works should be trimmed completely no later than tow weeks right after the machine is fixed.

Some straight cutting test was made in the HS3000 to investigate operational parameters for acceptable results.

April 1 : Received the fixture from the Corning.

April 3 : The NC program was received from the Corning. It was found that the program only offered three dimensional coordinate of the trim line only, it couldn't be run directly in our machine.

April 4 : The 5-axis AWJ machine was fixed to ready for machining.

April 5 : Tried downloading program from PC to the main memory of the 5-axis AWJ machine.

April 6-8 : Constructed a program to convert target coordinate to robot center coordinate. Corrected the NC program prepared by the Corning.

April 9 : Requested the machine shop making a frame to fasten the fixture on the carrier of the 5-axis AWJ machine.

April 10 : Tested the NC program and all settings.

April 11 - 12 : Finished trimming all 65 pieces of glass works.

I.2 Process Description

I.2.1 Robot Coordinate Conversion

The workpiece as shown in Fig. 48 was made of some special glass manufactured by the Corning. The required trimming contour shown in the same figure is a three dimensional close curve. With considering the robot orientation, this is a five dimensional machining work.

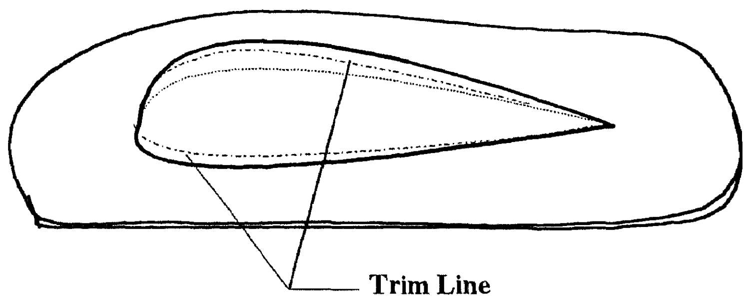

Figure 50 Glass Workpiece Manufactured by the Corning.

For this kind of complicated higher dimensional cutting, especially when the cutting path cannot be easily expressed in geometric equation, absolute coordinate system is usually a better choice than incremental one. The absolute coordinate system was hence used in this project.

In order to control the jet making a precise cut on desired location, it is required to know all the robot's five axis coordinate (X, Y, Z, A, and B) on each point. These values are rarely offered by the client. In most cases, only the coordinate of target points (i.e. the points on which jet should hit) were available. The coordinate conversion from target points to robot control's centers is discussed in the following.

As shown in Fig. 49, the Cartesian coordinate of target point is given as (a, b, c) and the orientation required is given as a vector <l, m, n>.

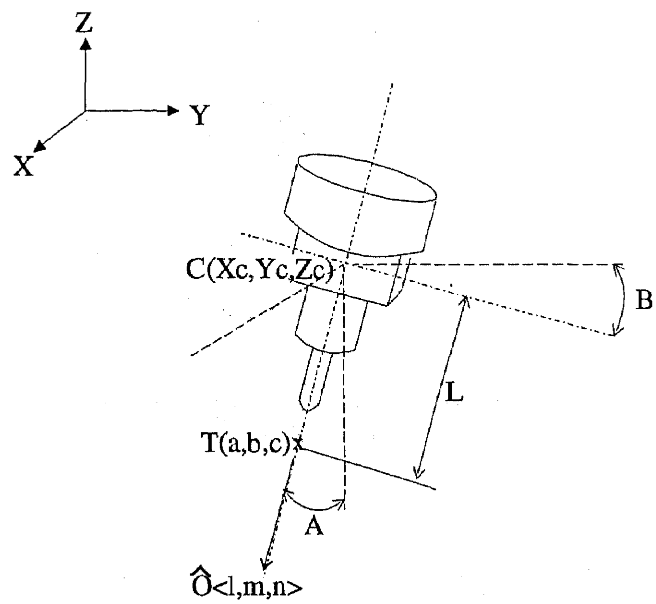

Figure 51 The Coordinates of Robot Motion

First, to find the coordinate of robot center (Xc, Yc, Zc):

Express the line passing through points C and T by

$$\begin{cases} a - Xc = t \cdot l \\ b - Yc = t \cdot m \\ c - Zc = t \cdot n \ . \end{cases} \tag{I.1}$$

L is figured from the distance between the robot center and the tip of nozzle plus the stand-off distance.

$$L = \sqrt{(Xc - a)^2 + (Yc - b)^2 + (Zc - c)^2}$$
$$= \sqrt{(t \cdot l)^2 + (t \cdot m)^2 + (t \cdot n)^2}$$

thus, $$t = \frac{L}{\sqrt{l^2 + m^2 + n^2}} \tag{I.2}$$

Substitute t in equation (1) with equation (2), we have

$$Xc = a - \frac{L \cdot l}{\sqrt{l^2 + m^2 + n^2}} \tag{I.3}$$

$$Yc = b - \frac{L \cdot m}{\sqrt{l^2 + m^2 + n^2}} \tag{I.4}$$

$$Zc = c - \frac{L \cdot n}{\sqrt{l^2 + m^2 + n^2}} \tag{I.5}$$

Second, to find angles A and B:

A is the angle between <l, m, n> and $-\hat{Z}<0, 0, -1>$,

$$\text{Cos } A = \frac{<l,\ m,\ n>}{\sqrt{l^2 + m^2 + n^2}} \cdot <0,\ 0,\ -1>$$

thus, we have

$$A = \text{Cos}^{-1}\left(\frac{-n}{\sqrt{l^2 + m^2 + n^2}}\right) = \text{Tan}\left(\frac{\sqrt{l^2 + m^2}}{-n}\right) \tag{I.6}$$

B is the angle between <l, m, 0> and $\hat{Y}<0, 1, 0>$,

$$\text{Cos } B = \frac{<l,\ m,\ 0>}{\sqrt{l^2 + m^2}} \cdot <0,\ 1,\ 0>$$

thus,

$$B = \text{Cos}^{-1}\left(\frac{m}{\sqrt{l^2 + m^2}}\right) = \text{Tan}\left(\frac{l}{m}\right) \tag{I.7}$$

Now that the conversion equations had been derived, we can readily find all the coordinate of required robot center points. A PC was used to carry out all these tedious calculation task. The program ROBOT listed in Appendix I.4 was written in PASCAL for this sake and had been successfully used in this project. The constructed NC program is listed in Appendix I.5.

I.2. 2 NC Program Transfer

There were 270 target points been used to cut the workpiece in this project. Including some other necessary process, the NC program is a 280 blocks (lines) long program. Keying the program of this size into our robot control will take more than 3 hours without counting the time of correcting manual mistakes. To save time and avoid error, transferring the NC program from a PC to the control was tried and then used in this project successfully. The communication software PC-TALK was used for this sake. The only problem in this transfer process is that there is a limit of program size on each program to be transferred. This limit is due to the available memory of control of which the exact amount is hardly decided. Ten blocks (lines) is a suggested program length after a series of tests. Dividing the long NC program into several sections which can be accepted by the robot control was also been considered in the created program ROBOT.

I.2.3 Machining Process

Following is a step-by-step description on the machining process.

1) Make a series of straight cutting test to find the optimal operational parameters.

   The following operational parameters were used in this project:

Water pressure	:	207 MPa
Water nozzle	:	0.254 mm ID
Focusing tube	:	0.867 mm ID
Abrasive	:	Barton 80 HP
Abrasive flow rate	:	210 g/min
Traverse rate	:	75 cm/min

2) Fasten the fixture on the frames (Fig. 50) and align the horizontal position.

3) Locate the workpiece in the fixture (Fig. 51) and check the level.

4) Find the trimming start point (Fig. 52) roughly by eyes.

5) Dry-run the NC program to test the robot motion and make necessary adjustment.

6) Start trimming.

I.3 Machining Results Discussion and Suggestion

In very limited time, this trimming work was done as shown in Fig. 53 with around fifteen percents of defective rate. These defects are mainly due to the cracks happened at the trimmed edge. The surface of workpiece wasn't eroded as expected by the spraying of abrasive particles. Several factors such as the loosening of workpiece, the uneven robot motion, the discreteness of the jet, the uneven distribution of abrasive particles in jet, and the defects of the workpiece itself could result in the happiness of cracks.

The success of this project widen the application of the AWJ technology, especially, in three-dimensional machining. However, the potential of WJ and AWJ is still not very clear in which a lot of studies on their applications are very valuable to be carried. Besides these, the study on current hardware such as the reliability of the robot and the flexibility and accuracy of fixtures should be done as soon as possible. The productivity will be hardly raised and a lot of time will be wasted if the complete knowledge on the ability of our equipment is not available.

Figure 52 Fixture Setup.

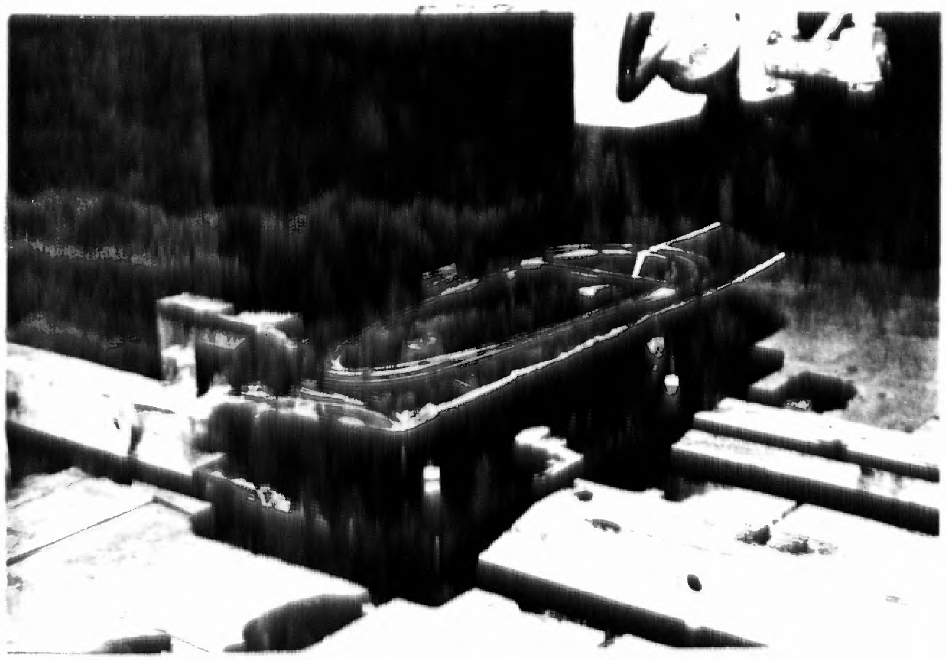

Figure 53 Photograph of the Workpiece Holding by the Fixture.

Figure 54 Locating the Trimming Start Point.

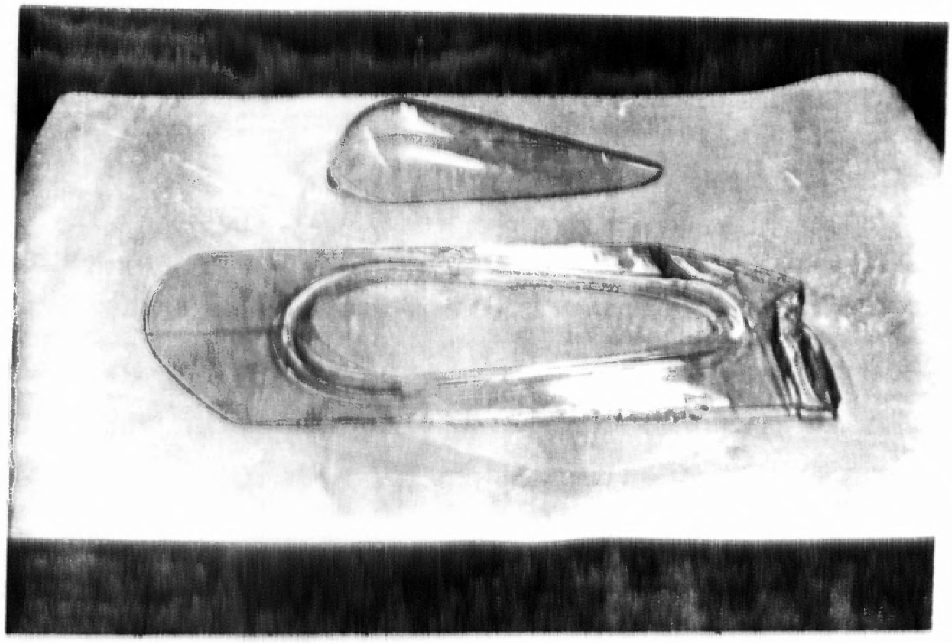

Figure 55 Workpiece Been Trimmed

APPENDIX I.4
PROGRAM "ROBOT" FOR CONVERTING COORDINATES OF TARGET TO THE CENTER OF ROBOT CONTROL

```
PROGRAM ROBOTMOTION;   (* To transfer target coordinate and orientation  *)
                       (* to robot center coordinate and orientation.    *)
CONST  N=700;
TYPE   CORN = ARRAY[1..N,1..3] OF REAL;
VAR    I,J,K,NCN,
    BN,EN      : INTEGER;      (* L -- Distance between target & robot center *)
    COOR,ORIN  : CORN;         (* COOR -- Coordinate *)
                               (* ORIN -- Orientation *)
    OFFSET,MF,                 (* OFFSET -- Tool offset *)
    TX,TY,TZ,                  (* MF -- Magnification factor *)
    OL,OM,ON,
    X,Y,Z,A,B,
    L          : REAL;         (* X, Y, Z, A, B -- Robot's 5 axis *)
    NC         : CHAR;
    INF,OUTF   : TEXT;         (* INF & OUTF -- Input and output file *)
    INFN,OUTFN : STRING[12];
    NCF,S      : STRING[4];


PROCEDURE TRANSFER (VAR X,Y,Z,A,B:REAL);
BEGIN
  X:= TX-L*OL/SQRT(SQR(OL)+SQR(OM)+SQR(ON));
  Y:= TY-L*OM/SQRT(SQR(OL)+SQR(OM)+SQR(ON));
  Z:= TZ-L*ON/SQRT(SQR(OL)+SQR(OM)+SQR(ON));
  IF ON=0 THEN
      BEGIN
        A:=90;
        B:=-180;
      END
   ELSE
    A:= -57.29578*ARCTAN(SQRT(SQR(OL)+SQR(OM))/(-ON));
  IF ON<>0 THEN
    CASE ORD(OM>0) OF
      1: CASE ORD(OL>0) OF
           1: B:= 90-57.29578*ARCTAN(OL/OM);
           0: IF OL=0 THEN B:=90 ELSE
                B:= 90-57.29578*ARCTAN(OL/OM)
         END;
      0: CASE ORD(OM<0) OF
           1: CASE ORD(OL>0) OF
                1: B:=-57.29578*ARCTAN(OL/OM)-90;
                0: IF OL=0 THEN B:=-90 ELSE
                     B:= -57.29578*ARCTAN(OL/OM)-90
```

```
          END;
        0: IF OL>0 THEN B:=0 ELSE B:=-180
      END
    END
END;

PROCEDURE SAVEDATA;

BEGIN
  ASSIGN(OUTF,OUTFN);
  REWRITE(OUTF);
  FOR J:=BN TO EN DO
    BEGIN
      TX:=COOR[J,1];
      TY:=COOR[J,2];
      TZ:=COOR[J,3];
      OL:=ORIN[J,1];
      OM:=ORIN[J,2];
      ON:=ORIN[J,3];
      TRANSFER(X,Y,Z,A,B);
      IF NC='N' THEN WRITELN(OUTF,X:10:4,Y:10:4,Z:10:4,A:10:4,B:10:4)
        ELSE IF J<10 THEN
          WRITELN(OUTF,'N000',J:1,'X',X:5:3,'Y',Y:5:3,'Z',Z:5:3,
                  'A',A:4:2,'B',B:4:2)
          ELSE IF (9<J) AND (J<100) THEN
            WRITELN(OUTF,'N00',J:2,'X',X:5:3,'Y',Y:5:3,'Z',Z:5:3,
                    'A',A:4:2,'B',B:4:2)
            ELSE IF (J>99) AND (J<1000) THEN
              WRITELN(OUTF,'N0',J:3,'X',X:5:3,'Y',Y:5:3,'Z',Z:5:3,
                      'A',A:4:2,'B',B:4:2)
      ELSE
        WRITELN(OUTF,'N',J:4,'X',X:5:3,'Y',Y:5:3,'Z',Z:5:3,
                'A',A:4:2,'B',B:4:2);
    END;
  WRITELN(' ************* Complete transfer **************');
  WRITELN(' *** Transfered data were saved in : ',OUTFN);
  CLOSE(OUTF)
END;
BEGIN
  WRITELN('What is the distance between target and center of robot ?');
  WRITELN('(The unit using here must be consistant with the unit used in data file.)');
  WRITE('Key in the distance ==>');
  READLN(L);
  WRITELN;
  WRITE('Key in the name of input data file ==>');
  READLN(INFN);
  WRITELN;
  WRITE('What is the magnification factor? (1 for no magnification)==>');
  READLN(MF);
```

```
IF NOT (ABS(MF)>0) THEN MF:=1;
ASSIGN(INF,INFN);
RESET(INF);
I:=0;
WHILE NOT EOF(INF) DO                (* Read in target coordinate *)
  BEGIN                              (* and orientation.          *)
    I:=I+1;
    READLN(INF,COOR[I,1],COOR[I,2],COOR[I,3],ORIN[I,1],ORIN[I,2],
           ORIN[I,3]);
    COOR[I,1]:=COOR[I,1]*MF;
    COOR[I,2]:=COOR[I,2]*MF;
    COOR[I,3]:=COOR[I,3]*MF;
  END;
CLOSE(INF);
WRITELN;
WRITELN('Do you want to create a NC program in robot absolute coordinate?');
WRITE('Key in Y for Yes,  N for No ==>');
READLN(NC);
WRITELN;
IF NOT (NC='N') THEN
  BEGIN
    WRITELN('There are ',I,' points will be transfered...........');
    WRITELN('Into how many devided NC programs you want to store');
    WRITE('those transfered data ? ==>');
    READLN(NCN);
    WRITELN;
    WRITE('What is the first four characters of NC program?');
    READLN(NCF);
    FOR K:=1 TO NCN DO
      BEGIN
        IF K=NCN THEN
          BEGIN
            BN:=ROUND(I/NCN)*(K-1)+1;
            EN:=I;
            STR(K,S);
            OUTFN:=NCF+S;
            SAVEDATA;
          END
        ELSE
         BEGIN
           BN:=ROUND(I/NCN)*(K-1)+1;
           EN:=ROUND(I/NCN)*K;
           STR(K,S);
           OUTFN:=NCF+S;
           SAVEDATA;
         END;
      END;
    WRITELN;
  END
```

```
    ELSE
      BEGIN
        WRITE('Key in the name of output data file ==>');
        READLN(OUTFN);
      END;
END.
```

APPENDIX I.5
THE NC PROGRAM FOR TRIMMING THE CORNING GLASS

```
N0001 ((***Trimming Corning Glass***))
N0002G90G70F30
N0003G92X2.872Y-0.05Z2.31A-60.0B-180.0
N0004X2.872Y-0.05Z3.31A-10B-180.0
N0005X-2Y-0.05Z3.31A-60B-180
N0006G4M4F.5
N0007G4M13F.5
N0008X2.872Y-0.050Z3.310A-60.00B-180.00
N0009X2.872Y-0.050Z2.310A-60.00B-180.00
N0010X2.873Y0.037Z2.311A-60.00B-178.52
N0011X2.871Y0.124Z2.312A-60.00B-177.05
N0012X2.867Y0.210Z2.314A-60.00B-175.57
N0013X2.862Y0.296Z2.317A-60.00B-174.10
N0014X2.854Y0.381Z2.320A-60.00B-172.62
N0015X2.844Y0.465Z2.324A-60.00B-171.15
N0016X2.833Y0.548Z2.328A-60.00B-169.67
N0017X2.819Y0.630Z2.333A-60.00B-168.20
N0018X2.804Y0.711Z2.339A-60.00B-166.72
N0019X2.787Y0.791Z2.345A-60.00B-165.25
N0020X2.768Y0.870Z2.352A-60.00B-163.77
N0021X2.747Y0.947Z2.360A-60.00B-162.30
N0022X2.725Y1.024Z2.368A-60.00B-160.82
N0023X2.701Y1.099Z2.376A-60.00B-159.34
N0024X2.675Y1.172Z2.386A-60.00B-157.87
N0025X2.648Y1.244Z2.395A-60.00B-156.39
N0026X2.619Y1.314Z2.406A-60.00B-154.92
N0027X2.589Y1.384Z2.417A-60.00B-153.44
N0028X2.557Y1.451Z2.428A-60.00B-151.97
N0029X2.524Y1.517Z2.440A-60.00B-150.49
N0030X2.489Y1.581Z2.452A-60.00B-149.02
N0031X2.453Y1.644Z2.465A-60.00B-147.54
N0032X2.416Y1.705Z2.478A-60.00B-146.07
N0033X2.378Y1.765Z2.492A-60.00B-144.59
N0034X2.338Y1.823Z2.506A-60.00B-143.11
N0035X2.297Y1.880Z2.520A-60.00B-141.64
N0036X2.254Y1.935Z2.535A-60.00B-140.16
N0037X2.211Y1.988Z2.550A-60.00B-138.69
N0038X2.166Y2.040Z2.565A-60.00B-137.21
N0039X2.119Y2.090Z2.580A-60.00B-135.74
N0040X2.072Y2.139Z2.595A-60.00B-134.26
N0041X2.023Y2.187Z2.610A-60.00B-132.79
N0042X1.973Y2.233Z2.626A-60.00B-131.31
N0043X1.921Y2.277Z2.641A-60.00B-129.84
```

```
N0044X1.869Y2.320Z2.656A-60.00B-128.36
N0045X1.814Y2.362Z2.671A-60.00B-126.89
N0046X1.759Y2.403Z2.686A-60.00B-125.41
N0047X1.701Y2.442Z2.701A-60.00B-123.93
N0048X1.643Y2.479Z2.715A-60.00B-122.46
N0049X1.583Y2.516Z2.729A-60.00B-120.98
N0050X1.521Y2.550Z2.743A-60.00B-119.51
N0051X1.458Y2.584Z2.756A-60.00B-118.03
N0052X1.393Y2.616Z2.769A-60.00B-116.56
N0053X1.327Y2.647Z2.782A-60.00B-115.08
N0054X1.260Y2.676Z2.793A-60.00B-113.61
N0055X1.191Y2.703Z2.805A-60.00B-112.13
N0056X1.120Y2.729Z2.816A-60.00B-110.66
N0057X1.048Y2.754Z2.826A-60.00B-109.18
N0058X0.974Y2.777Z2.836A-60.00B-107.70
N0059X0.899Y2.798Z2.845A-60.00B-106.23
N0060X0.823Y2.818Z2.854A-60.00B-104.75
N0061X0.745Y2.836Z2.862A-60.00B-103.28
N0062X0.666Y2.852Z2.869A-60.00B-101.80
N0063X0.586Y2.867Z2.876A-60.00B-100.33
N0064X0.504Y2.880Z2.882A-60.00B -98.85
N0065X0.421Y2.890Z2.888A-60.00B -97.38
N0066X0.338Y2.899Z2.893A-60.00B -95.90
N0067X0.253Y2.906Z2.897A-60.00B -94.43
N0068X0.168Y2.911Z2.900A-60.00B -92.95
N0069X0.081Y2.914Z2.903A-60.00B -91.48
N0070X-0.006Y2.915Z2.906A-60.00B -90.00
N0071X-0.069Y2.914Z2.907A-60.00B -88.78
N0072X-0.171Y2.911Z2.908A-60.00B -87.57
N0073X-0.235Y2.907Z2.908A-60.00B -86.35
N0074X-0.291Y2.903Z2.909A-60.00B -85.14
N0075X-0.230Y2.908Z2.909A-60.00B -83.92
N0076X-0.233Y2.904Z2.909A-60.00B -82.70
N0077X-0.208Y2.899Z2.910A-60.00B -81.49
N0078X-0.047Y2.904Z2.911A-60.00B -80.27
N0079X0.287Y2.920Z2.913A-60.00B -79.05
N0080X1.095Y2.973Z2.918A-60.00B -77.84
N0081X2.020Y3.033Z2.923A-60.00B -76.62
N0082X2.375Y3.044Z2.925A-60.00B -75.41
N0083X2.473Y3.032Z2.926A-60.00B -74.19
N0084X2.519Y3.014Z2.927A-60.00B -72.97
N0085X2.566Y2.994Z2.928A-60.00B -71.76
N0086X2.650Y2.977Z2.929A-60.00B -70.54
N0087X2.741Y2.959Z2.930A-60.00B -69.32
N0088X2.838Y2.942Z2.931A-60.00B -68.11
N0089X2.934Y2.924Z2.932A-60.00B -66.89
N0090X3.024Y2.904Z2.933A-60.00B -65.68
N0091X3.111Y2.883Z2.934A-60.00B -64.46
N0092X3.198Y2.862Z2.935A-60.00B -63.24
```

```
N0093X3.286Y2.840Z2.936A-60.00B -62.03
N0094X3.371Y2.816Z2.936A-60.00B -60.81
N0095X3.444Y2.790Z2.937A-60.00B -59.59
N0096X3.508Y2.762Z2.938A-60.00B -58.38
N0097X3.567Y2.732Z2.939A-60.00B -57.16
N0098X3.630Y2.703Z2.940A-60.00B -55.95
N0099X3.697Y2.673Z2.940A-60.00B -54.73
N0100X3.709Y2.630Z2.941A-60.00B -53.51
N0101X3.773Y2.598Z2.942A-60.00B -52.30
N0102X3.831Y2.564Z2.942A-60.00B -51.08
N0103X3.884Y2.528Z2.943A-60.00B -49.86
N0104X3.933Y2.491Z2.944A-60.00B -48.65
N0105X3.981Y2.453Z2.944A-60.00B -47.43
N0106X4.029Y2.414Z2.945A-60.00B -46.22
N0107X4.078Y2.375Z2.946A-60.00B -45.00
N0108X4.121Y2.334Z2.946A-60.00B -43.78
N0109X4.157Y2.289Z2.947A-60.00B -42.57
N0110X4.132Y2.223Z2.947A-60.00B -41.35
N0111X4.160Y2.174Z2.948A-60.00B -40.14
N0112X4.185Y2.123Z2.948A-60.00B -38.92
N0113X4.207Y2.071Z2.948A-60.00B -37.70
N0114X4.228Y2.018Z2.949A-60.00B -36.49
N0115X4.249Y1.964Z2.949A-60.00B -35.27
N0116X4.270Y1.910Z2.950A-60.00B -34.05
N0117X4.290Y1.855Z2.950A-60.00B -32.84
N0118X4.312Y1.801Z2.951A-60.00B -31.62
N0119X4.331Y1.744Z2.951A-60.00B -30.41
N0120X4.345Y1.685Z2.951A-60.00B -29.19
N0121X4.357Y1.624Z2.952A-60.00B -27.97
N0122X4.367Y1.561Z2.952A-60.00B -26.76
N0123X4.375Y1.496Z2.952A-60.00B -25.54
N0124X4.381Y1.430Z2.952A-60.00B -24.32
N0125X4.388Y1.364Z2.953A-60.00B -23.11
N0126X4.392Y1.295Z2.953A-60.00B -21.89
N0127X4.380Y1.212Z2.953A-60.00B -20.68
N0128X4.384Y1.141Z2.953A-60.00B -19.46
N0129X4.387Y1.068Z2.954A-60.00B -18.24
N0130X4.388Y0.994Z2.954A-60.00B -17.03
N0131X4.388Y0.918Z2.954A-60.00B -15.81
N0132X4.389Y0.842Z2.954A-60.00B -14.59
N0133X4.389Y0.764Z2.954A-60.00B -13.38
N0134X4.384Y0.678Z2.954A-60.00B -12.16
N0135X4.384Y0.598Z2.954A-60.00B -10.95
N0136X4.387Y0.519Z2.954A-60.00B  -9.73
N0137X4.390Y0.441Z2.955A-60.00B  -8.51
N0138X4.394Y0.362Z2.955A-60.00B  -7.30
N0139X4.398Y0.283Z2.955A-60.00B  -6.08
N0140X4.402Y0.204Z2.955A-60.00B  -4.86
N0141X4.407Y0.123Z2.955A-60.00B  -3.65
```

```
N0142X4.413Y0.042Z2.955A-60.00B -2.43
N0143X4.427Y-0.007Z2.955A-60.00B-1.22
N0144X4.438Y-0.030Z2.955A-60.00B 0.00
N0145X4.428Y 0.007Z2.955A-60.00B 1.18
N0146X4.414Y-0.042Z2.955A-60.00B 2.37
N0147X4.409Y-0.121Z2.955A-60.00B 3.55
N0148X4.404Y-0.199Z2.955A-60.00B 4.74
N0149X4.400Y-0.276Z2.955A-60.00B 5.92
N0150X4.396Y-0.354Z2.955A-60.00B 7.11
N0151X4.393Y-0.430Z2.955A-60.00B 8.29
N0152X4.390Y-0.506Z2.954A-60.00B 9.47
N0153X4.387Y-0.582Z2.954A-60.00B10.66
N0154X4.385Y-0.658Z2.954A-60.00B11.84
N0155X4.389Y-0.740Z2.954A-60.00B13.03
N0156X4.388Y-0.816Z2.954A-60.00B14.21
N0157X4.388Y-0.891Z2.954A-60.00B15.39
N0158X4.388Y-0.966Z2.954A-60.00B16.58
N0159X4.387Y-1.039Z2.953A-60.00B17.76
N0160X4.387Y-1.112Z2.953A-60.00B18.95
N0161X4.385Y-1.183Z2.953A-60.00B20.13
N0162X4.382Y-1.253Z2.953A-60.00B21.32
N0163X4.350Y-1.300Z2.953A-60.00B22.50
N0164X4.343Y-1.366Z2.952A-60.00B23.68
N0165X4.335Y-1.430Z2.952A-60.00B24.87
N0166X4.326Y-1.494Z2.952A-60.00B26.05
N0167X4.315Y-1.557Z2.952A-60.00B27.24
N0168X4.304Y-1.618Z2.951A-60.00B28.42
N0169X4.290Y-1.678Z2.951A-60.00B29.61
N0170X4.274Y-1.736Z2.951A-60.00B30.79
N0171X4.258Y-1.792Z2.950A-60.00B31.97
N0172X4.236Y-1.846Z2.950A-60.00B33.16
N0173X4.214Y-1.900Z2.949A-60.00B34.34
N0174X4.192Y-1.953Z2.949A-60.00B35.53
N0175X4.170Y-2.005Z2.949A-60.00B36.71
N0176X4.147Y-2.057Z2.948A-60.00B37.89
N0177X4.125Y-2.108Z2.948A-60.00B39.08
N0178X4.100Y-2.158Z2.947A-60.00B40.26
N0179X4.071Y-2.206Z2.947A-60.00B41.45
N0180X4.038Y-2.252Z2.946A-60.00B42.63
N0181X4.000Y-2.295Z2.946A-60.00B43.82
N0182X3.954Y-2.336Z2.945A-60.00B45.00
N0183X3.904Y-2.375Z2.944A-60.00B46.18
N0184X3.853Y-2.413Z2.944A-60.00B47.37
N0185X3.802Y-2.451Z2.943A-60.00B48.55
N0186X3.752Y-2.489Z2.942A-60.00B49.74
N0187X3.698Y-2.525Z2.942A-60.00B50.92
N0188X3.639Y-2.559Z2.941A-60.00B52.11
N0189X3.574Y-2.591Z2.940A-60.00B53.29
N0190X3.500Y-2.621Z2.939A-60.00B54.47
```

```
N0191X3.431Y-2.650Z2.939A-60.00B55.66
N0192X3.365Y-2.681Z2.938A-60.00B56.84
N0193X3.303Y-2.711Z2.937A-60.00B58.03
N0194X3.236Y-2.740Z2.936A-60.00B59.21
N0195X3.159Y-2.767Z2.935A-60.00B60.39
N0196X3.072Y-2.791Z2.935A-60.00B61.58
N0197X2.980Y-2.814Z2.934A-60.00B62.76
N0198X2.890Y-2.837Z2.933A-60.00B63.95
N0199X2.801Y-2.859Z2.932A-60.00B65.13
N0200X2.707Y-2.880Z2.931A-60.00B66.32
N0201X2.609Y-2.900Z2.930A-60.00B67.50
N0202X2.508Y-2.918Z2.929A-60.00B68.68
N0203X2.413Y-2.937Z2.928A-60.00B69.87
N0204X2.325Y-2.956Z2.927A-60.00B71.05
N0205X2.213Y-2.972Z2.926A-60.00B72.24
N0206X2.009Y-2.979Z2.925A-60.00B73.42
N0207X1.320Y-2.944Z2.921A-60.00B74.61
N0208X0.391Y-2.887Z2.916A-60.00B75.79
N0209X0.032Y-2.874Z2.913A-60.00B76.97
N0210X-0.222Y-2.868Z2.912A-60.00B78.16
N0211X-0.320Y-2.873Z2.911A-60.00B79.34
N0212X-0.378Y-2.879Z2.909A-60.00B80.53
N0213X-0.372Y-2.888Z2.909A-60.00B81.71
N0214X-0.425Y-2.887Z2.909A-60.00B82.89
N0215X-0.366Y-2.895Z2.910A-60.00B84.08
N0216X-0.307Y-2.900Z2.911A-60.00B85.26
N0217X-0.261Y-2.904Z2.911A-60.00B86.45
N0218X-0.161Y-2.909Z2.911A-60.00B87.63
N0219X-0.065Y-2.912Z2.911A-60.00B88.82
N0220X-0.004Y-2.912Z2.910A-60.00B90.00
N0221X0.082Y-2.911Z2.908A-60.00B91.45
N0222X0.168Y-2.907Z2.906A-60.00B92.90
N0223X0.252Y-2.902Z2.903A-60.00B94.35
N0224X0.336Y-2.895Z2.900A-60.00B95.81
N0225X0.419Y-2.886Z2.896A-60.00B97.26
N0226X0.501Y-2.875Z2.891A-60.00B98.71
N0227X0.581Y-2.862Z2.886A-60.00B 100.16
N0228X0.661Y-2.848Z2.880A-60.00B 101.61
N0229X0.739Y-2.831Z2.873A-60.00B 103.06
N0230X0.816Y-2.814Z2.866A-60.00B 104.52
N0231X0.892Y-2.794Z2.858A-60.00B 105.97
N0232X0.966Y-2.773Z2.849A-60.00B 107.42
N0233X1.039Y-2.750Z2.840A-60.00B 108.87
N0234X1.111Y-2.726Z2.831A-60.00B 110.32
N0235X1.181Y-2.700Z2.820A-60.00B 111.77
N0236X1.249Y-2.673Z2.809A-60.00B 113.23
N0237X1.316Y-2.644Z2.798A-60.00B 114.68
N0238X1.382Y-2.614Z2.786A-60.00B 116.13
N0239X1.446Y-2.583Z2.774A-60.00B 117.58
```

```
N0240X1.508Y-2.550Z2.761A-60.00B 119.03
N0241X1.569Y-2.516Z2.748A-60.00B 120.48
N0242X1.628Y-2.481Z2.734A-60.00B 121.94
N0243X1.686Y-2.445Z2.720A-60.00B 123.39
N0244X1.742Y-2.407Z2.706A-60.00B 124.84
N0245X1.797Y-2.368Z2.691A-60.00B 126.29
N0246X1.851Y-2.328Z2.676A-60.00B 127.74
N0247X1.903Y-2.287Z2.661A-60.00B 129.19
N0248X1.953Y-2.244Z2.646A-60.00B 130.65
N0249X2.003Y-2.200Z2.630A-60.00B 132.10
N0250X2.051Y-2.155Z2.615A-60.00B 133.55
N0251X2.097Y-2.108Z2.600A-60.00B 135.00
N0252X2.142Y-2.060Z2.584A-60.00B 136.45
N0253X2.186Y-2.011Z2.569A-60.00B 137.90
N0254X2.229Y-1.960Z2.554A-60.00B 139.35
N0255X2.271Y-1.908Z2.539A-60.00B 140.81
N0256X2.311Y-1.855Z2.524A-60.00B 142.26
N0257X2.350Y-1.800Z2.509A-60.00B 143.71
N0258X2.388Y-1.744Z2.495A-60.00B 145.16
N0259X2.425Y-1.686Z2.481A-60.00B 146.61
N0260X2.460Y-1.627Z2.468A-60.00B 148.06
N0261X2.495Y-1.566Z2.455A-60.00B 149.52
N0262X2.528Y-1.504Z2.442A-60.00B 150.97
N0263X2.559Y-1.440Z2.430A-60.00B 152.42
N0264X2.590Y-1.375Z2.418A-60.00B 153.87
N0265X2.619Y-1.309Z2.407A-60.00B 155.32
N0266X2.646Y-1.240Z2.397A-60.00B 156.77
N0267X2.673Y-1.171Z2.387A-60.00B 158.23
N0268X2.698Y-1.100Z2.377A-60.00B 159.68
N0269X2.721Y-1.028Z2.369A-60.00B 161.13
N0270X2.743Y-0.954Z2.360A-60.00B 162.58
N0271X2.763Y-0.879Z2.353A-60.00B 164.03
N0272X2.782Y-0.803Z2.346A-60.00B 165.48
N0273X2.799Y-0.726Z2.339A-60.00B 166.94
N0274X2.814Y-0.647Z2.333A-60.00B 168.39
N0275X2.828Y-0.567Z2.328A-60.00B 169.84
N0276X2.839Y-0.487Z2.324A-60.00B 171.29
N0277X2.850Y-0.405Z2.320A-60.00B 172.74
N0278X2.858Y-0.323Z2.317A-60.00B 174.19
N0279X2.864Y-0.240Z2.314A-60.00B 175.65
N0280X2.868Y-0.156Z2.312A-60.00B 177.10
N0281X2.871Y-0.072Z2.311A-60.00B 178.55
N0282X2.872Y 0.013Z2.310A-60.00B 180.00
N0283G4M4F.5
N0284X2.872Y-0.05Z3.81A-60B180
N0285M2
```

APPENDIX II.
DATABASE OF EXPERIMENTAL RESULTS

Pi -- Initial water pressure (MPa)
Po -- Operating water pressure (MPa)
Do -- Diameter of jewel nozzle orifice (mm)
Dt -- Diameter of focus tube (mm)
Sa -- Size of abrasive (mesh)
Ma -- Mass flow rate of abrasive (g/min)
Sd -- Stand off distance (mm)
U -- Cutting speed (cm/min)
H -- Depth of cut (mm)
Wt -- Top kerf width (mm)
Wb -- Buttom kerf Width at 8 mm deep (mm)
Tp -- Taper of kerf (degree)

Database I

(*** Use water nozzles and nozzle body of old design ***)
Pi = 331 MPa, Sa = 120 mesh, Sd = 2.5 mm

Cut No.	Do	Dt	Ma	U	H	Wt	Wb	Tp
S0012	0.305	1.143	266	10.16	21.85			
S0013	0.305	1.143	266	10.16	22.37			
S0014	0.305	1.143	266	15.24	17.51			
S0015	0.305	1.143	266	15.24	17.3			
S0016	0.305	1.143	266	15.24	17.83			
S0017	0.305	1.143	266	15.24	17.89			
S0018	0.305	1.143	266	15.24	17.13			
S0019	0.305	1.143	266	15.24	17.55			
S001A	0.305	1.143	266	10.16	24.59			
S001B	0.305	1.143	266	10.16	22.92			
S001C	0.305	1.143	266	10.16	22.84			
S0021	0.305	1.143	330	20.32	9.1	1.209	0.725	1.733
S0022	0.305	1.143	330	20.32	10.46	1.244	0.607	2.280
S0023	0.305	1.143	330	20.32	10.38	1.254	0.688	2.026
S0024	0.305	1.143	330	15.24	13.81	1.262	0.574	2.462
S0025	0.305	1.143	330	15.24	14.6	1.33	0.619	2.544
S0026	0.305	1.143	330	15.24	14.98	1.275	0.531	2.662
S0027	0.305	1.143	330	10.16	20.95	1.332	0.82	1.833
S0028	0.305	1.143	330	10.16	21.75	1.327	0.781	1.954
S0029	0.305	1.143	330	10.16	21.38	1.373	0.904	1.679
S002A	0.305	1.143	330	25.4	8.92	1.276	0.839	1.565
S002B	0.305	1.143	330	25.4	9.06	1.273	0.79	1.729
S002C	0.305	1.143	330	25.4	9.04	1.25	0.719	1.901

Database II

(*** Use water nozzle and nozzle body of new design ***)
Pi = 331 MPa, Sa = 120 mesh, Sd = 2.5 mm

Cut No.	Do	Dt	Ma	U	H	Wt	Wb	Tp
S0031	0.254	1.143	273	10.16	21.83	1.438	0.846	2.119
S0032	0.254	1.143	273	10.16	22.52	1.61	1.04	2.040
S0033	0.254	1.143	273	10.16	23.38	1.613	1.003	2.183
S0034	0.254	1.143	273	15.24	15.55	1.44	0.685	2.702
S0035	0.254	1.143	273	15.24	16.58	1.395	0.7	2.487
S0036	0.254	1.143	273	15.24	16.33	1.482	0.7	2.798
S0037	0.254	1.143	273	20.32	11.22	1.441	0.6	3.009
S0038	0.254	1.143	273	20.32	10.51	1.467	0.556	3.259
S0039	0.254	1.143	273	20.32	10.87	1.447	0.603	3.020
S003A	0.254	1.143	273	25.4	9.67	1.419	0.574	3.023
S003B	0.254	1.143	273	25.4	9.08	1.481	0.659	2.941
S003C	0.254	1.143	273	25.4	9.38	1.473	0.566	3.244

Database III

(*** Use water nozzles and nozzle body of old design ***)
Pi = 331 MPa, Sa = 50 mesh, Sd = 2.5 mm

Cut No.	Do	Dt	Ma	U	H
S0041	0.254	0.83	193	7.62	22.27
S0042	0.254	0.83	193	7.62	22.27
S0043	0.254	0.83	193	7.62	22.27
S0044	0.254	0.83	193	7.62	22.27
S0045	0.254	0.83	193	15.24	12.1
S0046	0.254	0.83	193	15.24	12.14
S0047	0.254	0.83	193	10.16	16.66
S0048	0.254	0.83	193	10.16	16.71
S0049	0.254	0.83	193	10.16	16.37
S004A	0.254	0.83	193	20.32	8.73
S004b	0.254	0.83	193	20.32	9.11
S004C	0.254	0.83	193	20.32	8.69
S0051	0.254	0.83	265	7.62	23.3
S0052	0.254	0.83	265	7.62	23.53
S0053	0.254	0.83	265	7.62	23.53
S0054	0.254	0.83	265	10.16	20.07
S0055	0.254	0.83	265	10.16	19.55
S0056	0.254	0.83	265	10.16	19.55
S0057	0.254	0.83	265	15.24	13.91
S0058	0.254	0.83	265	15.24	14.43
S0059	0.254	0.83	265	15.24	13.98
S005A	0.254	0.83	265	20.32	10.98
S005B	0.254	0.83	265	20.32	10.57
S005C	0.254	0.83	265	20.32	10.96

Database IV

(*** Use water nozzle and nozzle body of new design ***)
Pi = 345 MPa, Sa = 220 mesh, Sd = 2.5 mm

Cut No.	Do	Dt	Ma	U	H	Wt	Wb	Tp
S0081	0.254	0.84	132	6	22.78			
S0082	0.254	0.84	132	6	22.59			
S0083	0.254	0.84	132	6	23:07			
S0084	0.254	0.84	132	8	18.46			
S0085	0.254	0.84	132	8	18.55			
S0086	0.254	0.84	132	8	18.23			
S0087	0.254	0.84	132	10	14.75			
S0088	0.254	0.84	132	10	14.77			
S0089	0.254	0.84	132	10	14.98			
S008A	0.254	0.84	132	12	13.05			
S008B	0.254	0.84	132	12	13.06			
S008C	0.254	0.84	132	12	13.86			
S0091	0.254	0.84	155	7	22.25	1.061	0.581	1.718
S0092	0.254	0.84	155	7	20.94	1.016	0.532	1.733
S0093	0.254	0.84	155	7	20.57	0.998	0.551	1.600
S0094	0.254	0.84	155	9	17.98	0.971	0.449	1.869
S0095	0.254	0.84	155	9	17.8	0.977	0.451	1.883
S0096	0.254	0.84	155	9	18.05	1.003	0.476	1.886
S0097	0.254	0.84	155	12	14	0.958	0.33	2.248
S0098	0.254	0.84	155	12	14.88	0.973	0.428	1.951
S0099	0.254	0.84	155	12	14.55	0.98	0.451	1.894
S009A	0.254	0.84	155	15	11.64	0.96	0.272	2.462
S009B	0.254	0.84	155	15	11.98	0.935	0.391	1.947
S009C	0.254	0.84	155	15	11.96	0.831	0.311	1.861
S0101	0.254	0.84	195	8	22	1.099	0.587	1.833
S0102	0.254	0.84	195	8	21.36	1.13	0.64	1.754
S0103	0.254	0.84	195	8	21	1.102	0.629	1.693
S0104	0.254	0.84	195	11	16.63	1.044	0.502	1.940
S0105	0.254	0.84	195	11	15.48	1.028	0.449	2.072
S0106	0.254	0.84	195	11	15.76	1.041	0.444	2.137
S0107	0.254	0.84	195	13	14.73	1.009	0.516	1.765
S0108	0.254	0.84	195	13	14.66	1.029	0.454	2.058
S0109	0.254	0.84	195	13	13.95	1.032	0.434	2.140
S010A	0.254	0.84	195	15	12.68	1.027	0.348	2.430
S010B	0.254	0.84	195	15	12	1.033	0.379	2.341
S010C	0.254	0.84	195	15	12.24	1.014	0.313	2.509
S0111	0.362	1.078	165	7	17.97	1.197	0.499	2.498
S0112	0.362	1.078	165	7	19.06	1.329	0.712	2.208
S0113	0.362	1.078	165	7	18.47	1.251	0.653	2.140
S0114	0.362	1.078	165	9	15.03	1.249	0.591	2.355
S0115	0.362	1.078	165	9	15.34	1.256	0.563	2.480

Cut No.	Do	Dt	Ma	U	H	Wt	Wb	Tp
S0116	0.362	1.078	165	9	15.13	1.27	0.626	2.305
S0117	0.362	1.078	165	11	12.72	1.27	0.491	2.787
S0118	0.362	1.078	165	11	13.06	1.262	0.459	2.873
S0119	0.362	1.078	165	11	12.89	1.243	0.539	2.519
S011A	0.362	1.078	165	13	10.68	1.273	0.588	2.451
S011B	0.362	1.078	165	13	10.98	1.289	0.48	2.895
S011C	0.362	1.078	165	13	11.34	1.271	0.519	2.691
S0121	0.362	1.078	202	7	21.66	1.386	0.738	2.319
S0122	0.362	1.078	202	7	20.95	1.367	0.701	2.384
S0123	0.362	1.078	202	7	21.94	1.382	0.742	2.291
S0124	0.362	1.078	202	9	18.09	1.308	0.681	2.244
S0125	0.362	1.078	202	9	17.46	1.35	0.646	2.519
S0126	0.362	1.078	202	9	17.27	1.381	0.668	2.552
S0127	0.362	1.078	202	11	14.51	1.352	0.522	2.970
S0128	0.362	1.078	202	11	14.5	1.364	0.521	3.016
S0129	0.362	1.078	202	11	14:14	1.38	0.647	2.623
S012A	0.362	1.078	202	13	12.78	1.37	0.556	2.912
S012B	0.362	1.078	202	13	13.57	1.332	0.528	2.877
S012C	0.362	1.078	202	13	13.03	1.282	0.465	2.923
S0131	0.362	1.078	236	7	23.93	1.159	0.429	2.612
S0132	0.362	1.078	236	7	23.72	1.51	0.887	2.230
S0133	0.362	1.078	236	7	22.82	1.407	0.705	2.512
S0134	0.362	1.078	236	9	20.16	1.37	0.698	2.405
S0135	0.362	1.078	236	9	19.64	1.358	0.671	2.459
S0136	0.362	1.078	236	9	19.93	1.364	0.653	2.544
S0137	0.362	1.078	236	11	16.57	1.301	0.642	2.359
S0138	0.362	1.078	236	11	16.3	1.328	0.636	2.476
S0139	0.362	1.078	236	11	15.98	1.363	0.703	2.362
S013A	0.362	1.078	236	13	14.18	1.352	0.619	2.623
S013B	0.362	1.078	236	13	14.28	1.335	0.604	2.616
S013C	0.362	1.078	236	13	14.24	1.305	0.541	2.734

Database V

(*** Use water nozzles and nozzle body of new design ***)
P = 345 MPa, Sa = 80 mesh (Barton's HPE), Sd = 2.5 mm

Cut No.	Do	Dt	Ma	U	H	Wt	Wb	Tp
S0141	0.152	0.838	204	8	13.73	1.184	0.75	1.554
S0142	0.152	0.838	204	8	13.43	1.237	0.757	1.718
S0143	0.152	0.838	204	8	13.33	1.25	0.761	1.751
S0144	0.152	0.838	204	6	16.77	1.29	0.914	1.346
S0145	0.152	0.838	204	6	16.63	1.319	0.845	1.697
S0146	0.152	0.838	204	6	17.09	1.374	0.918	1.632
S0147	0.152	0.838	204	10	11.59	1.269	0.665	2.162
S0148	0.152	0.838	204	10	10.53	1.318	0.636	2.441
S0149	0.152	0.838	204	10	10.52	1.324	0.696	2.248
S014A	0.152	0.838	204	12	8.81	1.33	0.684	2.312
S014B	0.152	0.838	204	12	8.7	1.335	0.622	2.552
S014C	0.152	0.838	204	12	8.8	1.337	0.656	2.437
S0151	0.152	0.838	255	5	18.76	1.2	0.807	1.407
S0152	0.152	0.838	255	5	19.21	1.385	0.988	1.421
S0153	0.152	0.838	255	5	18.94	1.414	1.017	1.421
S0154	0.152	0.838	255	8	12.8	1.315	0.765	1.969
S0155	0.152	0.838	255	8	12.78	1.287	0.765	1.869
S0156	0.152	0.838	255	8	13.25	1.262	0.775	1.743
S0157	0.152	0.838	255	10	10.69	1.227	0.721	1.811
S0158	0.152	0.838	255	10	10.71	1.255	0.72	1.915
S0159	0.152	0.838	255	10	10.37	1.233	0.706	1.886
S015A	0.152	0.838	255	12	9	1.23	0.777	1.622
S015B	0.152	0.838	255	12	8.59	1.285	0.673	2.190
S015C	0.152	0.838	255	12	8.74	1.292	0.704	2.105
S0163	0.203	1.118	229	7	20.94	1.524	1.068	1.632
S0164	0.203	1.118	229	9	17.4	1.454	0.904	1.969
S0165	0.203	1.118	229	9	17.31	1.466	0.924	1.940
S0166	0.203	1.118	229	9	16.6	1.502	0.904	2.140
S0167	0.203	1.118	229	12	13.68	1.449	0.812	2.280
S0168	0.203	1.118	229	12	13.6	1.484	0.782	2.512
S0169	0.203	1.118	229	12	13.02	1.508	0.783	2.594
S016A	0.203	1.118	229	14	11.13	1.485	0.6	3.166
S016B	0.203	1.118	229	14	11.62	1.456	0.653	2.873
S016C	0.203	1.118	229	14	11.91	1.452	0.675	2.780
S0171	0.203	1.118	292	7	23.04	1.329	0.814	1.844
S0172	0.203	1.118	292	7	24.06	1.635	1.241	1.411
S0173	0.203	1.118	292	7	24.01	1.584	1.182	1.439
S0174	0.203	1.118	292	9	19.1	1.48	1.015	1.665
S0175	0.203	1.118	292	9	18.82	1.504	1.021	1.729
S0176	0.203	1.118	292	9	19.22	1.526	1.038	1.747

Cut No.	Do	Dt	Ma	U	H	Wt	Wb	Tp
S0177	0.203	1.118	292	12	14.7	1.496	0.88	2.205
S0178	0.203	1.118	292	12	14.16	1.5	0.95	1.969
S0179	0.203	1.118	292	12	14.41	1.545	0.89	2.344
S017A	0.203	1.118	292	14	12.59	1.517	0.744	2.766
S017B	0.203	1.118	292	14	12.74	1.55	0.79	2.720
S017C	0.203	1.118	292	14	11.83	1.494	0.764	2.612

Database VI

(*** Use water nozzles and nozzle body of new design ***)
P = 345 MPa, Sa = 50 mesh, Sd = 2.54 mm

Cut No.	Do	Dt	Ma	U	H	Wt	Wb	Tp
S0181	0.305	1.117	154	7	19.3	1.295	0.824	1.686
S0182	0.305	1.117	154	7	19.1	1.47	1.046	1.518
S0183	0.305	1.117	154	7	20.5	1.509	1.117	1.403
S0184	0.305	1.117	154	9	15.2	1.404	0.857	1.958
S0185	0.305	1.117	154	9	16	1.401	0.859	1.940
S0186	0.305	1.117	154	9	15.2	1.42	0.839	2.080
S0187	0.305	1.117	154	11	12.8	1.398	0.688	2.541
S0188	0.305	1.117	154	11	11.9	1.426	0.729	2.494
S0189	0.305	1.117	154	11	12.6	1.39	0.787	2.158
S018A	0.305	1.117	154	14	9.9	1.34	1.062	0.995
S018B	0.305	1.117	154	14	9.9	1.38	0.748	2.262
S018C	0.305	1.117	154	14	10.1	1.365	0.808	1.994
S0191	0.305	1.117	197	7	22.71	1.159	0.792	1.314
S0192	0.305	1.117	197	7	22.58	1.377	1.105	0.974
S0193	0.305	1.117	197	7	22.3	1.408	1.135	0.978
S0194	0.305	1.117	197	10	16.06	1.318	0.896	1.511
S0195	0.305	1.117	197	10	16.61	1.32	0.915	1.450
S0196	0.305	1.117	197	10	16.92	1.306	0.94	1.310
S0197	0.305	1.117	197	12	13.82	1.287	0.796	1.758
S0198	0.305	1.117	197	12	13.98	1.264	0.836	1.532
S0199	0.305	1.117	197	12	13.9	1.294	0.803	1.758
S019A	0.305	1.117	197	14	11.69	1.284	0.772	1.833
S019B	0.305	1.117	197	14	11.87	1.287	0.73	1.994
S019C	0.305	1.117	197	14	11.88	1.207	0.76	1.600
S0201	0.254	1.089	175	7	19.39	1.399	0.959	1.575
S0202	0.254	1.089	175	7	19.26	1.379	1.012	1.314
S0203	0.254	1.089	175	7	19.4	1.402	1.065	1.207
S0204	0.254	1.089	175	9	16.25	1.35	0.868	1.726
S0205	0.254	1.089	175	9	16.08	1.338	0.913	1.522
S0206	0.254	1.089	175	9	16.65	1.397	0.869	1.890
S0207	0.254	1.089	175	12	12.53	1.387	0.75	2.280
S0208	0.254	1.089	175	12	9.55	1.361	0.803	1.997
S0209	0.254	1.089	175	12	12.12	1.407	0.797	2.183
S020A	0.254	1.089	175	14	10.29	1.358	0.749	2.180
S020B	0.254	1.089	175	14	10.12	1.406	0.791	2.201
S020C	0.254	1.089	175	14	9.71	1.438	0.956	1.726
S0211	0.254	1.14	228	7	22.97	1.327		
S0212	0.254	1.14	228	8	19.95	1.481		
S0213	0.254	1.14	228	8	20.63	1.565		
S0214	0.254	1.14	228	10	16.74	1.441		
S0215	0.254	1.14	228	10	16.74	1.413		

Cut No.	Do	Dt	Ma	U	H	Wt	Wb	Tp
S0216	0.254	1.14	228	10	16.93	1.455		
S0217	0.254	1.14	228	12	14.06	1.432		
S0218	0.254	1.14	228	12	13.83	1.447		
S0219	0.254	1.14	228	12	14.19	1.471		
S021A	0.254	1.14	228	14	11.92	1.411		
S021B	0.254	1.14	228	14	11.48	1.434		
S021C	0.254	1.14	228	14	11.45	1.451		
S0221	0.254	0.869	228	8	22.39	1.102	0.732	1.325
S0222	0.254	0.869	228	9	20.11	1.212	0.882	1.182
S0223	0.254	0.869	228	9	20.23	1.164	0.86	1.088
S0224	0.254	0.869	228	11	16.8	1.158	0.75	1.461
S0225	0.254	0.869	228	11	16.8	1.131	0.77	1.293
S0226	0.254	0.869	228	11	17.4	1.166	0.747	1.500
S0227	0.254	0.869	228	13	15.06	1.14	0.677	1.658
S0228	0.254	0.869	228	13	14.94	1.14	0.721	1.500
S0229	0.254	0.869	228	13	14.38	1.167	0.749	1.497
S022A	0.254	0.869	228	15	13.49	1.151	0.683	1.675
S022B	0.254	0.869	228	15	12.62	1.167	0.722	1.593
S022C	0.254	0.869	228	15	13.27	1.154	0.656	1.783
S0231	0.254	0.9	180	8	20.65	0.966	0.724	0.867
S0232	0.254	0.9	180	8	20.21	1.176	0.931	0.877
S0233	0.254	0.9	180	8	20.18	1.12	0.876	0.874
S0234	0.254	0.9	180	10	16.71	1.053	0.783	0.967
S0235	0.254	0.9	180	10	16.24	1.109	0.78	1.178
S0236	0.254	0.9	180	10	16.66	1.111	0.766	1.235
S0237	0.254	0.9	180	12	14.3	1.077	0.762	1.128
S0238	0.254	0.9	180	12	14.49	1.114	0.73	1.375
S0239	0.254	0.9	180	12	13.78	1.156	0.77	1.382
S023A	0.254	0.9	180	16	10.77	1.17	0.749	1.507
S023B	0.254	0.9	180	16	10.44	1.178	0.719	1.643
S023C	0.254	0.9	180	16	11.3	1.246	0.701	1.951
S0241	0.254	1.773	209	8	12.45	2.011	1.14	3.116
S0242	0.254	1.773	209	8	12.57	2.08	1.13	3.398
S0243	0.254	1.773	209	8	12.29	2.053	1.162	3.187
S0244	0.254	1.773	209	6	17.22	2.279	1.542	2.637
S0245	0.254	1.773	209	6	17.07	2.079	1.321	2.712
S0246	0.254	1.773	209	6	17	2.205	1.435	2.755
S0247	0.254	1.773	209	10	9.17	2.054	0.995	3.787
S0248	0.254	1.773	209	10	8.1	2.029	0.944	3.879
S0249	0.254	1.773	209	10	8.75	2.072	1.08	3.548
S024A	0.254	1.773	209	12	7			
S024B	0.254	1.773	209	12	6.9			
S024C	0.254	1.773	209	12	7.14			

Database VII

(*** Use water nozzle and nozzle body of new design ***)
Pi = 345 MPa, Sd = 2.5 mm

Cut No.	Ds	Dt	Ma	U	H	Wt	Wb	Tp
S0251	0.254	0.851	211	8	25.6	1.072	0.777	1.056
S0252	0.254	0.851	211	9	25.22	1.297	0.945	1.260
S0253	0.254	0.851	211	10	23.82	1.204	0.824	1.361
S0254	0.254	0.851	211	13	18.87	1.143	0.695	1.604
S0255	0.254	0.851	211	13	19.45	1.119	0.71	1.464
S0256	0.254	0.851	211	13	19.16	1.14	0.715	1.522
S0257	0.254	0.851	211	15	16.17	1.148	0.644	1.804
S0258	0.254	0.851	211	15	16.21	1.128	0.642	1.740
S0259	0.254	0.851	211	15	16.13	1.193	0.681	1.833
S025A	0.254	0.851	211	17	14.68	1.182	0.609	2.051
S025B	0.254	0.851	211	17	14.34	1.203	0.633	2.040
S025C	0.254	0.851	211	17	15.03	1.142	0.584	1.997
S0261	0.254	0.851	256	11	23.75	1.203	0.803	1.432
S0262	0.254	0.851	256	11	22.92	1.315	0.9	1.486
S0263	0.254	0.851	256	11	21.83	1.234	0.849	1.378
S0264	0.254	0.851	256	14	18.95	1.19	0.752	1.568
S0265	0.254	0.851	256	14	18.78	1.156	0.66	1.776
S0266	0.254	0.851	256	14	19.17	1.209	0.775	1.554
S0267	0.254	0.851	256	17	15.89	1.229	0.653	2.062
S0268	0.254	0.851	256	17	15.16	1.192	0.661	1.901
S0269	0.254	0.851	256	17	15.88	1.25	0.722	1.890
S026A	0.254	0.851	256	17	16.46	1.2	0.698	1.797
S026B	0.254	0.851	256	20	13.22	1.163	0.624	1.929
S026C	0.254	0.851	256	20	13.88	1.217	0.562	2.344
S0271	0.254	1.195	209	10	20.34	1.558	1.014	1.947
S0272	0.254	1.195	209	10	19.58	1.511	0.986	1.879
S0273	0.254	1.195	209	10	20.18	1.575	1.042	1.908
S0274	0.254	1.195	209	12	17.42	1.487	0.875	2.190
S0275	0.254	1.195	209	12	16.68	1.48	0.85	2.255
S0276	0.254	1.195	209	12	16.29	1.504	0.85	2.341
S0277	0.254	1.195	209	14	13.91	1.479	0.79	2.466
S0278	0.254	1.195	209	14	14.13	1.477	0.77	2.530
S0279	0.254	1.195	209	14	14.9	1.529	0.82	2.537
S027A	0.254	1.195	209	16	12.43	1.48	0.753	2.602
S027B	0.254	1.195	209	16	12.99	1.501	0.727	2.770
S027C	0.254	1.195	209	16	12.52	1.491	0.671	2.934
S0281	0.254	1.195	262	12	19.68	1.454	0.923	1.901
S0282	0.254	1.195	262	12	19.16	1.548	1.005	1.944
S0283	0.254	1.195	262	12	19.03	1.488	0.956	1.904
S0284	0.254	1.195	262	16	13.11	1.444	0.745	2.502
S0285	0.254	1.195	262	16	14	1.468	0.75	2.569

Cut No.	Ds	Dt	Ma	U	H	Wt	Wb	Tp
S0286	0.254	1.195	262	16	14.25	1.513	0.759	2.698
S0287	0.254	1.195	262	14	15.47	1.533	0.832	2.509
S0288	0.254	1.195	262	14	15.6	1.537	0.864	2.409
S0289	0.254	1.195	262	14	15.72	1.561	0.866	2.487
S028A	0.254	1.195	262	18	12.14	1.514	0.711	2.873
S028B	0.254	1.195	262	18	12.4	1.536	0.742	2.841
S028C	0.254	1.195	262	18	11.94	1.515	0.659	3.062
S0291	0.254	1.81	263	12	11.89	2.11	0.97	4.075
S0292	0.254	1.81	263	12	12.17	2.11	0.862	4.460
S0293	0.254	1.81	263	12	11.94	2.16	0.926	4.410
S0294	0.254	1.81	263	10	15.18	2.18	1	4.218
S0295	0.254	1.81	263	10	14.33	2.21	1.013	4.278
S0296	0.254	1.81	263	10	14.03	2.218	1.011	4.314
S0297	0.254	1.81	263	8	17.25	2.303	1.224	3.858
S0298	0.254	1.81	263	8	18.24	2.22	1.264	3.419
S0299	0.254	1.81	263	8	17.92	2.204	1.202	3.583
S029A	0.254	1.81	263	14	9.42	2.192	0.973	4.357
S029B	0.254	1.81	263	14	9.22	2.256	0.965	4.613
S029C	0.254	1.81	263	14	9.18	2.3	0.831	5.246
S0301	0.254	1.81	295	8	19.12	2.16	1.3	3.077
S0302	0.254	1.81	295	8	18.32	2.17	1.34	2.970
S0303	0.254	1.81	295	8	18.97	2.16	1.31	3.041
S0304	0.254	1.81	295	10	14.95	2.14	1.04	3.933
S0305	0.254	1.81	295	10	14.05	2.14	1.08	3.790
S0306	0.254	1.81	295	10	14.75	2.2	1.1	3.933
S0307	0.254	1.81	295	12	10.98	2.17	1.03	4.075
S0308	0.254	1.81	295	12	11.32	2.28	0.93	4.823
S0309	0.254	1.81	295	12	11.94	2.21	0.97	4.432
S030A	0.254	1.81	295	14	9.13	2.26	0.94	4.716
S030B	0.254	1.81	295	14	8.94	2.27	0.97	4.645
S030C	0.254	1.81	295	14	8.84	2.22	0.78	5.143
S0311	0.308	0.825	212	7	25.5	1.004	0.416	2.105
S0312	0.308	0.825	212	8	25.3	1.278	0.881	1.421
S0313	0.308	0.825	212	8	25.5	1.36	0.884	1.704
S0314	0.308	0.825	212	11	19.6	1.227	0.712	1.844
S0315	0.308	0.825	212	11	21.3	1.166	0.655	1.829
S0316	0.308	0.825	212	11	21.1	1.239	0.68	2.001
S0317	0.308	0.825	212	14	16.8	1.203	0.6	2.158
S0318	0.308	0.825	212	14	17.1	1.199	0.692	1.815
S0319	0.308	0.825	212	14	15.8	1.241	0.655	2.098
S031A	0.308	0.825	212	17	14.2	1.241	0.55	2.473
S031B	0.308	0.825	212	17	14.9	1.189	0.55	2.287
S031C	0.308	0.825	212	17	14	1.196	0.56	2.276
S0321	0.308	0.825	275	9	25.6	1.077	0.656	1.507
S0322	0.308	0.825	275	10	24.6	1.383	0.969	1.482
S0323	0.308	0.825	275	10	25	1.265	0.85	1.486
S0324	0.308	0.825	275	13	21.2	1.195	0.714	1.722

Cut No.	Ds	Dt	Ma	U	H	Wt	Wb	Tp
S0325	0.308	0.825	275	13	20.7	1.141	0.715	1.525
S0326	0.308	0.825	275	13	20.7	1.178	0.695	1.729
S0327	0.308	0.825	275	16	16.6	1.149	0.544	2.165
S0328	0.308	0.825	275	16	16.7	1.157	0.671	1.740
S0329	0.308	0.825	275	16	16.1	1.163	0.677	1.740
S032A	0.308	0.825	275	20	14.6	1.15	0.624	1.883
S032B	0.308	0.825	275	20	14.1	1.168	0.595	2.051
S032C	0.308	0.825	275	20	14.2	1.136	0.61	1.883
S0331	0.308	1.146	278	10	24.6	1.249	0.646	2.158
S0332	0.308	1.146	278	10	23.7	1.46	0.994	1.668
S0333	0.308	1.146	278	10	22.7	1.435	0.965	1.683
S0334	0.308	1.146	278	13	18.9	1.423	0.857	2.026
S0335	0.308	1.146	278	13	19.6	1.398	0.856	1.940
S0336	0.308	1.146	278	13	20	1.383	0.868	1.844
S0337	0.308	1.146	278	16	15.1	1.381	0.751	2.255
S0338	0.308	1.146	278	16	16.4	1.374	0.729	2.308
S0339	0.308	1.146	278	16	15	1.414	0.787	2.244
S033A	0.308	1.146	278	19	13.4	1.366	0.734	2.262
S033B	0.308	1.146	278	19	13.2	1.404	0.698	2.527
S033C	0.308	1.146	278	19	12.2	1.358	0.718	2.291
S0341	0.308	1.146	210	10	18.5	1.386	0.784	2.155
S0342	0.308	1.146	210	10	18.6	1.42	0.802	2.212
S0343	0.308	1.146	210	10	19.8	1.502	0.923	2.072
S0344	0.308	1.146	210	12	16.9	1.408	0.935	1.693
S0345	0.308	1.146	210	12	17.4	1.461	0.836	2.237
S0346	0.308	1.146	210	12	16.8	1.379	0.803	2.062
S0347	0.308	1.146	210	15	12.6	1.385	0.689	2.491
S0348	0.308	1.146	210	15	12.5	1.39	0.739	2.330
S0349	0.308	1.146	210	15	13	1.41	0.756	2.341
S034A	0.308	1.146	210	18	10.7	1.391	0.693	2.498
S034B	0.308	1.146	210	18	10.4	1.387	0.663	2.591
S034C	0.308	1.146	210	18	11	1.413	0.671	2.655
S0351	0.308	1.86	210	9	13	1.98	1.055	3.309
S0352	0.308	1.86	210	9	14.6	2.029	1.058	3.473
S0353	0.308	1.86	210	9	14.5	2.073	1.014	3.787
S0354	0.308	1.86	210	7	18.2	2.077	1.258	2.930
S0355	0.308	1.86	210	7	18	2.115	1.221	3.198
S0356	0.308	1.86	210	7	18.5	2.132	1.154	3.498
S0357	0.308	1.86	210	11	10.1	2.06	0.862	4.282
S0358	0.308	1.86	210	11	9.3	2.101	0.747	4.837
S0359	0.308	1.86	210	11	10.2	2.093	0.958	4.058
S035A	0.308	1.86	210	13	7.7	2.08	0.747	4.837
S035B	0.308	1.86	210	13	7.8	2.058	0.747	4.837
S035C	0.308	1.86	210	13	7.8	2.083	0.747	4.837
S0361	0.308	1.86	277	9	17	1.999	1.116	3.159
S0362	0.308	1.86	277	9	16.5	2.097	1.191	3.241
S0363	0.308	1.86	277	9	17.5	2.131	1.197	3.341

Cut No.	Ds	Dt	Ma	U	H	Wt	Wb	Tp
S0364	0.308	1.86	277	11	12.2	2.044	0.964	3.862
S0365	0.308	1.86	277	11	12.6	2.066	0.954	3.976
S0366	0.308	1.86	277	11	12.7	2.084	0.929	4.129
S0367	0.308	1.86	277	7	20.8	2.134	1.416	2.569
S0368	0.308	1.86	277	7	20.8	2.091	1.33	2.723
S0369	0.308	1.86	277	7	20.8	2.3	1.479	2.937
S036A	0.308	1.86	277	14	8.6	2.103	0.922	4.221
S036B	0.308	1.86	277	14	9	2.056	0.958	3.926
S036C	0.308	1.86	277	14	8.8	2.122	0.957	4.164
S0371	0.365	0.902	284	8	25.4	1.186	0.714	1.690
S0372	0.365	0.902	284	9	25.3	1.274	0.86	1.482
S0373	0.365	0.902	284	10	24.6	1.252	0.833	1.500
S0374	0.365	0.902	284	13	24.1	1.259	0.773	1.740
S0375	0.365	0.902	284	13	23.1	1.196	0.751	1.593
S0376	0.365	0.902	284	13	23.2	1.21	0.732	1.711
S0377	0.365	0.902	284	16	18.8	1.138	0.716	1.511
S0378	0.365	0.902	284	16	19.2	1.194	0.712	1.726
S0379	0.365	0.902	284	16	18.9	1.198	0.71	1.747
S037A	0.365	0.902	284	19	15.9	1.163	0.64	1.872
S037B	0.365	0.902	284	19	16.3	1.187	0.701	1.740
S037C	0.365	0.902	284	19	16.2	1.117	0.616	1.793
S0381	0.365	0.902	220	9	25.5	1.289	0.884	1.450
S0382	0.365	0.902	220	10	22.8	1.323	0.904	1.500
S0383	0.365	0.902	220	10	23.4	1.259	0.793	1.668
S0384	0.365	0.902	220	13	18.8	1.214	0.7	1.840
S0385	0.365	0.902	220	13	18.5	1.26	0.723	1.922
S0386	0.365	0.902	220	13	18.9	1.21	0.712	1.783
S0387	0.365	0.902	220	16	16	1.205	0.623	2.083
S0388	0.365	0.902	220	16	15.9	1.188	0.65	1.926
S0389	0.365	0.902	220	16	15.2	1.182	0.688	1.768
S038A	0.365	0.902	220	19	12	1.221	0.601	2.219
S038B	0.365	0.902	220	19	12.9	1.157	0.581	2.062
S038C	0.365	0.902	220	19	12.5	1.18	0.6	2.076
S0391	0.365	1.186	218	10	20.3	1.258	0.538	2.577
S0392	0.365	1.186	218	10	20.8	1.541	1.005	1.919
S0393	0.365	1.186	218	10	20.8	1.457	0.882	2.058
S0394	0.365	1.186	218	13	15.5	1.432	0.742	2.469
S0395	0.365	1.186	218	13	16.3	1.426	0.732	2.484
S0396	0.365	1.186	218	13	16.4	1.441	0.749	2.476
S0397	0.365	1.186	218	8	22.8	1.491	0.937	1.983
S0398	0.365	1.186	218	8	23.7	1.443	0.964	1.715
S0399	0.365	1.186	218	8	23.6	1.619	1.23	1.393
S039A	0.365	1.186	218	15	13.9	1.41	0.754	2.348
S039B	0.365	1.186	218	15	14.1	1.446	0.808	2.283
S039C	0.365	1.186	218	15	13.9	1.41	0.766	2.305
S0401	0.365	1.186	280	10	22.7	1.512	0.976	1.919
S0402	0.365	1.186	280	10	23.9	1.582	1.012	2.040

Cut No.	Ds	Dt	Ma	U	H	Wt	Wb	Tp
S0403	0.365	1.186	280	10	24.1	1.554	1.027	1.886
S0404	0.365	1.186	280	13	18.4	1.452	0.829	2.230
S0405	0.365	1.186	280	13	19.5	1.461	0.841	2.219
S0406	0.365	1.186	280	13	19.7	1.503	0.905	2.140
S0407	0.365	1.186	280	16	16.1	1.463	0.761	2.512
S0408	0.365	1.186	280	16	15.3	1.454	0.787	2.387
S0409	0.365	1.186	280	16	15.2	1.497	0.822	2.416
S040A	0.365	1.186	280	19	12.5	1.448	0.738	2.541
S040B	0.365	1.186	280	19	13.1	1.468	0.685	2.802
S040C	0.365	1.186	280	19	13.5	1.414	0.697	2.566
S0411	0.365	1.79	273	10	16	2.188	1.03	4.140
S0412	0.365	1.79	273	10	15.1	2.219	1.19	3.680
S0413	0.365	1.79	273	10	15.7	2.192	1.143	3.751
S0414	0.365	1.79	273	8	18.5	2.18	1.28	3.219
S0415	0.365	1.79	273	8	18.8	2.242	1.345	3.209
S0416	0.365	1.79	273	8	18.8	2.193	1.315	3.141
S0417	0.365	1.79	273	13	11.1	2.104	0.976	4.033
S0418	0.365	1.79	273	13	12.7	2.156	0.957	4.286
S0419	0.365	1.79	273	13	11.6	2.131	0.906	4.378
S041A	0.365	1.79	273	15	8.8	2.169	1.082	3.887
S041B	0.365	1.79	273	15	9.4	2.059	1.239	2.934
S041C	0.365	1.79	273	15	9.3	2.107	1.097	3.612
S0421	0.226	0.812	210	10	19.8	1.219	0.636	2.087
S0422	0.226	0.812	210	10	19.8	1.261	0.846	1.486
S0423	0.226	0.812	210	10	20.1	1.251	0.861	1.396
S0424	0.226	0.812	210	13	16.6	1.194	0.684	1.826
S0425	0.226	0.812	210	13	15.7	1.151	0.691	1.647
S0426	0.226	0.812	210	13	15.5	1.169	0.672	1.779
S0427	0.226	0.812	210	16	12.4	1.143	0.617	1.883
S0428	0.226	0.812	210	16	13.1	1.161	0.655	1.811
S0429	0.226	0.812	210	16	13	1.133	0.619	1.840
S042A	0.226	0.812	210	19	11.6	1.137	0.514	2.230
S042B	0.226	0.812	210	19	11.3	1.193	0.574	2.216
S042C	0.226	0.812	210	19	11.9	1.104	0.493	2.187
S0431	0.226	0.812	276	10	22.1	1.274	0.867	1.457
S0432	0.226	0.812	276	10	22	1.317	0.944	1.335
S0433	0.226	0.812	276	10	21.8	1.276	0.909	1.314
S0434	0.226	0.812	276	13	17.9	1.208	0.77	1.568
S0435	0.226	0.812	276	13	18.2	1.194	0.757	1.565
S0436	0.226	0.812	276	13	18.2	1.2	0.778	1.511
S0437	0.226	0.812	276	16	14.6	1.172	0.696	1.704
S0438	0.226	0.812	276	16	14.4	1.15	0.708	1.582
S0439	0.226	0.812	276	16	15.2	1.215	0.769	1.597
S043A	0.226	0.812	276	19	12.2	1.15	0.642	1.819
S043B	0.226	0.812	276	19	11.2	1.156	0.626	1.897
S043C	0.226	0.812	276	19	11.3	1.14	0.538	2.155
S0441	0.226	1.153	277	10	19	1.46	0.826	2.269

Cut No.	Ds	Dt	Ma	U	H	Wt	Wb	Tp
S0442	0.226	1.153	277	10	20	1.62	1.09	1.897
S0443	0.226	1.153	277	10	20.5	1.61	1.05	2.005
S0444	0.226	1.153	277	13	15.2	1.529	0.87	2.359
S0445	0.226	1.153	277	13	14.4	1.537	0.829	2.534
S0446	0.226	1.153	277	13	14.6	1.591	0.87	2.580
S0447	0.226	1.153	277	16	12.2	1.548	0.671	3.137
S0448	0.226	1.153	277	16	12.5	1.48	0.711	2.752
S0449	0.226	1.153	277	16	12.5	1.528	0.763	2.737
S044A	0.226	1.153	277	19	10.6	1.493	0.668	2.952
S044B	0.226	1.153	277	19	10.1	1.498	0.83	2.391
S044C	0.226	1.153	277	19	9.8	1.57	0.734	2.991
S0451	0.226	1.153	214	9	19.3	1.508	1.047	1.650
S0452	0.226	1.153	214	9	17	1.41	0.989	1.507
S0453	0.226	1.153	214	9	20.2	1.485	1.056	1.536
S0454	0.226	1.153	214	12	14.6	1.37	0.782	2.105
S0455	0.226	1.153	214	12	13.8	1.396	0.763	2.266
S0456	0.226	1.153	214	12	15.5	1.352	0.781	2.044
S0457	0.226	1.153	214	15	11.2	1.341	0.654	2.459
S0458	0.226	1.153	214	15	11.6	1.359	0.704	2.344
S0459	0.226	1.153	214	15	11.6	1.349	0.649	2.505
S045A	0.226	1.153	214	18	9.5	1.339	0.616	2.587
S045B	0.226	1.153	214	18	9.5	1.306	0.683	2.230
S045C	0.226	1.153	214	18	8.8	1.359	0.739	2.219

Database VIII

Sa = 80 mesh, Sd = 2.5 mm

Cut No.	Pi	Po	Do	Dt	Ma	U	H	Wt	Wb	Tp
S0461	345	317	0.254	1.155	242	12	17.57	1.476	1	1.704
S0462	345	317	0.254	1.155	242	12	17.44	1.478	0.981	1.779
S0463	345	317	0.254	1.155	242	12	17.4	1.479	0.985	1.768
S0464	310	286	0.254	1.155	242	12	14.59	1.411	0.844	2.030
S0465	310	286	0.254	1.155	242	12	14.49	1.412	0.832	2.076
S0466	310	286	0.254	1.155	242	12	14.48	1.431	0.873	1.997
S0467	283	262	0.254	1.155	242	12	13.08	1.429	0.815	2.198
S0468	283	262	0.254	1.155	242	12	13.29	1.43	0.819	2.187
S0469	283	262	0.254	1.155	242	12	13.06	1.418	0.779	2.287
S046A	245	221	0.254	1.155	242	12	10.04	1.46	0.74	2.577
S046B	245	221	0.254	1.155	242	12	10.51	1.426	0.741	2.451
S046C	245	221	0.254	1.155	242	12	11	1.422	0.774	2.319
S0471	210	193	0.254	1.179	242	12	8.86	1.415	0.843	2.047
S0472	215	193	0.254	1.179	242	12	9.26	1.441	0.764	2.423
S0473	210	193	0.254	1.179	242	12	8.95	1.447	0.793	2.341
S0474	178	159	0.254	1.179	242	12	6.87	1.383		
S0475	178	159	0.254	1.179	242	12	6.81	1.444		
S0476	178	159	0.254	1.179	242	12	6.81	1.398		
S0477	135	124	0.254	1.179	242	12	4.11	1.392		
S0478	134	124	0.254	1.179	242	12	4.07	1.39		
S0479	135	124	0.254	1.179	242	12	4.08	1.415		
S047A	106	97	0.254	1.179	242	12	2.56	1.38		
S047B	104	97	0.254	1.179	242	12	2.53	1.358		
S047C	104	97	0.254	1.179	242	12	2.54	1.387		
S0481	106	97	0.254	0.916	303	12	2.65	1.133		
S0482	104	97	0.254	0.916	303	12	2.63	1.117		
S0483	104	97	0.254	0.916	303	12	2.67	1.145		
S0484	139	130	0.254	0.916	303	12	5.11	1.167		
S0485	140	130	0.254	0.916	303	12	5.02	1.192		
S0486	139	130	0.254	0.916	303	12	5.04	1.165		
S0487	213	194	0.254	0.916	303	12	11.07	1.219	0.695	1.876
S0488	214	194	0.254	0.916	303	12	10.8	1.203	0.651	1.976
S0489	214	192	0.254	0.916	303	12	10.66	1.201	0.684	1.851
S048A	284	255	0.254	0.916	303	12	16.34	1.297	0.901	1.418
S048B	277	255	0.254	0.916	303	12	16.27	1.264	0.817	1.600
S048C	277	255	0.254	0.916	303	12	15.79	1.211	0.675	1.919
S0491	315	290	0.254	0.958	303	12	18.52	1.253	0.879	1.339
S0492	318	293	0.254	0.958	303	12	18.98	1.304	0.851	1.622
S0493	323	293	0.254	0.958	303	12	19.54	1.226	0.867	1.285
S0494	346	317	0.254	0.958	303	12	21.29	1.274	0.947	1.171
S0495	345	317	0.254	0.958	303	12	20.7	1.292	0.858	1.554
S0496	345	317	0.254	0.958	303	12	20.67	1.251	0.847	1.446

Cut No.	Pi	Po	Do	Dt	Ma	U	H	Wt	Wb	Tp
S0497	345	317	0.254	0.958	303	15	16.59	1.251	0.787	1.661
S0498	345	317	0.254	0.958	303	15	16.59	1.262	0.834	1.532
S0499	345	317	0.254	0.958	303	15	17	1.324	0.813	1.829
S049A	345	317	0.254	0.958	303	18	14.68	1.3	0.744	1.990
S049B	345	317	0.254	0.958	303	18	14.19	1.252	0.632	2.219
S0591	345	335	0.177	0.894	207	10	15.62	1.128	0.628	1.790
S0592	345	335	0.177	0.894	207	10	15.45	1.206	0.765	1.579
S0593	345	335	0.177	0.894	207	80	18.58	1.298	0.902	1.418
S0594	345	335	0.177	0.894	207	80	18.44	1.226	0.831	1.414
S0595	281	269	0.177	0.894	207	80	13.12	1.201	0.704	1.779
S0596	281	269	0.177	0.894	207	80	13.55	1.232	0.732	1.790
S0597	281	269	0.177	0.894	207	10	11.29	1.258	0.675	2.087
S0598	281	269	0.177	0.894	207	10	11.13	1.241	0.66	2.080
S0599	216	206	0.177	0.894	207	10	7.89	1.259		
S059A	216	206	0.177	0.894	207	10	7.64	1.229		
S059B	216	206	0.177	0.894	207	80	9.21	1.246	0.713	1.908
S059C	216	206	0.177	0.894	207	80	9.01	1.288	0.734	1.983
S0601	179	172	0.177	0.894	215	80	7.02	1.302		
S0602	179	172	0.177	0.894	215	80	6.54	1.239		
S0603	179	172	0.177	0.894	215	100	5.46	1.219		
S0604	179	172	0.177	0.894	215	100	5.47	1.243		
S0605	130	124	0.177	0.894	215	100	3.00	1.203		
S0606	130	124	0.177	0.894	215	100	3.02	1.241		
S0607	130	124	0.177	0.894	215	80	3.83	1.22		
S0608	130	124	0.177	0.894	215	80	3.75	1.243		
S0609	94	90	0.177	0.894	215	80	1.80	1.252		
S060A	94	90	0.177	0.894	215	80	1.81	1.231		
S060B	94	90	0.177	0.894	215	100	1.30	1.175		
S060C	94	90	0.177	0.894	215	100	1.29	1.193		

Database IX

Po = 317 MPa, Sa = 80 mesh

Cut No.	Do	Dt	Ma	U	Sd	H	Wt	Wb	Tp
SB501	0.254	0.959	272	12	1.27	18.9	1.014	0.623	1.400
SB502	0.254	0.959	272	12	1.27	18.6	1.204	0.902	1.081
SB503	0.254	0.959	272	12	1.27	19.12	1.219	0.893	1.167
SB504	0.254	0.959	272	12	2.54	18.49	1.325	0.896	1.536
SB505	0.254	0.959	272	12	2.54	18.42	1.299	0.865	1.554
SB506	0.254	0.959	272	12	2.54	18.22	1.279	0.855	1.518
SB507	0.254	0.959	272	12	3.81	18.02	1.48	0.862	2.212
SB508	0.254	0.959	272	12	3.81	17.61	1.538	0.884	2.341
SB509	0.254	0.959	272	12	3.81	17.88	1.615	0.958	2.351
SB50A	0.254	0.959	272	12	5.08	16.57	1.706	0.918	2.820
SB50B	0.254	0.959	272	12	5.08	15.94	1.745	0.925	2.934
SB50C	0.254	0.959	272	12	5.08	16.6	1.674	0.853	2.937
SB511	0.254	0.973	272	12	6.35	16.85	1.901	0.948	3.409
SB512	0.254	0.973	272	12	6.35	15.9	1.866	0.981	3.166
SB513	0.254	0.973	272	12	6.35	16.09	1.902	1.001	3.223
SB514	0.254	0.973	272	12	7.62	15.38	2.114	0.942	4.189
SB515	0.254	0.973	272	12	7.62	15.49	2.097	0.919	4.211
SB516	0.254	0.973	272	12	7.62	15.29	2.052	0.946	3.954
SB517	0.254	0.973	272	12	8.89	15.28	2.223	1.174	3.751
SB518	0.254	0.973	272	12	8.89	15	2.209	0.971	4.424
SB519	0.254	0.973	272	12	8.89	14.72	2.302	0.978	4.730
SB51A	0.254	0.973	272	12	10.16	14.12	2.477	0.908	5.601
SB51B	0.254	0.973	272	12	10.16	14.2	2.452	0.968	5.299
SB51C	0.254	0.973	272	12	10.16	14.04	2.484	0.94	5.512

Database X

Sa = 80 mesh, Sd = 2.5 mm

Cut No.	Po	Do	Dt	Ma	U	H	Wt	Wb	Tp
S0521	317	0.254	0.865	28	14	3.34	1.033		
S0522	317	0.254	0.865	28	14	2.85	1.022		
S0523	317	0.254	0.865	83	14	8.18	1.094	0.604	1.754
S0524	317	0.254	0.865	83	14	8.14	1.096	0.709	1.386
S0525	317	0.254	0.865	122	14	10.94	1.141	0.606	1.915
S0526	317	0.254	0.865	122	14	10.92	1.149	0.504	2.308
S0527	317	0.254	0.865	171	14	13.5	1.158	0.607	1.972
S0528	317	0.254	0.865	171	14	13.78	1.183	0.65	1.908
S0529	317	0.254	0.865	217	14	15.75	1.236	0.748	1.747
S052A	317	0.254	0.865	217	14	15.17	1.23	0.717	1.836
S052B	317	0.254	0.865	254	14	17.44	1.275	0.791	1.733
S052C	317	0.254	0.865	254	14	16.09	1.281	0.718	2.015
S0531	317	0.254	0.865	283	14	16.81	1.268	0.733	1.915
S0532	317	0.254	0.865	283	14	17.62	1.372	0.849	1.872
S0533	317	0.254	0.865	308	14	17.61	1.352	0.846	1.811
S0534	317	0.254	0.865	308	14	17.21	1.309	0.791	1.854
S0535	317	0.254	0.865	335	14	17.4	1.365	0.832	1.908
S0536	317	0.254	0.865	335	14	17.7	1.358	0.823	1.915
S0537	317	0.254	0.865	351	14	17.47	1.371	0.828	1.944
S0538	317	0.254	0.865	351	14	17.59	1.374	0.908	1.668
S0539	317	0.254	0.865	368	14	16.86	1.38	0.88	1.790
S053A	317	0.254	0.865	368	14	17.5	1.389	0.912	1.708
S053B	317	0.254	0.865	367	14	16.35	1.437	0.93	1.815
S053C	317	0.254	0.865	367	14	16.93	1.323	0.863	1.647
S0541	331	0.177	0.906	29	14	2.31	1.171		
S0542	331	0.177	0.906	29	14	2.13	1.15		
S0543	331	0.177	0.906	51.	14	3.96	1.154		
S0544	331	0.177	0.906	51.	14	3.78	1.155		
S0545	331	0.177	0.906	79.	14	5.79	1.188		
S0546	331	0.177	0.906	79.	14	5.95	1.21		
S0547	331	0.177	0.906	121	14	8.2	1.27		
S0548	331	0.177	0.906	121	14	8.1	1.285		
S0549	331	0.177	0.906	167	14	9.15	1.349	0.524	2.952
S054A	331	0.177	0.906	167	14	9.46	1.337	0.622	2.559
S054B	331	0.177	0.906	212	14	10.53	1.395	0.714	2.437
S054C	331	0.177	0.906	212	14	10.13	1.4	0.658	2.655
S0561	331	0.177	0.986	255	14	10.24	1.419	0.715	2.519
S0562	331	0.177	0.986	255	14	10.06	1.44	0.754	2.455
S0563	331	0.177	0.986	280	14	10.31	1.462	0.757	2.523
S0564	331	0.177	0.986	280	14	10.29	1.481	0.724	2.709
S0565	331	0.177	0.986	302	14	9.9	1.51	0.735	2.773
S0566	331	0.177	0.986	302	14	10.19	1.532	0.745	2.816

Cut No.	Po	Do	Dt	Ma	U	H	Wt	Wb	Tp
S0567	331	0.177	0.986	323	14	9.98	1.53	0.761	2.752
S0568	331	0.177	0.986	323	14	10.12	1.552	0.739	2.909
S0569	331	0.177	0.986	343	14	9.54	1.488	0.698	2.827
S056A	331	0.177	0.986	343	14	10.13	1.515	0.751	2.734
S056B	331	0.177	0.986	355	14	9.82	1.567	0.762	2.880
S056C	331	0.177	0.986	355	14	9.77	1.557	0.751	2.884
S0571	197	0.177	1.015	28	10	0.86	1.236		
S0572	197	0.177	1.015	28	10	0.77	1.246		
S0573	197	0.177	1.015	50	10	1.56	1.326		
S0574	197	0.177	1.015	50	10	1.60	1.318		
S0575	197	0.177	1.015	82	10	2.66	1.358		
S0576	197	0.177	1.015	82	10	2.58	1.335		
S0577	197	0.177	1.015	126	10	3.85	1.423		
S0578	197	0.177	1.015	126	10	3.68	1.468		
S0579	197	0.177	1.015	169	10	4.65	1.477		
S057A	197	0.177	1.015	169	10	4.52	1.491		
S057B	197	0.177	1.015	213	10	4.98	1.495		
S057C	197	0.177	1.015	213	10	4.99	1.513		
S0581	197	0.177	1.015	243	10	5.24	1.52		
S0582	197	0.177	1.015	243	10	5.16	1.516		
S0583	197	0.177	1.015	274	10	5.40	1.541		
S0584	197	0.177	1.015	274	10	5.30	1.525		
S0585	197	0.177	1.015	297	10	5.44	1.52		
S0586	197	0.177	1.015	297	10	5.36	1.522		
S0587	197	0.177	1.015	321	10	5.53	1.499		
S0588	197	0.177	1.015	321	10	5.18	1.542		
S0589	197	0.177	1.015	342	10	5.52	1.575		
S058A	197	0.177	1.015	342	10	5.46	1.58		
S058B	197	0.177	1.015	356	10	5.59	1.588		
S058C	197	0.177	1.015	356	10	5.44	1.572		

Database XI

(Grooving Test on Steel)
Sa = 80 mesh, Sd = 2.5 mm

Cut No.	Po	Do	Dt	Ma	U	Hmax	Hmin	H	Wt
SN011	304	0.229	0.89	219	10				1.263
SN012	304	0.229	0.89	219	10				1.151
SN013	304	0.229	0.89	219	10				1.157
SN014	304	0.229	0.89	219	13				1.167
SN015	304	0.229	0.89	219	13				1.192
SN016	324	0.229	0.89	219	10	20.9	20.9	20.90	1.18
SN017	324	0.229	0.89	219	10	19.6	19.6	19.60	1.17
SN018	324	0.229	0.89	219	13	17.5	15.2	16.30	1.164
SN019	324	0.229	0.89	219	13	17.3	15.1	16.08	1.171
SN01A	324	0.229	0.89	219	16	13.9	12.9	13.35	1.181
SN01B	324	0.229	0.89	219	16	14.5	12.2	13.60	1.161
SN01C	324	0.229	0.89	219	19	11.9	11	11.42	1.143
SN021	324	0.229	0.89	290	10	22.6	22.6	22.60	1.144
SN022	324	0.229	0.89	290	10	22.3	22.3	22.30	1.176
SN023	324	0.229	0.89	290	10	21.8	21.8	21.80	1.189
SN024	324	0.229	0.89	290	13	19.6	17.2	18.32	1.169
SN025	324	0.229	0.89	290	13	19.4	16.2	17.75	1.16
SN026	324	0.229	0.89	290	13	18.4	16	17.60	1.189
SN027	324	0.229	0.89	290	16	15.9	14.5	15.25	1.151
SN028	324	0.229	0.89	290	16	16.2	13.8	15.07	1.152
SN029	324	0.229	0.89	290	16	16.4	13.2	15.23	1.154
SN02A	324	0.229	0.89	290	19	13.5	12.3	12.85	1.131
SN02B	324	0.229	0.89	290	19	13.2	12.3	12.80	1.139
SN02C	324	0.229	0.89	290	19	13.6	12.6	13.07	1.138
SN031	324	0.254	1.132	123	12	12.1	10.62	11.25	1.352
SN032	324	0.254	1.132	123	12	11.94	10.76	11.53	1.381
SN033	324	0.254	1.132	196	12	16.09	14.4	15.24	1.381
SN034	324	0.254	1.132	196	12	16.2	14.68	15.47	1.439
SN035	324	0.254	1.132	250	12	18.37	16.81	17.66	1.401
SN036	324	0.254	1.132	250	12	17.72	15.64	16.51	1.419
SN037	324	0.254	1.132	274	12	19.55	17.41	18.78	1.459
SN038	324	0.254	1.132	274	12	19.38	18.25	18.85	1.426
SN039	324	0.254	1.132	304	12	19.23	18.01	18.63	1.428
SN03A	324	0.254	1.132	304	12	19.71	18.32	19.19	1.455

Database XII

(Deep Grooving on Steel)
Sa = 80 mesh, Sd = 2.5 mm

Cut No.	Po	Do	Dt	Ma	U	H	Wt
SN011	317	0.254	0.91	275	2	60.33	1.446
SN012	317	0.254	0.91	275	2	63.58	1.492
SN013	317	0.254	0.91	275	4	36.26	1.371
SN014	317	0.254	0.91	275	4	33.4	1.359
SN021	317	0.254	0.91	209	2	55.16	1.44
SN022	317	0.254	0.91	209	2	54.64	1.497
SN023	317	0.254	0.91	209	4	34.3	1.398
SN024	317	0.254	0.91	209	4	31.1	1.422

Database XIII

Sa = 80 mesh, Sd = 2.5 mm

Cut No.	Po	Do	Dt	Ma	U	H	Wt
AP011	317	0.254	0.947	190.0	25	21.63	1.329
AP012	317	0.254	0.947	190.0	25	20.46	1.269
AP013	317	0.254	0.947	190.0	28	18.99	1.294
AP014	317	0.254	0.947	190.0	28	19.19	1.25
AP023	317	0.254	0.947	222	28	19.75	1.352
AP024	317	0.254	0.947	222	28	18.74	1.32
AP027	317	0.254	0.947	243	28	20.66	1.356
AP028	317	0.254	0.947	243	28	20.25	1.354
AP018	317	0.254	0.947	46.6	32	5.59	1.132
AP017	317	0.254	0.947	46.6	32	6.17	1.13
AP019	317	0.254	0.947	95.7	32	11.46	1.163
AP01A	317	0.254	0.947	95.7	32	10.57	1.18
AP01C	317	0.254	0.947	152.3	32	14.21	1.258
AP01B	317	0.254	0.947	152.3	32	14.77	1.267
AP016	317	0.254	0.947	190.0	32	17.03	1.273
AP015	317	0.254	0.947	190.0	32	16.89	1.24
AP021	317	0.254	0.947	222	32	17.36	1.342
AP022	317	0.254	0.947	222	32	17.40	1.331
AP026	317	0.254	0.947	243	32	17.69	1.351
AP025	317	0.254	0.947	243	32	18.14	1.342
AP029	317	0.254	0.947	274	32	19.50	1.383
AP02A	317	0.254	0.947	274	32	18.22	1.387
AP02B	317	0.254	0.947	300	32	19.76	1.406
AP02C	317	0.254	0.947	300	32	19.28	1.37
AP031	317	0.254	0.947	220	32	20.06	1.353
AP032	317	0.254	0.947	220	32	17.41	1.402
AP033	248	0.254	0.947	220	32	12.49	1.366
AP034	248	0.254	0.947	220	32	12.07	1.387
AP035	188	0.254	0.947	220	32	8.27	1.373
AP036	188	0.254	0.947	220	32	8.33	1.38
AP037	150	0.254	0.947	220	32	5.69	1.378
AP038	150	0.254	0.947	220	32	5.78	1.405
AP039	110	0.254	0.947	220	32	3.09	1.301
AP03A	110	0.254	0.947	220	32	3.02	1.296
AP03B	82	0.254	0.947	220	32	1.53	1.304
AP03C	82	0.254	0.947	220	32	1.53	1.315

Database XIV

Sa = 80 mesh, Sd = 2.5 mm

Cut No.	Pi	Po	Do	Dt	Ma	U	H	Wt
TP011	345	317	0.254	0.96	27.3	14	4.25	1.183
TP012	345	317	0.254	0.96	27.3	14	4.40	1.1
TP013	345	317	0.254	0.96	81.6	14	11.06	1.21
TP014	345	317	0.254	0.96	81.6	14	10.99	1.193
TP015	345	317	0.254	0.96	119.5	14	13.99	1.264
TP016	345	317	0.254	0.96	119.5	14	14.25	1.244
TP017	345	317	0.254	0.96	162.0	14	17.56	1.34
TP018	345	317	0.254	0.96	162.0	14	16.45	1.299
TP019	345	317	0.254	0.96	162.0	17	14.66	1.305
TP01A	345	317	0.254	0.96	162.0	17	14.11	1.315
TP01B	345	317	0.254	0.96	162.0	20	12.47	1.303
TP01C	345	317	0.254	0.96	162.0	20	11.68	1.312
TP01D	345	317	0.254	0.96	162.0	23	10.82	1.313
TP01E	345	317	0.254	0.96	162.0	23	10.63	1.301
TP022	95	90	0.1778	0.884	214	8	2.56	1.108
TP021	95	90	0.1778	0.884	214	8	2.57	1.116
TP028	129	117	0.1778	0.884	214	8	5.64	1.106
TP027	129	117	0.1778	0.884	214	8	5.71	1.113
TP02A	186	175	0.1778	0.884	214	8	10.99	1.165
TP029	186	175	0.1778	0.884	214	8	10.75	1.165
TP033	230	220	0.1778	0.884	214	8	14.68	1.297
TP034	230	220	0.1778	0.884	214	8	14.94	1.251
TP035	279	268	0.1778	0.884	214	8	18.29	1.245
TP036	279	268	0.1778	0.884	214	8	18.11	1.272
TP024	95	90	0.1778	0.884	214	10	2.01	1.063
TP023	95	90	0.1778	0.884	214	10	2.09	1.086
TP026	129	117	0.1778	0.884	214	10	4.53	1.096
TP025	129	117	0.1778	0.884	214	10	4.70	1.116
TP02B	186	175	0.1778	0.884	214	10	8.87	1.175
TP02C	186	175	0.1778	0.884	214	10	8.86	1.182
TP031	230	220	0.1778	0.884	214	10	12.04	1.187
TP032	230	220	0.1778	0.884	214	10	11.91	1.214
TP038	279	268	0.1778	0.884	214	10	15.58	1.262
TP037	279	268	0.1778	0.884	214	10	15.32	1.269

Database XV

Sa = 80 mesh, Sd = 2.5 mm

Cut No.	Po	Do	Dt	Ma	U	H	Wt
TP041	317	0.254	0.901	235	15		1.255
TP042	317	0.254	0.901	235	15		1.247
TP043	317	0.254	0.901	235	13		1.252
TP044	317	0.254	0.901	235	13		1.273
TP045	317	0.254	0.901	235	17		1.253
TP046	317	0.254	0.901	235	17		1.271
TP047	317	0.254	0.901	235	20	15.06	1.275
TP048	317	0.254	0.901	235	20	15.45	1.259
TP049	267	0.254	0.901	235	13	16.33	1.289
TP04A	267	0.254	0.901	235	13	16.80	1.293
TP04B	267	0.254	0.901	235	17	13.03	1.29
TP051	162	0.254	0.901	235	17	8.09	1.272
TP052	162	0.254	0.901	235	17	8.08	1.237
TP053	162	0.254	0.901	235	13	10.36	1.293
TP054	162	0.254	0.901	235	13	10.37	1.293
TP055	102	0.254	0.901	235	13	4.85	1.207
TP056	102	0.254	0.901	235	13	4.87	1.216
TP057	102	0.254	0.901	235	17	3.62	1.215
TP058	102	0.254	0.901	235	17	3.56	1.198
TP059	102	0.254	0.901	235	20	2.93	1.175
TP05A	102	0.254	0.901	235	20	2.92	1.176
TP05B	102	0.254	0.901	235	10	6.19	1.278
TP05C	102	0.254	0.901	235	10	6.27	1.27

BIBLIOGRAPHY

1. Geskin, E. S., W. L. Chen, and W.Z. Lee. " Glass Shaping by the Use of Abrasive Waterjet. " *Glass Digest.* November, 1989, pp. 60-64.

2. Vora, A. " Investigation of the Characteristics of the Kerf and the Surface Generated in the Course of Cutting Titanium with Abrasive Waterjets." *Master Thesis.* New Jersey Institute of Technology, May 1988.

3. Donnan, P . H. " Abrasive Jet Cutting Development for Specialist Industrial Application ". *Proceedings of the 7th International Symposium on Jet Cutting Technology.* June 1984, pp. 481-492.

4. Hashish, M. " Application of Abrasive Waterjet to Metal Cutting". *Proceedings of Conference on Nontraditional Machining.* 1986, pp. 1-11.

5. Yie, G. G. " Cutting Hard Material with Abrasive-Entrained Waterjet - A Progress Report ". *Proceedings of the 7th International Symposium on Jet Cutting Technology.* 1984, pp. 481-492.

6. Neusen, K. F., P.K. Rohatgi, C. Vaidyanathan, and D. Alberts. " Abrasive Waterjet Cutting of Metal Matrix Composites". *Proceedings of the 4th American Water Jet Conference.* 1987, pp. 175-182.

7. Hashish, M., " Turning, Milling and Drilling with Abrasive-Waterjets (AWJ) ". *Proceedings of the 9th International Symposium on Jet Cutting Technology.* October, 1988, pp. 113-132.

8. Ohya, H. and M. Hoshina. " Research and Development into Ultra-high Pressure Jet Boring Machine " *Proceedings of the 10th International Symposium on Jet Cutting Technology.* Amsterdam (1990), paper H4.

9. Schroter, D.C. " Motion Equipment Designs for Hydrobrasive Waterjet Systems". *Proceedings of the 10th International Symposium on Jet Cutting Technology.* Amsterdam (1990), paper H1.

10. Johnson, S.T. "Integration of Ultra-High Water Pressure Jet Cutting with Multi Axis Control Devices ". *Proceedings of the 6th American Water Jet Conference.* Houston (1990), pp. 263-274.

11. Shah, S.C. "Integration of CAD/CAM System into a Waterjet Cutting Cell". *Master Thesis.* New Jersey Institute of Technology, May 1988.

12. Hu, F., Y. Yang, E.S. Geskin and Y. Chung. "Characterization of Material Removal in the Course of Abrasive Waterjet Machining ". *Proceedings of the 6th American Water Jet Conference.* Houston (1990), pp.17-29.

13. Blickwedel, H. N.S. Guo, H. Haferkamp, and H. Louis. " Prediction of Abrasive Jet Cutting Efficiency and Quality ". *Proceedings of the 10th International Symposium on Jet Cutting Technology.* Amsterdam (1990).

14. Kovacevic, R. " Surface Texture in Abrasive Waterjet Cutting ". *Journal of Manufacturing Systems.* Jan. 1991, Vol. 10, No. 1, pp. 32-40.

15. Chalmers, E.J. "Effect of Parameter Selection on Abrasive Waterjet Performance". *Proceedings of the 6th American Water Jet Conference.* Houston (1990), pp.345-354.

16. Matsui, S., H. Matsumura, Y. Ikemoto, Y. Kumon, and H. Shimizu. "Prediction Equations for Depth of Cut Made By Abrasive Water Jet". *Proceedings of the 6th American Water Jet Conference.* Houston (1991), pp. 31-41.

17. Hu, F. "Investigation of Material Erosion by Abrasive Waterjet Cutting". *Master thesis.* New Jersey Institute of Technology, May 1990.

18. Hashish, M. "Prediction Equations Relating High Velocity Jet Cutting Performance to Stand Off Distance and Multipasses ". *Journal of Engineering Industry.* August 1979, Vol. 101, pp.311-318.

19. Wulf, C. and W. Konig. "The Influence of the Cutting Parameters on Jet Forces and on the Geometry of the Kerf ". *Proceedings of the 7th International Symposium on Jet Cutting Technology.* June 1984, pp. 179-191.

20. Shih, L.Y. "Development of Technology for Glass Shaping by the Use of Abrasive Water-Jet". *Master Thesis.* New Jersey Institute of Technology, September 1991.

21. Finnie, I. "Erosion of Surfaces By Solid Particles". *Wear.* vol. 3, 1960, pp. 87-103.

22. Bitter, J.G.A. "A Study of Erosion Phenomena - Part I and Part II". *Wear.* vol. 6, 1963, pp. 169-190.

23. Neilson, J.H. and A. Gilchrist. "Erosion by a Stream of Solid Particles". *Wear.* vol. 11, 1968, pp. 111-122.

24. Hashish, M. " An Improved Model of Erosion by Solid Particle Impact ". *Proceedings of the 7th Conference on Erosion by Liquid and Solid Impact.* ELSI VII, Cambridge, England, September 1987, pp. 66/1-66/9.

25. Hashish, M. "A Model for Abrasive-Waterjet (AWJ) Machining". *ASME Journal of Engineering Materials and Technology.* Apr. 1989, Vol. 111, pp. 154-162.

26. Hashish, M. " Visualization of the Abrasive-Waterjet Cutting Process ". *Experimental Mechanics.* Jun. 1988, pp. 159-169.

27. Hashish, M. " Pressure Effects in Abrasive-Waterjet (AWJ) Machining". *ASME Journal of Engineering Materials and Technology.* Jul. 1989, Vol. 111, pp. 221-228.

28. Labus, T. J. et. al. " Factors Influencing the Abrasive Mixing Process ". *Proceedings of the 5th American Water Jet Conference.* Toronto, August 1989, pp. 205-215.

29. Mazurkiewicz, M. P. Oliko and R. Jordan. " Abrasive Particles Distribution in a High Pressure Hydroabrasive Jet". *Proceedings of International Waterjet Symposium.* Beijing, China, September 1987, Paper4: pp. 1-10.

30. Simpson, M. " Abrasive Particle Study in High Pressure Waterjet Cutting". *International Journal of Water Jet Technology.* March 1990, Vol. 1, pp. 17-28.

31. Yang, Y. " Characterization of Material Removal in the Course of Abrasive Waterjet (AWJ) Machining ". *Master Thesis.* New Jersey Institute of Technology, December 1990.

32. Finnie, I. " Erosion by Solid Particle in a Fluid Stream ". *ASTM Technical Publication 307.* 1961.

33. Hinze, J.O. *Turbulence.* McGraw-Hill Book Company, Inc., 1959.

34. Hjelmfelt, A.T. Jr. and L.F. Mockros. "Motion of Discrete Particles in a Turbulent Fluid". *Appl. Sci. Res.* 1965.

35. Danon, H.; M. Wolfshtein, and G. Hetsroni. "Numerical Calculation of Two-Phase Turbulent Round Jet". *Int. J. Multiphase Flow.* vol. 3, 1977, pp. 223-234.

36. Melville, W.K. and K.N.C. Bray. "A Model of the Two-Phase Turbulent Jet". *Int. J. Heat Mass Transfer.* vol. 22, 1979.

37. Maxey, M.R. and J.J. Riley. "Equation of Motion for a Small Rigid Sphere in a Nonuniform Flow". *Phys. Fluids.* 26(4), April 1983.

38. Situ, M. and J.A. Schetz. "Numerical Calculations of the Breakup of Highly Loaded Slurry Jets". *Journal of Fluids Engineering.* September 1987.

39. Givler, R.C. and R.R. Mikatarian. "Numerical Simulation of Fluid-Particle Flows: Geothermal Drilling Applications". *Journal of Fluids Engineering.* September 1987.

40. Ahmadi, G. and H. Ounis. "Dispersion of Small Rigid Spheres in a Turbulent Flow Field". *Proceedings of International Conference on Mechanics of Two-Phase Flow.* June, 1989.

41. Swanson, R.K. M. Kilman, S. Cerwin and W. Tarver. "Study of Particle Velocities in Water Driven Abrasive Jet Cutting", *Proceedings of the 4th American Water Jet Conference.* 1987.

42. Chen, W.L. "Correlation Between Particles Velocities and Conditions of Abrasive Waterjet Formation", *Ph.D. Dissertation.* New Jersey Institute of Technology, January 1990.

43. Himmelreich, U. and Riess, W. "Laser-Velocimetry Investigations of the Flow In Abrasive Water Jets with Varying Cutting Head Geometry". *Proceedings of the 6th American Water Jet Conference.* Houston (1990), pp. 355-370.

44. Bridgman, P.N. *The Physics of High Pressure.* First Edition, Dover Publications, Inc., New York, 1970.

45. Chen, W. L. and E. S. Geskin. " Correlation Between Particle Velocity and Conditions of Abrasive Waterjet Formation" *Proceedings of the 6th American Water Jet Conference.* Houston (1990), pp.305-313.

46. Hashish, M. " Steel Cutting with Abrasive Water Jets". *Proceedings of the 6th International Symposium on Jet Cutting Technology.* University of Surrey, U.K. (1982), Paper K3.

47. Beyer, W.H. *Handbook of Mathematical Sciences.* 6th edition, CRC press., pp.700.

48. Ipsen, D.C. *Units, Dimensions and Dimensionless Numbers.* McGraw-Hill Book Company, New York, 1951.

49. Buckingham, E. "Model Experiments and the Forms of Empirical Equations". *Trans. ASME,* 37, (1915), 263.